

Simulation, optimization and development of thermo-chemical diffusion processes

by

Yingying Wei

A dissertation submitted to the faculty

of the

WORCESTER POLYTECHNIC INSTITUTE

in partial fulfillment of the requirements for the

Degree of

Doctor of Philosophy

in

Material Science and Engineering

April 2013

Approved by: _____

Prof. Richard D. Sisson, Jr., Advisor

George F. Fuller Professor
Director of Manufacturing and Materials Engineering

ABSTRACT

Thermo-chemical diffusion processes play an important part in modern manufacturing technologies. They exist in many varieties depending on the type of diffusing elements used and the respective process objectives and procedures.

To improve wear and/or corrosion performance of precisely machined steel components, gas nitriding is selected as the most preferred thermo-chemical surface treatment. Conventional gas nitriding of steels is a multi-hour, sometimes multi-day hardening process carried out at ferritic temperatures and including a complete heat treatment cycle: normalizing, austenitizing, martensitic quenching and tempering. An alternative, subcritical-temperature austenitic nitriding process is evaluated with the purpose of accelerating the treatment and optimizing the hardness and toughness of nitrided layers while minimizing the distortion of steel parts treated. The alternative process involves liquefied nitrogen cryogenic quenching as well as aging. This study presents results of experimental work on AISI 4140 steel, examining the interplay between the nitriding and tempering conditions and phase transformations in both ferritic (525°C) and subcritical, nitrogen-austenitic (610°C) processes. Thermodynamic models, used to design processing conditions, are applied also in the microstructural interpretation of nitrided layers. Results are verified using the SEM, EPMA and EDS techniques. Kinetics of interstitial diffusion, isothermal martensite transformation, as well as dimensional control of nitrided parts is also presented.

Carburizing is, by far, the most widely adopted method in surface hardening. Problems with intergranular oxidation (IGO), energy efficiency and carbon footprint of conventional endothermic atmosphere (CO-H₂-N₂) carburizing is forcing heat treating and manufacturing companies to move toward increasingly capital- and operating-cost expensive, low-pressure (vacuum furnace) carburizing methods. In response, a new activated and alternate carburizing method (A2A carburizing) has recently been developed, bridging the endothermic atmosphere and vacuum processes, where a plasma-activated, oxygen-free, non-equilibrium nitrogen-hydrocarbon gas blend is utilized. The optimization of industrial A2A carburizing processes involves improvement of case uniformity of parts at different locations in the charge as well as between different sides

on the parts. Connected to the optimization, a computational fluid dynamics (CFD) study is conducted for examination of gas flow field inside the furnace and trays holding steel parts treated. To mitigate soot in the atmosphere and minimize the poorly carburized contact area between parts, effects of different combinations of nitrogen-hydrocarbons mixture on soot formation in atmosphere, deposition on metal surface and graphite growth at carburizing temperature are investigated. N₂-0.4%C₃H₈-1%CH₄ mixture is proven to be able to provide proper carburizing hardened case with less soot in atmosphere, less coke deposition on metal surface, as well as minimized marginally carburized contact zone. A soot formation mechanism for non-equilibrium atmosphere in A2A carburizing is discussed.

The carburizing processes have been investigated for decades, yet it still faces challenges concerning performance, reliability and process control. Since carburized parts must meet tolerances and specifications of particular applications, it is necessary to accurately predict carbon concentration profiles as a function of processing conditions. Proper carbon distribution is critical for satisfactory and reliable service life of carburized parts. Based on experimental work and theoretical developments, a software CarbTool© has been created for atmosphere and low pressure carburizing methods which consider the thermodynamics, mass transfer kinetics and carbon diffusion aspects of the carburizing process and the gas-steel interface condition. The models are capable now to accurately predict the surface carbon concentration and the carbon concentration profile in the steel, i.e. the most important outcomes of the process.

ACKNOWLEDGEMENTS

Without support and guidance from many individuals, it would not be enjoyable and challenging to complete this work. I feel deeply indebted to them all and would like to convey my gratitude in this acknowledgement.

I wish to express my sincere gratitude to my advisor Prof. Richard D. Sisson, Jr., for his constant support, guidance, advice, enthusiasm and encouragement throughout the years when I am studying at Worcester Polytechnic Institute. It is my honor to be his student. Not only does his insight and profound knowledge inspire me, but also his affirmative attitude for both research and life encourages me to conquer difficulties in this journey.

I owe my greatest appreciation to Mr. Zbigniew Zurecki, my co-advisor at Air Products and Chemicals, Inc. It is enjoyable to work with and learn from him. His ways of problem solving and thinking motivate my pursuit for the better, deeper and boarder understanding in the field of my work.

I deeply grateful to Prof. Diran Apelian, Prof. Makhlouf M. Makhlouf, Prof. Satya Shivkumar, Prof. Kevin Rong and Prof. Jianyu Liang for sharing their vision of research, their continuous encouragements and invaluable feedback through my academic years. I am grateful to Ms. Rita Shilansky for her constant assistance and Dr. Boquan Li for helping me to carry out the experiments.

I deeply appreciate opportunities that I have received through my internship with the Metal Processing Center of Excellence in Air Products and Chemicals, Inc. A lot of my work would have not been possible without their generous support. I give my sincere thanks to Mr. Ranajit Ghosh, Ms. Anna K. Wehr-Auckland and Mr. John L. Green for their valuable discussions, challenging my growth as a student, team player and an independent researcher. I am thankful to my friends and colleagues in Air Products for providing the support while pursuing my academic and personal goals.

I would like to thank the Center for Heat Treating Excellence at the Metal Processing Institute and the consortium member companies for their financial support and oversight of the project. I am so grateful for every little help that was provided on my way up.

It is a pleasure to be part of Materials Science and Engineering program and Metal Processing Institute. Friends and colleagues here made my years at WPI an enjoyable experience.

At Last, I am grateful to my parents and my boyfriend Mike Hu for being my everyday inspiration. Their love and belief in me lit my path in life and helped me strive to reach towards horizon and beyond.

TABLE OF CONTENTS

ABSTRACT	II
ACKNOWLEDGEMENTS	IV
TABLE OF CONTENTS	VI
CHAPTER I. INTRODUCTION	1
1.1 Conventional nitriding and subcritical temperature austenitic nitriding.....	2
1.2 Activated and alternate atmosphere carburizing and simulation of carburizing processes	4
1.3. Objective.....	6
CHAPTER II. LITERATURE REVIEW.....	7
2.1 Nitriding.....	7
2.1.1 Fe-N martensite transformation during cryogenic treatment	7
2.1.2 Atmosphere control of nitriding atmosphere	10
2.2 Carburizing.....	11
2.2.1 Atmosphere control of gas carburizing	12
2.2.2 Intergranular oxides formation in gas carburizing	14
2.2.3 Vacuum carburizing.....	17
2.2.4 Plasma activated and alternate atmosphere (A2A) carburizing.....	19
2.2.5 Carbon transfer mechanisms and its analytical models.....	23
2.2.6 Numerical Simulation	24
CHAPTER III. PUBLICATIONS	35
Paper #1: Nitrogen diluted ammonia atmosphere subcritical temperature nitriding on AISI 4140 steel: microstructure evolution, layer growth kinetics and cryogenic treatment (<i>to be submitted to Surface and Coatings Technology</i>).....	35
Paper #2: Subcritical temperature austenitic nitriding and cryogenic treatment on low alloy steel (<i>published in Proceedings of Materials Science and Technology (MS&T) 2012, Pittsburgh, PA, October, 2012</i>).....	57
Paper #3: Process Optimization for Industrial Practices of Plasma Activated Nitrogen-Hydrocarbons Atmosphere Carburizing (<i>to be submitted to International Heat Treatment and Surface Engineering</i>).....	73
Paper #4: Modeling of carbon distribution during atmosphere and low pressure carburizing processes (<i>published in Journal of Materials Engineering and Performance, Vol.22(1), 2013, DOI:10.1007/s11665-012-0353-6</i>)	103

Paper #5: Intelligent Heat Treating: Simulation of Carburization Process (*published in Proceedings of the 26th ASM Heat Treating Society Conference, Cincinnati, OH, Nov 2011, pp. 91-98*) 118

CHAPTER IV. RESEARCH CONCLUSIONS 134

CHAPTER I. INTRODUCTION

Thermochemical processes have several methods depending on the processing temperature and interstitial atoms diffused in. For ferrous alloys, in general, it is divided into two major categories, ferritic and austenitic regions, based on the different processing temperature range.

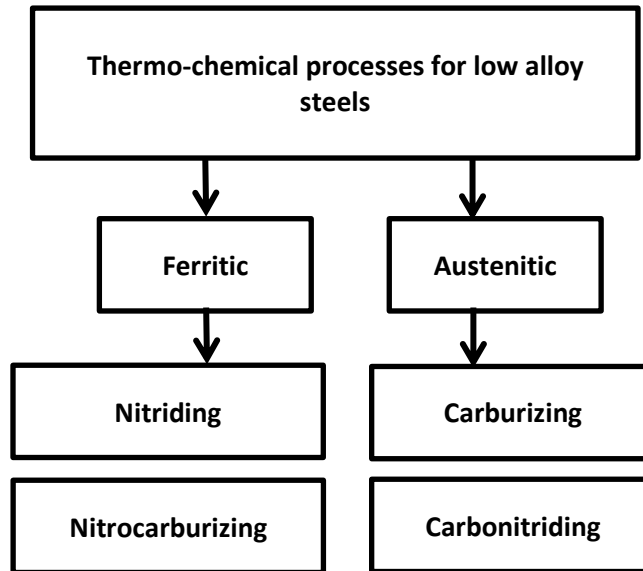


Figure 1 Categories of thermo-chemical processes

Shown in Fe-C phase diagram in figure 2, in ferritic region, which is below the eutectoid temperature, nitriding (350-590° C) and nitrocarburizing (400-590°C) are usually conducted. Above austenitic region, carburizing (800-1200° C) and carbonitriding (750-900° C) are processed. In this study, simulation and process optimization carburizing and development of nitriding will be focused on and discussed.

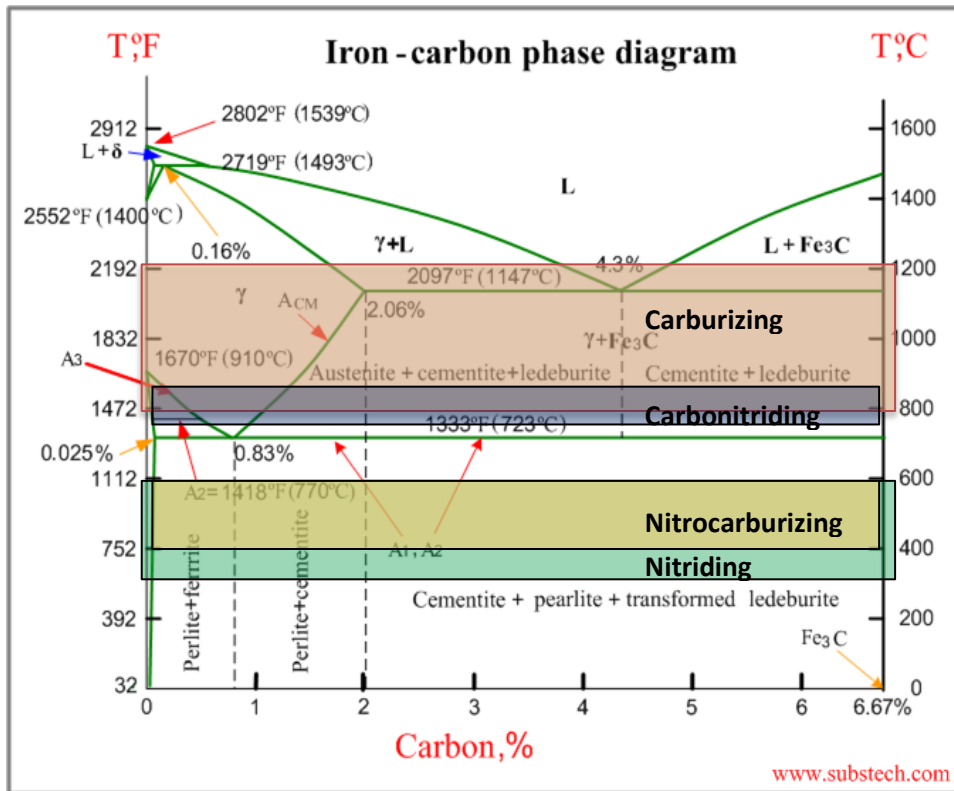


Figure 2 Temperature range of thermo-chemical processes on low alloy steels

1.1 Conventional nitriding and subcritical temperature austenitic nitriding

Nitriding is a thermo-chemical process that diffuses nitrogen atoms into surface of metals, most frequently steels, to create hardened case. Nitriding can be divided into several categories based on its interstitial atom carrier. During the recent decades, gas nitriding has become the dominant method in the metals processing industry. Conventional gas nitriding (ferritic-phase nitriding) usually takes place in the 350-590 °C range, i.e. in the ferritic phase region of low-alloyed steels. Rapid quenching is not required following the conventional, ferritic gas nitriding operations, and this prevents dimensional distortions, normally produced by the classic, carbon austenite to martensite phase transformation.

Nitrided layer is comprises compound layer and diffusion zone. Compound layer, consisting of γ' -Fe₄N and ϵ -Fe₂₋₃N, determines tribological and corrosion properties. Diffusion zone consists of α phase and different kinds of carbides, which determine its mechanical properties though their hardness and distribution. Ferritic nitriding of steels

produces less distortion and deformation than either carburizing or conventional transformation hardening. However, due to the limited nitrogen solubility of ferrite (figure 3) and a low diffusion coefficient caused by low process temperatures, the hardened case is relatively shallow even for the treatments taking many hours or days. Also, the nitrogen concentration decreases very quickly beneath the compound layer which results in an undesired, sudden drop of metal hardness.

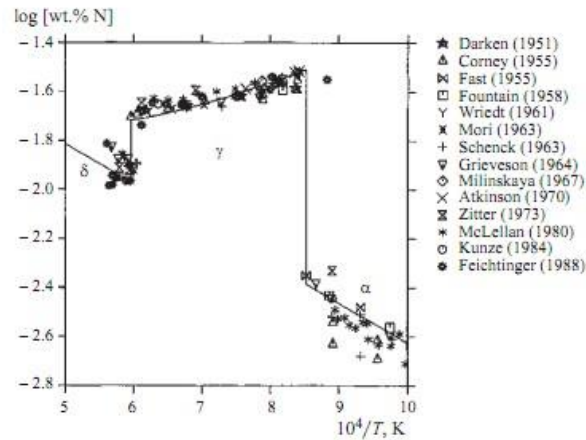


Figure 3 Solubility of nitrogen in iron at 0.1 MPa [1]: the symbols reflect data of various researchers.

A modified method is employed for accelerating nitriding treatments and optimizing the hardness and toughness of the core and the nitrided layers while minimizing the distortion of steel parts treated. The method involves increasing the nitriding temperature to sub-critical temperature, the temperature above the eutectoid temperature in the Fe-N system but below the corresponding temperature in the Fe-C system, and combined with quenching and further cooling to the cryogenic temperature range, in order to assure a complete transformation of nitrogen-formed austenite into nitrogen-formed martensite.

It is verified within the present research program that the core of the parts treated according to the proposed method retain its original ductile phases, carbon ferrite and carbides, whereas the surface layer comprises the conventional, hard compound layer (γ' -Fe₄N and ϵ -Fe₂₋₃N) and, an additional, somewhat softer transition layer of N-martensite. Thus, the thickness of the hardened case increases because of the transition layer and,

importantly, the phase transformation on quenching only occurs inside this layer which, in turn, will minimize distortion.

1.2 Activated and alternate atmosphere carburizing and simulation of carburizing processes

Carburizing of ferrous alloys is the introduction of carbon atoms into a solid alloys by holding above the temperature at which austenite begins to form, the critical temperature (A1) of the material in contact with a suitable source of carbonaceous material, which may be solid, liquid or gas.

The current prevalent carburizing methods in industry are atmosphere/gas and low pressure/vacuum carburizing. Gas carburizing uses equilibrium atmosphere controlled by carbon potential, which can be calculated from carbon activity from gas reactions. Vacuum carburizing uses non-equilibrium atmosphere at low pressure, in this case, carbon potential for equilibrium status is not applicable any more, in this study, carbon flux from atmosphere into component is used as controlling parameter of vacuum carburizing. There are three major steps in carburizing: 1) carbon carrier gases diffusion from atmosphere to component surface, controlled by mass transfer coefficient; 2) reaction at the surface and carbon chem-absorption by the surface, driven by activity gradient and 3) adsorbed carbon diffusion from the surface into the bulk materials, controlled by Fick's diffusion laws.

Endothermic gas is the major carbon carrier atmosphere used in industrial gas carburizing, which in average contains approximately 40% N₂, 40% H₂, 20% CO, 0.2-0.5% CO₂, trace amount of water vapor and methane/propane, depending on the original feeding gas into the endogas generator. [2]. The final production level of CO varies with various feed gas and will directly affect the atmosphere carbon potential, therefore, the controlling system in endothermic gas generator need to be precisely regulated. In addition, in certain regions of the world, where natural gas or propane may not be available, gaseous nitrogen and liquid methanol are used as alternate atmosphere and fed directly into furnace without generator. However, there are some problems exist with this kind of atmosphere in terms of quality of both atmosphere and workload. [3].

Because of the existence of oxidizing species (H_2O , CO_2) in the atmosphere of gas carburizing, the ferrous alloys with high content of Ti, Si, Mn, and Cr will be easily oxidized at the grain boundary and forms so-called intergranular oxide (IGO), which is brittle therefore could be the initial point of fatigue crack propagation during service. In industry, post-carburizing grinding is utilized to get rid of IGO layer, but additional stress is introduced onto the components, and also increased the cost. To avoid the formation of IGO, low pressure carburizing is employed to treat components with high quality requirements. Hydrocarbon, usually acetylene, is purged into furnace at 2-20 mbar. Nevertheless, the investment of vacuum carburizing furnace is much more expensive than gas carburizing furnace, and requires more frequent and careful maintenance.

The A2A technology introduced by Air Products and Chemicals, Inc. has been developed to eliminate oxides, improve carburized quality, remove endo-gas generator, reduce capital- and operational- cost saving by using less toxic and more environmental friendly gas in 1-atm pressure furnace, where nitrogen and hydrocarbon blends are introduced and activated through cold plasma injector. In this work, implementation of industrial process optimization has been conducted by both experimental trials and Computational fluid dynamics simulation (CFD), two methods of flux controlling are also used. Soot/tar formation on low alloy steel components, which is existing problem in both gas and vacuum carburizing is investigated.

Carbon concentration profile is one of the most important criterions for quality evaluation of carburized components, therefore, to have satisfied and reliable service of the components, precise control of carbon distribution is imperative. A simulation tool CarbTool© has been developed based on experimental data and theoretical development. In this study, vacuum carburizing model with non-equilibrium atmosphere is improved regarding to the quick carbon saturation and carbides formation on interested alloys by thermodynamics simulation. The accurate prediction for both gas and vacuum carburizing has been verified.

1.3. Objective

The aim of this research is to develop and optimize the conventional nitriding and carburizing processes using modified atmosphere and process parameters with assistance from simulation and modeling.

The aim of subcritical temperature nitriding process development is to investigate the kinetics, behavior and properties of N-austenite and N-martensite formed during gas nitriding and cryogenic quenching in the surface of low-alloy, low-cost steels.

To commercialized the feasibility-proven plasma activated and alternate atmosphere carburizing, industrial trials with plasma injector retrofit on exist integral quench furnace are conducted and evaluated. The purpose of this work is to verify the feasibility of this technology in practical industrial production in the extent of improvement of case uniformity, assurance of atmosphere and components quality, as well as development of process controls.

The simulation work provides better understanding of carburizing processes in equilibrium and non-equilibrium atmosphere, as well as possibility of optimizing the material, process and design for achieving the optimum performance.

Ultimately, the objective of this study is to provide the metals processing industry with more cost-effective, better quality thermo-chemical processes alternatives.

CHAPTER II. LITERATURE REVIEW

Case hardening processes are used to form a hard case or shell around the still tough core of a steel component. In general terms the harder a piece the less it wears. So if produce a component like gear we want it to be as hard as possible to be not worn out. However, high hardness in steel will decrease the ductility so that the components tend to be brittle. When the component is shocked, for instant, change the gear, the gear teeth would fracture and fall off. Therefore, case hardening would be employed as the solution, to create a hard wear resistant outside and keep the tough, ductile and shock resistant core [4].

2.1 Nitriding

Compare to carburizing, the benefits of conventional nitriding result from relatively lower process temperature, which is in ferritic region. Thus it does not undergo structural-mechanical change at the core upon quenching, and consequently minimizes dimensional change and distortion. However, the low solubility of ferrite and low processing temperature lead to shallow case of compound layer and hardness quickly drop within diffusion zone. Fe-N austenite with subsequent transformed Fe-N martensite could create a transition layer between hard but poorly supported compound layer and soft diffusion zone.

2.1.1 Fe-N martensite transformation during cryogenic treatment

Fe-N austenite formed at high temperature nitriding (over 1000 °C) in stainless steels has been investigated by Berns, et al [5-9]. Fattah [10] has compared the corrosion properties of AISI 4140 steel treated by plasma ferritic and austenitic nitriding followed by a slow cooling with furnace. Yasumaru[11] compared the results from nitriding at three different temperatures and water quenching on pure iron.

Regarding cryogenic treatments of steels after quenching from austenitic temperatures and before tempering, their effect on transformation of retained austenite and carbide precipitation (aging) has been investigated extensively. Claimed advantages of these

“deep freezing” treatments (-195°C) on transformation hardenable alloys are captured in the following three aspects:

1) Conversion of retained austenite to martensite and preventing excessive distortion during subsequent tempering due to austenite decomposition, as well as increasing hardness.

A large number of references [12-19] have stated delay between room temperature quench and cryogenic treatment may introduce austenite stabilization, hindering the subsequent martensitic transformation. However, investigations by Stratton et al. on AISI 8620 steel grade [20] shows when temperature is lower than -120 °C, the driving force is sufficient to convert even stabilized austenite.

2) Clustering of carbon atoms (distributed randomly over c-type of octahedral interstices) is activated during soaking steel in liquid nitrogen. This effect promotes precipitation of ultra-fine carbides, hence, it increase the hardness, wear- and corrosion-resistance.

3) According to the current state of knowledge the transformations of cryogenically treated steels during the subsequent aging and tempering include the following four stages: carbon clustering; transition carbides (ϵ/η) precipitation, martensite decomposition into a low carbon martensite; retained austenite decomposition into cementite and ferrite, and conversion of transition carbides to cementite.

Meanwhile, microstructure evolution on aging and tempering of cryogenically quenched Fe-N martensite have been researched using elemental, carbon-free iron as the starting material [10, 21-28].

Comparing to Fe-C martensite transformation during aging and tempering, the Fe-N transformations differ slightly. At the first stage, Mittemeijer [23] found no evidence of nitrogen clustering. Instead, segregation and ordering of interstitial atoms to c-type octahedral interstices occurs during aging at room temperature, which was confirmed by Gavdijuk [27, 29] using Mössbauer methods and Monte Carlo simulation. Gavriljuk [29]

observes that N tend to be short-range ordering and C tend to clustering, and that the distribution of Cr, Mn, Ni, Mo in austenite is more homogeneous in the presence of N than C. However, transition of carbides η and ϵ (original specimen included 0.5 wt. % C) does not take place, whereas coherent transition nitrides α'' precipitate [23] which results in increasing hardness while. In the next step, incoherent transition nitrides α'' form and reduce hardness. In the last steps of described aging-tempering sequence, α'' converts to γ' further reducing material hardness and, finally, retained austenite decomposes into ferrite and carbides.

Few only publications [30-34] were found to focus on the precipitation behavior of Fe-C-N martensite during aging and tempering and discuss the early stages of aging. Ferguson [35] and Wierszyllowski [36] proposed that the early clustering involves both nitrogen and carbon, and leads to the formation of carbonitrides $\alpha''\text{-Fe}_{16}(\text{C,N})_2$ during the subsequent tempering.

In contrast, experimental results from Mittemeijer and et. al. [30, 32, 34] indicated that nitrocarbides or carbonitrides do not form. It is rather the stress-driven local redistribution of C and N atoms to a-, b- and c- type of octahedral interstitials and α'' nitrides and ϵ/η carbides that is responsible for co-development of Fe-C-N martensite. When the atomic ratio of carbon and nitrogen varies but the total amount of interstitial atoms is constant, the amount of α'' and ϵ/η is dependent on the C/N ratio. This leads to the conclusion that carbon and nitrogen follow separate precipitation routes, with one part of the enrichments containing (mainly) carbon and that the other part mainly nitrogen atoms.

The precipitation process of Fe-C-N martensite can be divided into five steps according to Cheng et al. [34]: 1) local enrichment of interstitial atoms below 97 °C; 2) formation of nitrogen-containing α'' and carbon-containing ϵ/η ; 3) α'' conversion to γ' along with coarsening of ϵ/η ; 4) decomposition of retained austenite; 5) ϵ/η conversion to cementite.

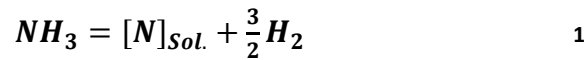
In terms of alloy effects on transformation of N containing martensite during aging, only Cheng et al. [37] reported on tempering of FeNiN martensite. Ni was found to suppress

the development of α'' -(Fe,Ni)₁₆N₂; γ' -(Fe,Ni)₄N precipitated from a randomly distributed N-enriched matrix and was followed by retained austenite decomposition.

Considering the martensite transformation starting point (Ms), N stabilized austenite more effectively than C. Ms was only 120K for Fe-2.75 wt. %N alloy according to [27]. When nitrogen content exceeds 2.2 wt. %, the N-austenite is stable at room temperature due to its Ms point located below the room temperature [11]. T. Bell [38] proposed the relationship between Ms and N-concentration as Ms (°C) = 533-228NC (wt. %). In this case, cryogenic soaking treatment is, simply, indispensable for transforming austenite to martensite.

2.1.2 Atmosphere control of nitriding atmosphere

Partially dissociated ammonia is used in conventional nitriding. Before feeding into the furnace, ammonia is dissociated through an ammonia dissociate, where addition of H₂ is produced to improve the control of nitriding potential in some cases. At the metal surface, ammonia dissociates to provide nitrogen dissolution via equation 18,



For local equilibrium between N in the atmosphere and N dissolve by metal surface, the activity of nitrogen is given by,

$$a_N = k_{18} \frac{P_{NH_3}}{P_{H_2}^{3/2}} \quad 2$$

where k_{18} is equilibrium constant of reaction 18, P is partial pressure of respective gas phases.

Nitriding potential is defined as,

$$K_N = \frac{P_{NH_3}}{P_{H_2}^{3/2}} \quad 3$$

Lehrer diagram for pure iron in figure 4 has been universally adopted for nitriding process control. This diagram presents the relationship between phases formed under local equilibrium and the nitriding potential as a function of temperature for pure iron. The

methodology of Lehrer diagram creation for alloy steels is developed by M. Yang [39] by Thermo-Calc [40].

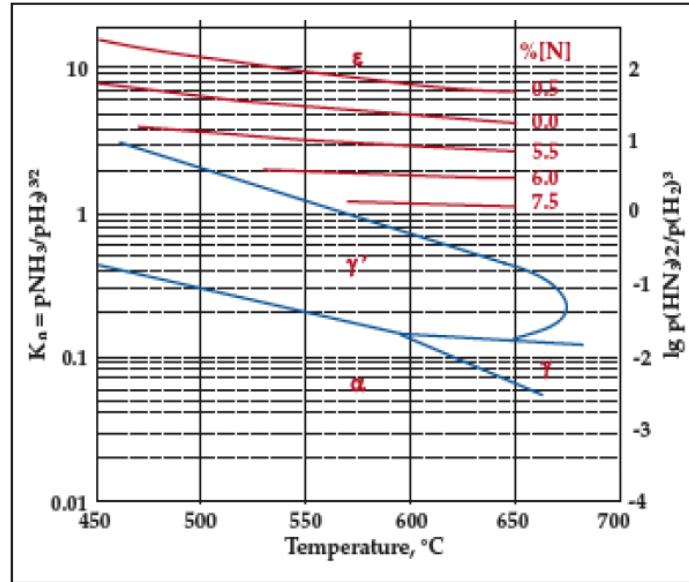


Figure 4 The experimental Lehrer diagram of the pure iron [41] with isoconcentration lines added [42]

2.2 Carburizing

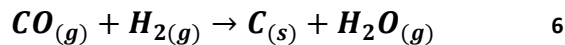
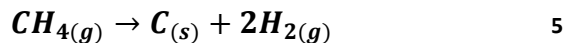
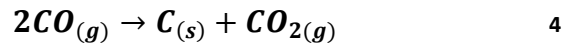
Of the many technologies available today to improve the performance of engineered surfaces, carburizing is one of the most common. It is enduringly popular because it uses a higher temperature than most thermochemical processes so that a deep hard layer can be formed in a short time [43]. It has been used in many industrial applications, especially automobile and aerospace components. To enrich the surface layer of steel and achieve the desired carbon solubility and penetration depth, the treatment is usually carried out at 800-1200° C [44], depending on the process objective and procedures. There are several categories of carburizing processes regarding to the carbon carrier medium: liquid, carbonaceous solid and atmosphere. This review will focus on process modeling, atmosphere control and development of carburizing processes using gas carbon carrier medium.

2.2.1 Atmosphere control of gas carburizing

The current prevalent carburizing processes include gas carburizing using either endothermic atmosphere or nitrogen/methanol mixture, and low pressure carburizing which is usually referred as vacuum carburizing.

The endothermic gas is a common equilibrium atmosphere used in many heat-treatment furnaces for applications that require a strong oxygen reducing atmosphere [2]. It is commonly generated from an endo-gas generator, which is comprised of an air/gas mixing system that supplies a mixture of air and natural gas (or propane) through a heated retort that contains a nickel coated ceramic catalyst where the air/gas mixture converted to the final gas production at 1900° F to 2000° F [2]. Upon the completion of the reaction, the production gas is quickly cooled from elevated temperature to 300° F to freeze the gas and prevent possible reverse reaction and carbon fallout to cooling system and pipeline downstream [2, 3]. The production gas is primarily composed of 31 – 40% H₂, 40 – 46% nitrogen, 19 – 23 % CO, 0.2 – 0.5% CO₂, less than 0.1 % water vapor and less than 0.1 % hydrocarbon depending on the original feeding gas in the generator.

This production gas would be feed directly into furnace as carbon carrier atmosphere during gas carburizing process. To achieve the desired carbon potential, an enrichment gas, e.g. methane or propane may be added. There are three main reactions take place in the furnace at the processing temperature.



Among above three reactions, the last one has been proved to be the fastest and therefore the rate-determining reaction in the carburizing atmosphere with CO and H₂ as major components [45]. According to the fundamental principle of chemistry, the equilibrium condition for reaction 3 is described by equilibrium constant k_3 [46]:

$$k_3 = a_C \cdot \frac{P_{H_2O}}{P_{CO}P_{H_2}} \quad 7$$

Where a_c is carbon activity, P is partial pressure of respective gas species. The value of equilibrium constant is dependent on temperature and can be calculated from equation [47].

$$\ln k_3 = -\frac{\Delta G^\circ}{RT} = -\frac{16333.11}{T} - 17.26 \quad 8$$

where ΔG° stands for standard Gibbs free energy for the reaction, T is the temperature, R is the ideal gas constant. From equation 4 and 5, carbon activity can be calculated. Carbon activity gradient is the driving force of transferring carbon atoms from atmosphere to metal surface. When gas composition (dew point, CO, H₂) is controlled and then carbon activity is controlled.

Since equilibrium is assumed in this kind of atmosphere, the equilibrium also exists in the reaction 1 and another carbon transferring reaction 6.



$$k_1 = a_c \cdot \frac{P_{CO_2}}{P_{CO}^2} \quad 10$$

$$k_6 = a_c \cdot \frac{P_{O_2}^{1/2}}{P_{CO}} \quad 11$$

Therefore, carbon activity can also be controlled by CO/CO₂ ratio or O₂ content. CO₂ is commonly controlled with an IR instrument and O₂ is with an oxygen probe.

However, in practical production, instead of carbon activity, another term called carbon potential is used in the process. The carbon potential of a furnace atmosphere is equal to the carbon content that pure iron would have in equilibrium with the gas [48]. The relationship between carbon activity a_c and carbon potential C_p is expressed by [48],

$$a_c = \gamma \cdot \frac{X_C}{1-2X_C} \quad 12$$

$$X_C = \frac{C_p/12.01}{C_p/12.01 + (100 - C_p)/55.85} \quad 13$$

$$\gamma = EXP\left(\frac{5115.9 + 8339.9X_C/(1-X_C)}{T} - 1.9096\right) \quad 14$$

where γ is activity coefficient and X_c is the carbon content expressed as a mole fraction. From above equations combined with calculated carbon activity, carbon potential can be calculated.

A simpler expression of the formula is usually used to calculate the relationship between carbon content in low-alloy case-hardening steel and carbon potential [48].

$$\log \frac{C_p}{X_c} = 0.55 \cdot (\%Si) - 0.013 \cdot (\%Mn) - 0.040 \cdot (\%Cr) + 0.014 \cdot (\%Ni) - 0.013 \cdot (\%Mo) \quad 15$$

In addition to endothermic gas, there is a competing process that was very popular in the late 1970's and early 1980's when natural gas curtailment took place. During this era the alternate atmosphere using gaseous nitrogen and liquid methanol was fed directly into the furnace [3]. The liquid methanol will be dripped into the furnace through the sprayer and cracks into carbon monoxide and hydrogen, at a rate to yield the 40% H₂ and 20% CO levels.

2.2.2 Intergranular oxides formation in gas carburizing

In both endogas and nitrogen/methanol mixture, the blend of the gas is formed by about 20% CO that is the most important in the exchange of the C from the atmosphere to the surface of the carburizing steel [49]. The standard Gibbs free energy change [50] for reaction 6 is

$$\Delta G^\circ = 111,700 + 87.65T \text{ J} \quad 16$$

The equilibrium constant k_6 of this reaction is

$$k_6 = e^{-\frac{\Delta G^\circ}{RT}} = e^{-\frac{111,700}{8.3144T} - \frac{87.65}{8.3144}} \quad 17$$

which gives k_6 equals to $e^{-21.74}$ at temperature 927 °C, together with equation 8

$$P_{O_2} = (e^{-21.74} \times 0.2)^2 = 10^{-20.28} \quad 18$$

and Nerst equation [49],

$$mV = 0.0496T \cdot \log \frac{O_2(air)}{O_2(furnace)} \quad 19$$

the reading on oxygen probe would be 1166 mV. From the table 1 [51], the carbon potential is found to be about 1.2%.

Table 1 Relationship between % CP and Probe mV at Various Temperatures for Endothermic Atmospheres Generated from Methane (20% CO)

% C _p	Temperature/ °C								
	800	825	850	875	900	925	950	975	1000
0.2	1034	1039	1043	1048	1053	1058	1062	1067	1072
0.25	1043	1048	1053	1058	1063	1068	1073	1078	1083
0.3	1051	1056	1061	1066	1072	1077	1082	1087	1092
0.35	1058	1063	1069	1074	1079	1085	1090	1095	1101
0.4	1065	1070	1076	1081	1087	1092	1098	1103	1109
0.45	1071	1076	1082	1088	1093	1099	1105	1110	1116
0.5	1076	1082	1088	1094	1100	1105	1111	1117	1123
0.55	1082	1088	1094	1099	1105	1111	1117	1123	1129
0.6	1087	1093	1099	1105	1111	1117	1123	1129	1135
0.65	1091	1097	1103	1110	1116	1122	1128	1134	1140
0.7	1096	1102	1108	1114	1120	1127	1133	1139	1145
0.75	1100	1106	1112	1119	1125	1131	1138	1144	1150
0.8	1104	1110	1116	1123	1129	1136	1142	1148	1155
0.85	1107	1114	1120	1127	1133	1140	1146	1153	1159
0.9	1111	1117	1124	1131	1137	1144	1150	1157	1163
0.95	1114	1121	1128	1134	1141	1148	1154	1161	1167
1	1118	1124	1131	1138	1144	1151	1158	1165	1171
1.05	1121	1127	1134	1141	1148	1155	1161	1168	1175
1.1	1124	1131	1137	1144	1151	1158	1165	1172	1179
1.15	1127	1133	1140	1147	1154	1161	1168	1175	1182
1.2	1129	1136	1143	1150	1157	1164	1171	1178	1185

Therefore, every element that in such atmosphere whose chemical equilibrium with the oxygen partial pressure equal or lower than $10^{-20.28}$ will form oxides. It is demonstrated in Ellingham diagram (Figure 5) that, Cr, Mn, Si and Al, which are the elements mostly

exist in steels will all form oxides in such atmosphere at 927° C. These oxides will be presented at the grain boundary as the so-called intergranular oxides (IGO).

IGO has been long known to degrade carburized components, in particular, it leads to low surface hardness and reduced component strength by depleting alloy elements in the matrix [52]. Moreover, IGO are stress raisers and are known to act as fatigue crack initiation sites, resulting in poor fatigue properties of the components [53, 54]. In addition, decarburization will also occur if oxygen is present leading to a lower hardenability at the surface [55]. However, from the above explanation of oxides formation, it has been proven that intergranular oxide is intrinsic propensity of components treated from either endogas or nitrogen/methanol atmosphere and barely can be prevented.

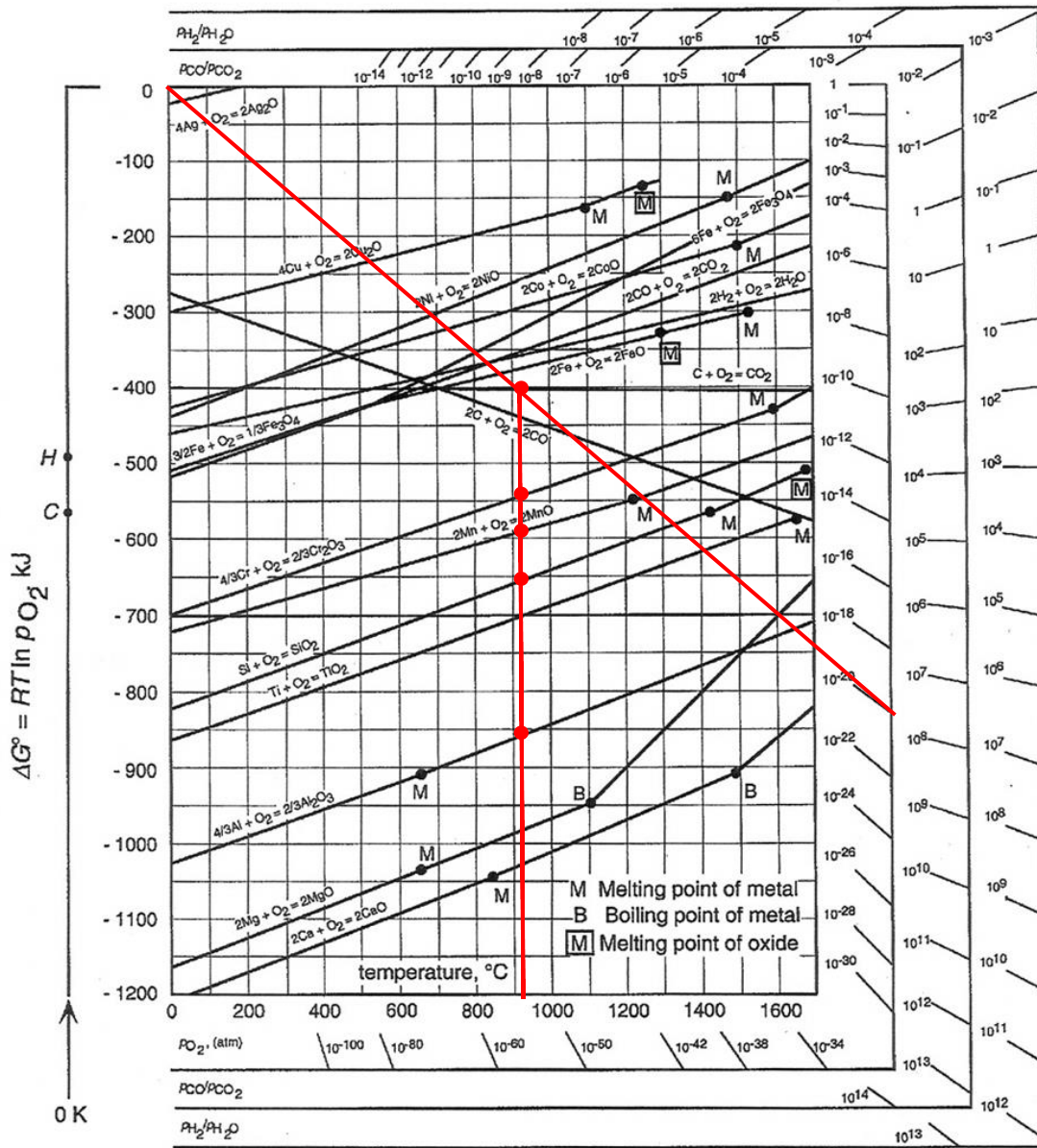


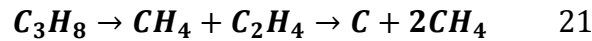
Figure 5 The Ellingham diagram for selected oxides [50]

2.2.3 Vacuum carburizing

Vacuum furnaces are typically utilized for heat treating precision parts with strict case hardening specifications. It avoids the formation of metal oxides because a hydrocarbon gas lacking oxygen is used and the furnace chamber is pumped down to a low pressure (2-20 mbar) to remove any oxygen that may be present [56]. Vacuum carburizing was introduced back to 1960s using methane at 500 mbar, however, it was unacceptable due

to the non-uniformity and heavy soot [57-61]. These problems were solved by reducing the pressure to 2-20 mbar [62, 63] and using propane, ethylene [64] or acetylene [65]. Methane is not used any more, due to its low dissociation at this low pressure [66].

Carbon is delivered to the steel surface in vacuum carburizing via reactions such as these [66]:



In the past, propane is the primary medium used in vacuum carburizing. However, propane dissociation occurs before the gas comes in contact with the surface of the steel, thus producing free carbon or soot. This uncontrolled soot formation results in poor carbon transfer to the part and loss of up-time productivity due to the need for additional heat treat equipment maintenance. Development work done in the past few years has demonstrated that acetylene is a good performing gas for vacuum carburizing. This is because the chemistry of acetylene is vastly different from that of propane or ethylene. Dissociation of acetylene delivers two carbon atoms to the one produced by dissociation of either propane or ethylene and avoids formation of nonreactive methane [66].

Under the high temperature, hydrocarbon gas with high decomposition rate makes the surface of components saturate very rapidly. Oversaturation leads to carbide formation, which should be avoided whenever possible. The only way to prevent carbide forming in processes with high carbon transfer coefficients is to divide the process into several boost-diffuse cycles [43]. If the carbide formation limit of the steel is exceeded, carbides can form in the outer surface of the components become barrier for further carbon atoms diffusion. The maximum length of carburizing boost steps is therefore given by the carbide formation limit of the steel at process temperature. The diffusion step is carried out until the surface carbon content has been lowered enough to attach another boost step of reasonable duration. The process ends with a diffusion step to adjust the desired carbon profile.

Compared to gas carburizing, which is controllable by measurement and adjustment of the carbon potential, vacuum carburizing cannot be controlled by carbon potential due to absence of thermodynamic equilibrium.

Components carburized at low pressure show no signs of internal oxidation, but other effects are reported, including: effusion of elements, especially manganese, formation of carbides on grain boundaries if the carburizing parameters are less than optimal, as well as etching at austenite grain boundaries during the carburizing step [67].

2.2.4 Plasma activated and alternate atmosphere (A2A) carburizing

Oxygen-free, hydrocarbon heat treating atmospheres have been an object of industrial and research interest for over quarter century. The early work of Kaspersma [68] and the subsequent studies of 1-atm pressure [69, 70] or higher pressure [49], nitrogen-hydrocarbon blends (N₂-HC) have demonstrated that, due to a relatively high thermochemical stability, acceptable reaction rates can be obtained only at temperatures markedly higher than for the typical nitrocarburizing treatments.

To accelerate the process, bridge the gas carburizing and vacuum carburizing, eliminate intergranular oxides, reduce capital/operational cost and promote usage of more safety and environmental friendly atmosphere, a plasma activation and alternate atmosphere heat treatment technology (A2A technology) has been introduced by Air Products and Chemicals, Inc [71]. A series of gas stream-activating, cold-plasma (figure 7) injectors have been developed at Air Products during the recent few years. The injectors [72] comprise two high voltage electrodes positioned across the stream of gas directed from gas supply into heat treating furnace. A DC or AC source-powered electric discharge between these electrodes ionizes, partially dissociates and converts the gas molecules on their way into the furnace. In contrast to the conventional, low-pressure plasma ion furnaces, metal load is not an electrode. A high-voltage/low-amperage, low power supply is used (typically below 2 kW) which forms a cold discharge combining self-pulsed, non-equilibrium arc and abnormal glow plasma modes [73] inside the passing gas stream. The low thermal energy of the discharge assures long electrode lifetime and prevents gas pyrolysis and sooting. The plasma injector can be easily retrofitted to various types of the

conventional, radiant tube or electrically heated and 1-atm pressure furnaces in order to carry out carburizing, carbonitriding, neutral carbon annealing, as well as nitrocarburizing operations falling into a relatively low temperature range [74]. So far, this technology has been tested on carburizing of low-alloy and stainless steels [74], low- and high-temperature nitriding of carbon, alloy and stainless steels [75].

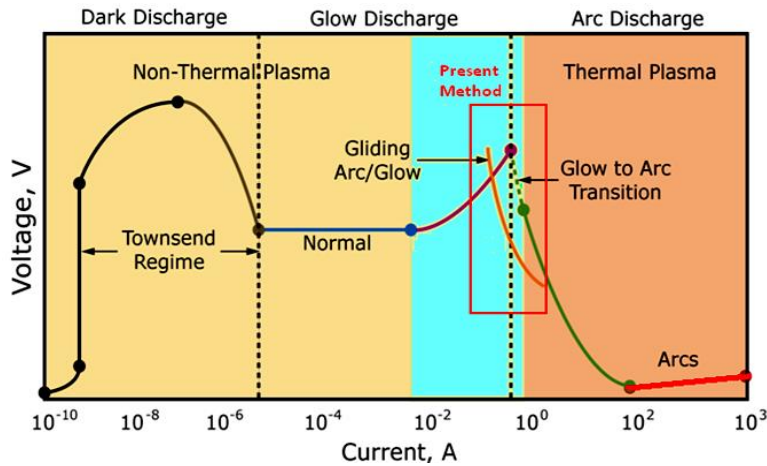


Figure 6 Non-thermal (cold) plasma and thermal plasma [75].

During A2A carburizing, instead of using endothermic gas in atmosphere furnace, the alternate nitrogen-hydrocarbons blend is used. Through the cold plasma, hydrocarbon could be activated into active species, numerous long- and short-lived, equilibrium and non-equilibrium gas products are formed in the N₂-hydrocarbons blend passing the discharge. As shown in figure 8, carbon flux obtained on low alloy steel AISI 1010 under activated N₂-4.5% CH₄ carburizing is more than twice on the same steel under only thermal treatment.

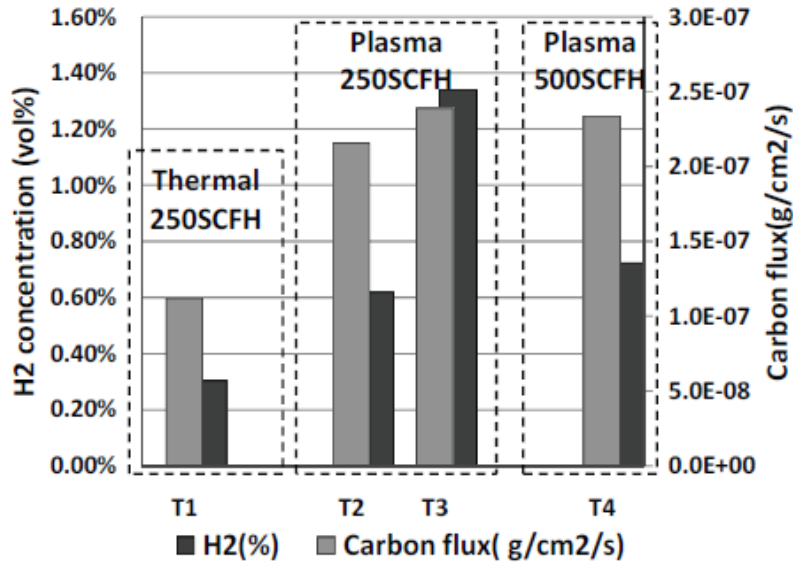


Figure 7 Thermal and plasma carburizing using N2-4.5% CH4 gas blend (AISI 1010 steel) [74]

Comparison between activated hydrocarbon treated and endo-gas treated AISI 8620 is demonstrated in Figure 9 [74], the endo-carburized part revealed a clearly developed intergranular oxidation zone. The enrichment of the oxidized boundaries with Mn, Cr and Si is observed and agrees with the metal oxides found from Ellingham diagram (figure 5) in previous sections.

The control of N2-NC atmosphere is more challenging than controlling equilibrium endo-gas by carbon potential. Normally, flowrate and concentration of the process gas are used to control the non-equilibrium N2-NC blend, the same approach as vacuum atmosphere. The development of carburizing recipes may require more trials, and the cycle may include carbon boost and diffuse with necessitate real-time, dynamic corrections to the processing parameters using a feedback loop. And many in situ sensors have been developed over the years to address the difficulties of process control in non-equilibrium as well as equilibrium atmospheres by testing the electrical resistance of carburized samples which directly related to carbon concentration [51, 76-78].

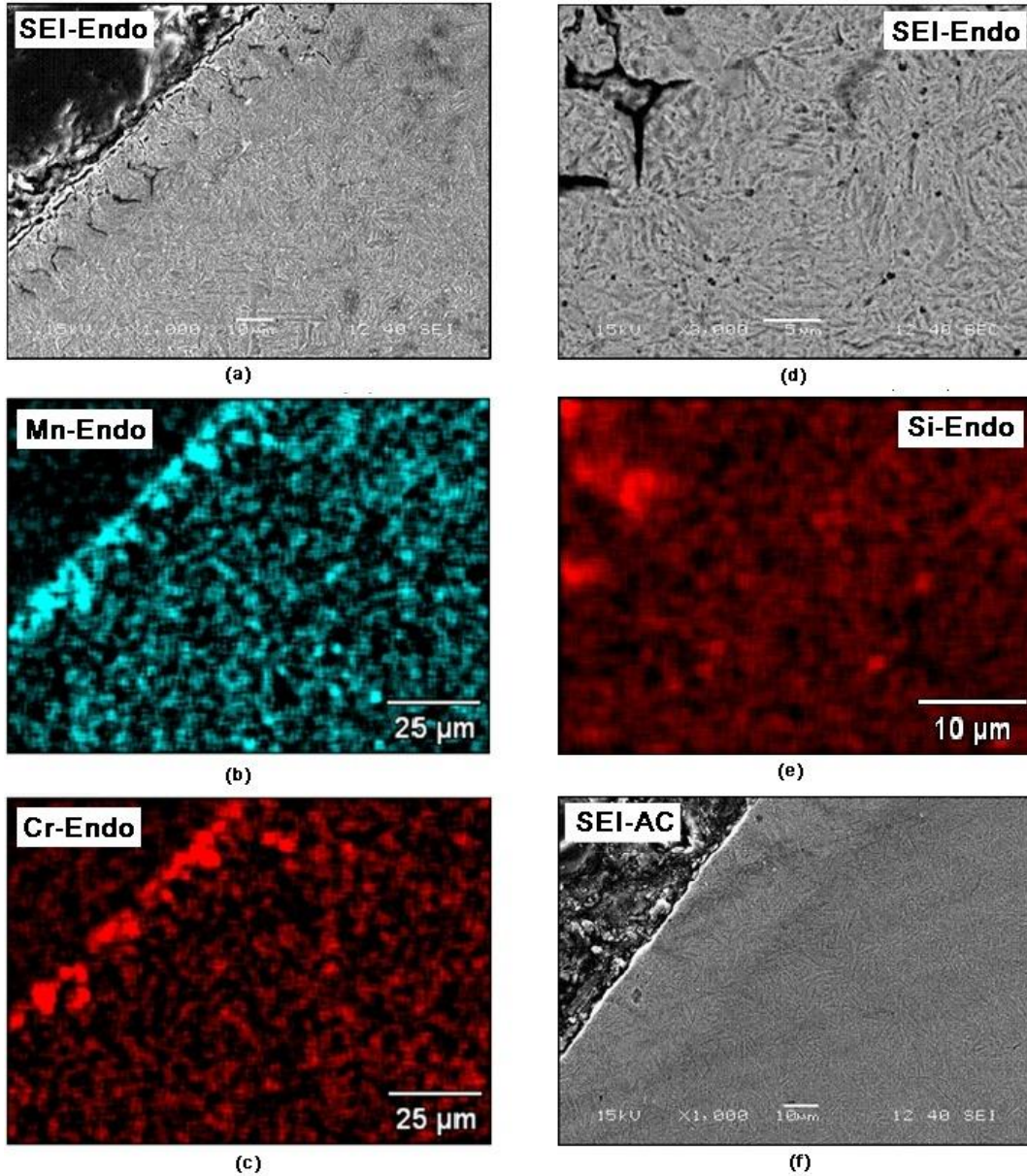


Figure 8 SEM-SEI-EDS cross-sectional images of subsurface regions of AISI 8620 after completed carburizing, quenching and tempering cycle. Etched in 2% Nital. (a) SEI image of endo-atmosphere carburized part; (b-c) Mn and Cr EDS-maps of area (a), (d) higher magnification of area (a), (e) Si EDS-map of area (d); and (f) SEI image of AC-plasma carburized part.

2.2.5 Carbon transfer mechanisms and its analytical models

There are three major steps in carburizing, shown as in figure 6: 1) carbon carrier gases diffusion from atmosphere to component surface, controlled by mass transfer coefficient; 2) reaction at the surface and carbon chem-absorption by the surface, driven by activity gradient; and 3) adsorbed carbon diffusion from the surface into the bulk materials, controlled by Fick's diffusion laws. The effect of process parameters on these kinetic parameters has been investigated by many researchers [79-88]. In particular, the mass transfer coefficient has been reported to be a complex function of the atmosphere gas composition, carburizing potential, temperature and surface carbon content [47, 79-84]. The coefficient of carbon diffusion in steel is another parameter defining the rate of carbon transport, which is strongly influenced by the carburizing temperature and steel carbon concentration [85-88].

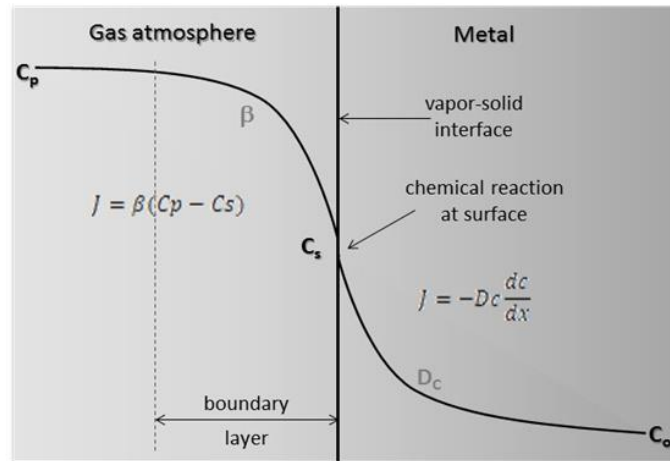


Figure 9 Carburizing mechanism [47]

In figure 6, J is the flux which represents the amount of atoms pass through unit area of plane per unit of time. In gas carburizing, it is assumed that the amount of carbon atoms transport from atmosphere to surface equals to the amount of atoms from the surface diffuse into bulk of steel, then the following equation will be obtained, which has been taken as boundary condition in gas carburizing simulation.

$$\beta(C_p - C_s) = -D_c \frac{dC}{dx} \quad 23$$

In the above equation, β is mass transfer coefficient, C_P is carbon potential of atmosphere, C_S is surface carbon concentration, D_C is diffusion coefficient of carbon in steel, C is carbon concentration and x is the depth from the surface.

However, this equation is not applicable in low pressure and plasma carburizing due to the intrinsic non-equilibrium of the process. In this case, flux has been used as boundary condition [89]. It can be measured by either weight gain after vacuum carburizing, or calculated from direct integration of carbon concentration profile [47],

$$J = \frac{\Delta m}{A \cdot t} \quad 24$$

$$J = \frac{\partial}{\partial t} \int_{x_\infty}^{x_0} C(x, t) dx \quad 25$$

where Δm is the weight change after carburizing, A is the area of treated surface, t is time and $C(x, t)$ is the carbon concentration as a function of depth and time.

Nevertheless, during vacuum carburizing, the hydrocarbon decomposition rate is so fast that the surface carbon concentration will build up and excess the austenite solubility easily. Once the austenite solubility is reached, carbides will start to form and block further carbon atoms absorption. If the model does not take into account the phase transformation, the carbon concentration calculation of following segments would be influenced and deviates from the reality.

The diffusion process is governed by Fick's second law with modification of surface curvature condition,

$$\frac{\partial C}{\partial t} = \frac{\partial}{\partial x} \left(D_C \frac{\partial C}{\partial x} \right) + u \cdot \frac{D_C}{r+ux} \cdot \frac{\partial C}{\partial x} \quad 26$$

where $u=-1$ for convex surface, $u=0$ for plane surface and $u=1$ for concave surface, r is radius of the curvature.

2.2.6 Numerical Simulation

Since an analytical solution to carbon diffusion in steel with the flux balance boundary condition is not available for concentration dependent diffusivity, the carburizing processes need to be modeled numerically. The governing partial differential equation

with the corresponding boundary condition can be transformed into a set of finite difference equations and solved numerically [47].

References

[1] N.I. Kardonina, A.S. Yurovskikh and A. S. Kolpakov, 2011, "Transformations in the Fe – N System," *Metal Science and Heat Treatment*, **52**(9) pp. 457-467.

[2] Jossart, J., "Endothermic Gas Production Overview," Atmosphere Engineering Company,.

[3] Bernard, W. J., Poor, R. P., Barbee, G. W., 2012, "Surface Treatment of Metallic Articales in an Atmospheric Furnace," **12/085,209**(US 8,293167 B2) .

[4] The Linde Group, "The principles of carburizing and carbonitriding,"

[5] Berns, H., 2007, "Advantages in Solution Nitriding of Stainless Steels," *Metal Science and Heat Treatment*, **49**(11) pp. 578-580.

[6] Berns, H., 2003, "Case Hardening of Stainless Steel using Nitrogen," *Industrial Heating*, **70**(5) pp. 47.

[7] Tschiptschin, A., 2002, "Predicting Microstructure Development during HighTemperature Nitriding of Martensitic Stainless SteelsUsing Thermodynamic Modeling," *Materials Research (S ão Carlos, S ão Paulo, Brazil)*, **5**(3) pp. 257-262.

[8] D. M. Larinin, L. M. Kleiner and A. A. Shatsov, 2008, "High-Temperature Nitriding of Low-Carbon Martensitic Steel 12Kh2G2NMFb in Nontoxic Salt Melts," *Metal Science and Heat Treatment*, **50**(9) pp. 502-507.

[9] H.W. Lee, J.H. Kong, D.J. Lee and et al., 2009, "A Study on High Temperature Gas Nitriding and Tempering Heat Treatment in 17Cr-1Ni-0.5C," *Materials & Design*, **30**(5) pp. 1691-1696.

- [10] M. Fattah, F. M., 2010, "Comparison of Ferritic and Austenitic Plasma Nitriding and Nitrocarburizing Behavior of AISI 4140 Low Alloy Steel," *Materials & Design*, **31**(8) pp. 3915-3921.
- [11] Yasumaru, N., 1992, "Formation of Austenite and Martensite in Surface Layer of Pure Iron with Ion Nitriding," *Materials Transactions, JIM*, **33**(1) pp. 7-10.
- [12] A. Saha Podder, H.K.D.H. Bhadeshia, 2010, "Thermal Stability of Austenite Retained in Bainitic Steels," *Materials Science & Engineering.A, Structural Materials : Properties, Microstructure and Processing*, **527**(7-8) pp. 2121-2128.
- [13] Zrn k, J., 2006, "Retained Austenite Stability Investigation in TRIP Steel using Neutron Diffraction," *Materials Science & Engineering.A, Structural Materials : Properties, Microstructure and Processing*, **437**(1) pp. 114-119.
- [14] Herring, D., 2005, "A Discussion of Retained Austenite," *Industrial Heating*, **72**(3) pp. 14.
- [15] Kokosza, A., 2005, "Evaluation of Retained Austenite Stability in Heat Treated Cold Work Tool Steel," *Journal of Materials Processing Technology*, **162-163**pp. 327-331.
- [16] Van Der Zwaag, S., 2001, "Stabilization Mechanisms of Retained Austenite in Transformation-Induced Plasticity Steel," *Metallurgical and Materials Transactions.A, Physical Metallurgy and Materials Science*, **32**(6) pp. 1527-1539.
- [17] Ferrer, J. P., 2006, "Austenite Retention in Low Al/Si Multiphase Steels," *Scripta Materialia*, **55**(5) pp. 441-443.
- [18] De Moor, E., 2008, "Effect of Retained Austenite Stabilized Via Quench and Partitioning on the Strain Hardening of Martensitic Steels," *Metallurgical and Materials Transactions.A, Physical Metallurgy and Materials Science*, **39**(11) pp. 2586-2595.

- [19] Savchenkova, S., 2005, "Effect of Preliminary Heat Treatment on the Stability of Austenite in Steel 08Kh15N5D2T," *Metal Science and Heat Treatment*, **47**(5) pp. 232-234.
- [20] Paul Stratton, Cord Henrik Surberg, 2009, "Retained Austenite Stabilization: In Carburized SAE 8620 Alloy Steel: Case-Hardened Components made of Low-Alloy Steels often have Retained Austenite in the Case After Quenching, which can be Transformed to Martensite by further Cooling of the Component, Even if the Austenite Stabilizes during Aging at Room Temperature," *Heat Treating Progress*, **9**(2) pp. 25.
- [21] M.J. Van Genderen, A. Böttger and E.J. Mittemeijer, 1997, "Formation of A " Iron Nitride in FeN Martensite: Nitrogen Vacancies, Iron-Atom Displacements, and Misfit-Strain Energy," *Metallurgical and Materials Transactions.A, Physical Metallurgy and Materials Science*, **28**(1) pp. 63-77.
- [22] A. Van Gent, E.C. Van Doorn and E.J. Mittemeijer, 1985, "Crystallography and Tempering Behavior of Iron-Nitrogen Martensite," *Metallurgical Transactions.A, Physical Metallurgy and Materials Science*, **16**(8) pp. 1371-1384.
- [23] Liu Cheng, E. J. M., 1990, "The Tempering of Iron-Nitrogen Martensite; Dilatometric and Calorimetric Analysis," *Metallurgical Transactions.A, Physical Metallurgy and Materials Science*, **21**(1) pp. 13-26.
- [24] Liu Cheng, N.M. van der Pers and A. Böttger, 1990, "Lattice Changes of Iron-Nitrogen Martensite on Aging at Room Temperature," *Metallurgical Transactions.A, Physical Metallurgy and Materials Science*, **21**(11) pp. 2857-2867.
- [25] I. FALL, J. -. R. G., 1996, "Mössbauer Spectroscopy Study of the Aging and Tempering of High Nitrogen Quenched Fe-N Alloys: Kinetics of Formation of Fe₁₆N₂ Nitride by Interstitial Ordering in Martensite," *Metallurgical and Materials Transactions.A, Physical Metallurgy and Materials Science*, **27**(8) pp. 2160-2177.

- [26] Dongling Jiao, C.P. Luo and Jiangwen Liu, 2007, "Isothermal Transformation of High-Nitrogen Austenite," *Scripta Materialia*, **56**(7) pp. 613-616.
- [27] V.G. Gavdijuk, V.M. Nadutov and K. Ullakko, 1991, "Low Temperature Ageing of Fe-N Martensite," *Scripta Metallurgica Et Materialia*, **25**(4) pp. 905-910.
- [28] Lee, T., and Tae-Ho Lee, Chang-Seok Oh, Min-Ku Lee and et. al, 2010, "Nitride Precipitation in Salt-Bath Nitrided Interstitial-Free Steel," *Materials Characterization*, **61**(10) pp. 975-981.
- [29] Gavriljuk, V. G., 2006, "Austenite and Martensite in Nitrogen-, Carbon- and Hydrogen-Containing Iron Alloys: Similarities and Differences," *Materials Science & Engineering.A, Structural Materials : Properties, Microstructure and Processing*, **438-440**pp. 75-79.
- [30] Genderen, M.J. van, A. Böttger and E.J. Mittemeijer, 1992, "Ternary iron-carbon-nitrogen martensitic alloys: as-quenched state and development of transition precipitates," *Gilbert. R. Speich Symposium Proceedings, Iron & Steel Society*, pp. 29-38.
- [31] A. Böttger, P.J. Warren, G.D.W. Smith, M.J. van Genderen, S.J. Sijbrandij, 1999, "Tempering of iron-carbon-nitrogen martensites: (re)distribution of interstitial atoms," *Materials Science Forum*, **318-320**, pp. 103-108.
- [32] Genderen, M.J. van, A.J. Böttger and E.J. Mittemeijer, 1992, "First Stage of Precipitation in Iron-Carbon-Nitrogen Martensites; Diffraction Analysis using Synchrotron Radiation," *Scripta Metallurgica Et Materialia*, **26**(6) pp. 883-888.
- [33] Liu Cheng, A. Böttger and E.J. Mittemeijer, 1990, "The initial stages of tempering of iron-carbon-nitrogen martensite," *Proc. Sec. Int. Conf. on High Nitrogen Steels*, H. W. G. Stein, ed. *Stahleisen, Düsseldorf, Aachen, Germany*, pp. 52-56.
- [34] Liu Cheng, A. Böttger and E.J. Mittemeijer, 1992, "Tempering of Iron-Carbon-Nitrogen Martensites," *Metallurgical Transactions.A, Physical Metallurgy and Materials Science*, **23**(4) pp. 1129-1145.

- [35] P. Ferguson and K.H. Jack, 1984, *Scripta Metallurgica*, **18**pp. 1189.
- [36] I. Wierszylowski, L. M., 1988, *Proceeding of International Conference on High Nitrogen Steels*, Institute of Metals, London, Lille, France, pp. 338.
- [37] Liu Cheng, A. Böttger and E.J. Mittemeijer, 1991, "The Tempering of FeNiN Martensite," *Metallurgical Transactions.A, Physical Metallurgy and Materials Science*, **22**(9) pp. 1945-1956.
- [38] Bell, T., 1968, "Martensite Transformation Start Temperature in Iron-Nitrogen Alloys," *The Journal of the Iron and Steel Institute*, **206**(10) pp. 1017-1021.
- [39] Yang, M., 2012, "Nitriding – Fundamentals, Modeling and Process Optimization," Dissertation, Worcester Polytechnic Institute.
- [40] Andersson, J. O., and et al., 2002, "THERMO-CALC & DICTRA, Computational Tools for Materials Science," *Calphad*, **26**(2) pp. 273-312.
- [41] Lehrer, E., 1930, "The Equilibrium, Iron-Hydrogen-Ammonia," *Zeitschrift Fuer Elektrochemie Und Angewandte Physikalische Chemie*, **36**pp. 383.
- [42] Maldzinski, L., and P.Z., K., L., 1986, "Equilibrium between NH₃/H₂ and Nitrogen in ϵ Phase of Iron-Nitrogen System," **12**pp. 645-649.
- [43] The Linde Group, "Furnace Atmospheres No. 6: Low pressure carburising and high pressure gas quenching."
- [44] Herring, D., 2012, "All about Carburizing," .
- [45] Grabke, H. J., 1990, "Carburising Kinetics (in Germany)," *Harterei-Technische Mitteilungen*, **45**.pp. 110-118.
- [46] The Linde Group, "Furnace Atmosphere No. 1 Gas Carburizing and Carbonitriding,"

- [47] Karabelchtchikova, O., 2007, "Fundamentals of Mass Transfer in Gas Carburizing," Dissertation, Worcester Polytechnic Institute.
- [48] Holm, T., "Furnace atmospheres 1: Gas Carburizing and Carbonitriding," AGA AB,
- [49] Gianotti, E., 2006, "Hyper Baric Carburising Process," *La Metallurgia Italiana*, **7**(8) pp. 41-46.
- [50] Gaskell, D.R., 2008, "Introduction to the Thermodynamics of Materials - 5th Edition," Taylor & Francis Group, New York, NY, .
- [51] Eurothermo, 2008, "Carbon Probe Instruction Manual," pp. 28.
- [52] Naito, T., Ueda, H., and Kikuchi, M., 1984, "Fatigue Behavior of Carburized Steel with Internal Oxides and Nonmartensitic Microstructure Near the Surface," *Metall. Trans. A*, **15**(7) pp. 1431-1436.
- [53] Krauss, G., 1995, "Microstructure and Performance of Carburized Steel. Part IV: Oxidation and Inclusion," *Adv. Mater. Process*, **148**(6) pp. 36Z-36DD.
- [54] Dowling, W. E., Donlon, W. J., and Couppe, W. B., 1995, "Fatigue Behaviour of Two Carburized Low Alloy Steel," *Proceeding of the second international conference on carburizing and nitriding with atmosphere*, Cleveland, OH, J. Grosch, J. Morral and M. Schneider, eds. pp. 55.
- [55] Colombo, R. L., Fusani, F., and Lamberto, M., 1983, "On the Soft Layer in Carburized Gears," *Journal of Heat Treating*, **3**pp. 126-128.
- [56] Poor, R. P., Barbee, W., and Brug, J. E., 2007, "Furnace for Vacuum Carburizing with Unsaturated Aromatic Hydrocarbons," **11/404,459**(US 7,267,793 B2) pp. 1-14.
- [57] Limque, F., and Bless, F., 1980, "Erfahrungen Mit Überdruck-Gasabschrecken Sowie Aufkohlen in Vakuum öfen," *Härtereitechn. Mitt.*, **35**(5) pp. 238-244.

- [58] Chatterjee-Fischer, R., 1985, "Überblick Über Die Möglichkeiten Zur Verkürzung Der Aufkohlungsdauer," H ä r t e r e i - T e c h n . M i t t . , **40**(1) pp. 7-11.
- [59] Eysell, F. W., and Heumüller, E., 1979, "Entwicklungstendenzen Auf Dem Gebiet Der Unterdruckaufkohlung," H ä r t e r e i - T e c h n . M i t t . , **34**(2) pp. 83-89.
- [60] Chatterjee-Fischer, R., 1982, "Verfahrenstechnische Möglichkeiten einer randoxidationsarmen (-freien) Einsatzh ä r t u n g , " F V A - N r . 1 4 / I I A b s c h l u s s b e r i c h t , F V A F o r s c h u n g s h e f t 1 1 0 , F o r s c h u n g s v e r e i n i g u n g A n t r i e b s t e c h n i k e . V .
- [61] Luiten, C. H., Limque, F., and Bless, F., 1979, "Aufkohlen in Vakuum-Öfen," H ä r t e r e i - T e c h n . M i t t . , **34**(6) pp. 253-259.
- [62] Pourprix, Y., and Nandot, J., 1985, "La C é m e n t a t i o n S o u s B a s s e P r e s s i o n : U n M o y e n D ' i n t é g r e r L e T r a i t e m e n t T h e r m i q u e D a n s L e s L i g n e s D ' u s i n a g e D ' e n g r e n a g e s , " T r a i t e m e n t T h e r m i q u e , **197**pp. 51-58.
- [63] Altena, H., 1998, "Niederdruck-Aufkohlung Mit Hochdruckgasabschreckung," H ä r t e r e i - T e c h n . M i t t . , **53**(2) pp. 93-101.
- [64] Sugiyama, M., Ishikawa, K., and Iwata, H., 1998, "Using Acetylen for Superior Performance Vacuum Carburising," Proceedings of 18th ASM Heat Treating Society Conference, Anonymous Rosemont, Illinois, pp. 49-56.
- [65] Hayaud, C., Jacquot, P., Baravian, G., 1997, "Caract é r i s a t i o n P a r S p e c t r o m é t r i e D e M a s s e D e L ' a t m o s p h è r e D e T r a i t e m e n t D ' u n F o u r D e C é m e n t a t i o n B a s s e P r e s s i o n , " T r a i t e m e n t T h e r m i q u e , pp. 99-107.
- [66] Davis, J.R., 2002, "Surface Hardening of Steels: Understanding the Basics," ASM International, Materials Park, OH, pp. 349-91.
- [67] Clausen, B., Hoffmann, F., and Mayr, P., 2003, "Randschichtschädigung infolge Niederdruckaufkohlung," E u r o p ä i s c h e T a g u n g D a s E i n s a t z h ä r t e n , S V W / A S T T S c h w e i z e r V e r b a n d f ü r d i e W ä r m e b e h a n d l u n g d e r W e r k s t o f f e , Z ü r i c h , **3-4**, pp. 149-172.

- [68] Kaspersma, J. H., and Shay, R. H., 1982, "Carburization and Gas Reactions of Hydrocarbon-Nitrogen Mixtures at 850oC and 925oC," Metallurgical Transactions B, **13B**pp. 267-273.
- [69] Estrin, B. M., and et al, 1984, "Carburizing in a Nitrogen-Based Mixture with Additives of Pure Methane," Metallovedenie i Termicheskaya Obrabotka Metallov, **5**pp. 26-29.
- [70] Connery, K., and Ho, S., 2007, "Optimization of Oxygen-free Heat Treating," Proceeding of the 24th ASM Heat Treating Society Conference, Detroit, MI, pp. 17-19.
- [71] Wang, X., Zurecki, Z., and Sisson Jr., R. D., 2012, "Development of Nitrogen-Hydrocarbon Atmospheric Carburizing and Process Control Methods," Journal of Materials Engineering and Performance, DOI: 10.1007/s11665-012-0294-0.
- [72] Zurecki, Z., 2007, "Heat Treating Atmosphere Activation," Proceeding of the 24th ASM Heat Treating Society Conference, Detroit, MI, .
- [73] Fridman, A., 2008, "Plasma Chemistry," Cambridge University Press, New York, pp. 177-208.
- [74] Zurecki, Z., and Wang, X., 2009, "Atmosphere carburizing using electric discharge-activated nitrogen-natural gas mixtures," Heat Treating Conference and Exposition 2009, Indianapolis, IN .
- [75] Wang, X., 2011, "Activated Atmosphere Case Hardening of Steels," Dissertation, Worcester Polytechnic Institute.
- [76] Beuret, P., (US 5,064,620) .
- [77] Ghedid, L. G., and et al, (US 7,068,054) .
- [78] Winter, K., 2008, "A Guide to Better Atmosphere Carburizing using BothDynamic and Equilibrium-Based Measurements," Industrial Heating, pp. 91-94.

- [79] Stolar, P., and Prenosil, B., 1984, "Kinetics of Transfer of Carbon from Carburizing and Carbonitriding Atmospheres," *Metallic Materials (English Translation of Kovove Materialy)*, **22**(5) pp. 348-353.
- [80] Rimmer K., Schwarz-Bergkamp E., and Wunning J., 1975, "Surface Reaction Rate in Gas Carburizing," *Haerterei-Technische Mitteilungen*, **30**(3) pp. 152-160.
- [81] Munts, V. A., and Baskatov, A. P., 1980, "Rate of Carburizing of Steel," *Metal Science and Heat Treatment (English Translation of Metallovedenie i Termicheskaya Obrabotka Metallov)*, **22**(5-6) pp. 358-360.
- [82] Munts, V. A., and Baskatov, A. P., 1983, "Mass Exchange in Carburization and Decarburization of Steel," *Metal Science and Heat Treatment (English Translation of Metallovedenie i Termicheskaya Obrabotka Metallov)*, **25**(1-2) pp. 98-102.
- [83] Wunning, J., 1968, "Advances in Gas Carburizing Technique," *Haerterei-Technische Mitteilungen*, **23**(3) pp. 101-109.
- [84] Moiseev, B. A., Brunzel, Y. M., and Shvartsman, L. A., 1979, "Kinetics of Carburizing in an Endothermal Atmosphere," *Metal Science and Heat Treatment (English Translation of Metallovedenie i Termicheskaya Obrabotka Metallov)*, **21**(5-6) pp. 437-442.
- [85] Goldstein, J. I., and Moren, A. E., 1978, "Diffusion Modeling of the Carburization Process," *Metallurgical and Materials Transactions A*, **9**(11) pp. 1515-1525.
- [86] Totten, G.E., and Howes, M.A.H., 1997, "Steel Heat Treatment Handbook," Marcell Dekker, Inc., New York, NY, .
- [87] Agren, J., 1986, "Revised Expression for the Diffusivity of Carbon in Binary Fe-C Austenite," *Scripta Metallurgica*, **20**(11) pp. 1507-1510.
- [88] Asimow, R. M., 1964, "Analysis of the Variation of the Diffusion Constant of Carbon in Austenite with Concentration," *Transactions of AIME*, **230**(3) pp. 611-613.

[89] Kula, P., 2005, "Vacuum Carburizing—process Optimization," *Journal of Materials Processing Technology*, **164**pp. 876-881.

CHAPTER III. PUBLICATIONS

This section summarizes the results for the theoretical work and experimental investigations. The section is structured as a collection of papers.

Paper #1: Nitrogen diluted ammonia atmosphere subcritical temperature nitriding on AISI 4140 steel: microstructure evolution, layer growth kinetics and cryogenic treatment (*to be submitted to Surface and Coatings Technology*)

Yingying Wei¹, Zbigniew Zurecki², Richard D. Sisson, Jr.¹

1. *Center for Heat Treating Excellence, Worcester Polytechnic Institute, Worcester, MA, USA*

2. *Metal Processing Center of Excellence, Merchant Gases, Air Products and Chemicals, Inc., Allentown, PA, USA*

Abstract

An alternative, subcritical-temperature austenitic nitriding process is evaluated in this paper with the purpose of accelerating the treatment cycle, optimizing the hardness gradient in nitrided layers and seeking improved process control. Comparing to the conventional nitriding processed at ferritic temperature and followed by slow cooling, the alternative process includes nitriding at elevated austenitic temperature in nitrogen-dilute ammonia atmospheres and cryogenic quenching in liquefied nitrogen. This paper presents results of experimental work on low alloy steel AISI 4140 in both ferritic (525 °C) and subcritical austenitic (610 °C) processes, to investigate the interplay between the nitriding and cooling conditions as well as phase transformations. Thermodynamic models were used to design the process conditions and assist in the microstructural interpretation of the nitrided layers produced. Results were verified using the SEM, EPMA, and microhardness measurements. It is observed that in subcritical temperature austenitic nitriding, nitrogen absorption rate is accelerated, a transitional nitrogen-austenite sublayer is formed between compound layer and diffusion zone, meanwhile, the hardness in diffusion zone increases with the cryogenic soaking time ranging from 1 hour to 48 hours, suggesting that more mechanisms are operational than the classic nitrogen martensitic

transformation. The kinetics of interstitial diffusion and layer growth in non-equilibrium gas nitriding atmosphere are also discussed.

1. Introduction

During recent decades, gas nitriding has become increasingly popular as a surface hardening method used in the steel processing industry. Conventionally, gas nitriding of low-alloy steels (ferritic-phase nitriding) takes place in the temperature range of 495-565 °C, shown as lower shading area in figure 1. Rapid quenching is not required, preventing large dimensional distortion which is normally produced by the classic, carbon austenite-martensite phase transformation. However, due to the limited nitrogen solubility in ferrite [1] and low diffusion rates at low process temperatures, the nitrogen hardened layer is relatively shallow, even for the treatments lasting many hours or days. Also, the nitrogen concentration rapidly decreases from the surface to the core which results in an undesired, sharp hardness and stress gradient. In this paper, a modified method is explored for accelerating nitriding treatment and optimizing the hardness distribution from the surface layers to the core. This method involves increasing the nitriding temperature to the sub-critical temperature: above the austenite transformation temperature in the system with nitrogen but below the eutectoid temperature in the system without nitrogen, shown as top shading area in figure 1, combined with quenching and further cooling to cryogenic temperatures. The core of the parts treated according to the evaluated method is expected to retain its original microstructure and properties, whereas the surface layer, due to the nitrogen stabilized austenite, may comprises the conventional, hard compound layer (γ' -Fe₄N/ ϵ -Fe₂₋₃N) and, an additional, somewhat softer transition layer of nitrogen-martensite with a possible fraction of retained nitrogen-austenite, as well as diffusion zone.

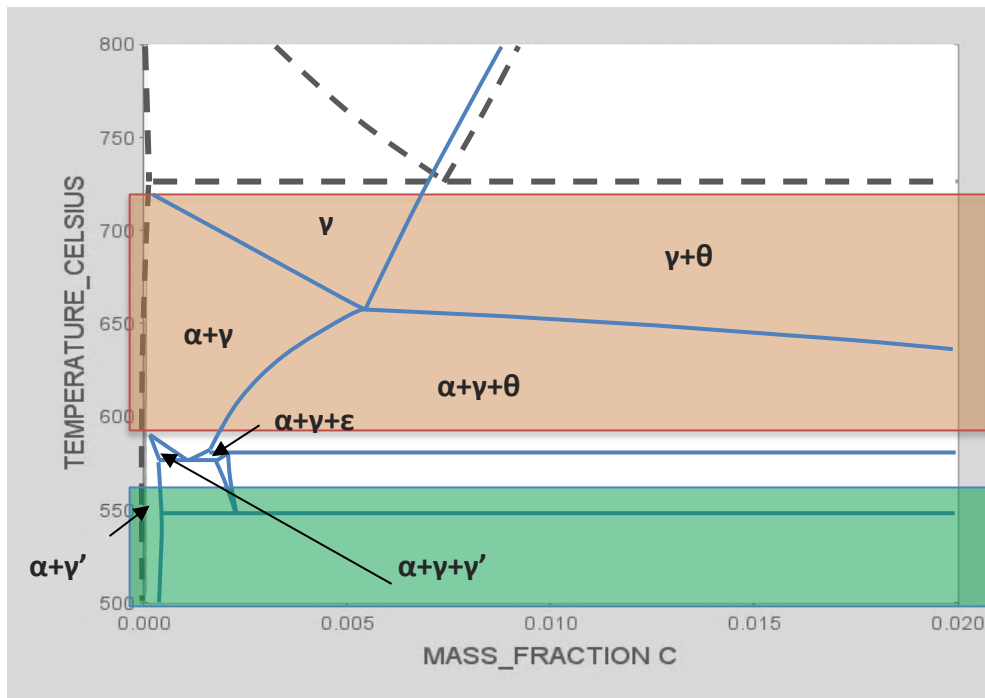


Figure 1 Temperature ranges for ferritic (bottom shade) and subcritical austenitic (top shade) nitriding. Dashed lines: Fe-C binary phase diagram; Solid lines: Fe-C isopleth with 1% nitrogen. α , γ , ϵ , θ , γ' are ferrite, austenite, Fe_{2-3}N , cementite and Fe_4N , respectively and indicate the phase regions of Fe-C isopleth with 1% nitrogen. generated by Thermo-Calc.

Fe-N austenite has been investigated by several authors. Fattah [2] compared corrosive properties of steel after plasma ferritic- and austenitic-nitriding followed with a slow cooling. Yasumaru [3] examined the effects of nitriding at three different temperatures and water quenching on pure iron. Most of microstructural evolution during aging and tempering of cryogenically quenched Fe-N martensite was analyzed using pure iron as the starting material [2, 4-6]. References published to date offer little on the physical metallurgy of Fe-N austenite formed in the popular industrial structural steels during the subcritical temperature nitriding and their transformation products in the subsequent cryogenic treatments. Thus, the further examination of this area is technologically justified.

This proposed method utilizes nitrogen diluted ammonia instead of traditional pure ammonia or partially dissociated ammonia, from the economic and ecological point of view. Diluting ammonia with second component in the atmosphere came into use about 50-60 years ago [7, 8]. The utility of nitrogen gas is due to its cheaper cost compare to ammonia and removal of ammonia dissociator. However, the utilization and atmosphere control is seldom investigated, a few of which are conducted by Sorokin [7], Maldzinski [9] and Michalski [10].

The purpose of cryogenic quenching and soaking in liquid nitrogen (LIN) is to promote the transformation of the nitrogen-formed austenite into nitrogen-formed martensite. Considering the martensite transformation starting point (Ms), nitrogen stabilizes austenite more effectively than carbon. Reference [5] reported Ms to be only 120K for Fe-2.75 wt.%N alloy. When nitrogen content exceeds about 2.2 wt.%, the N-austenite is stable at room temperature due to its Ms point located below the room temperature [3, 11]. In this view, a post-nitriding treatment involving cryogenic quenching and soaking appears to be advisable for transforming austenite to martensite.

2. Experimental procedures

AISI 4140 steel, characterized by high hardenability, was selected as the test materials. The composition of 4140 is listed in table 1.

Table 1 Composition of Low-alloy Steel Tested

		C	Cr	Fe	Mn	Mo	P	S	Si
AISI 4140	minimum	0.38	0.8	Bal.	0.75	0.15	0	0	0.15
	maximum	0.43	1.1	Bal.	1	0.25	0.035	0.04	0.35

Material was processed in the sequence illustrated in figure 2: normalizing, rough machining, austenitizing, oil and LIN quenching, tempering and oil quenching, finish machining, nitriding, and finish cooling of nitrided samples in three different ways. Ferritic nitriding (FN) at 525 °C and austenitic nitriding (AN) at 610 °C lasted 4 hours in N₂-diluted 25% NH₃ atmosphere. The three finish cooling paths examined were: (a) slow

cooling inside furnace, (b) fast cooling in liquid nitrogen bath (-195°C) and holding for 1 hour (LIN 1 hr), as well as (c) fast cooling in liquid nitrogen combined with holding for 48 hours (LIN 48 hrs). Figure 3 shows the atmosphere nitriding apparatus used.

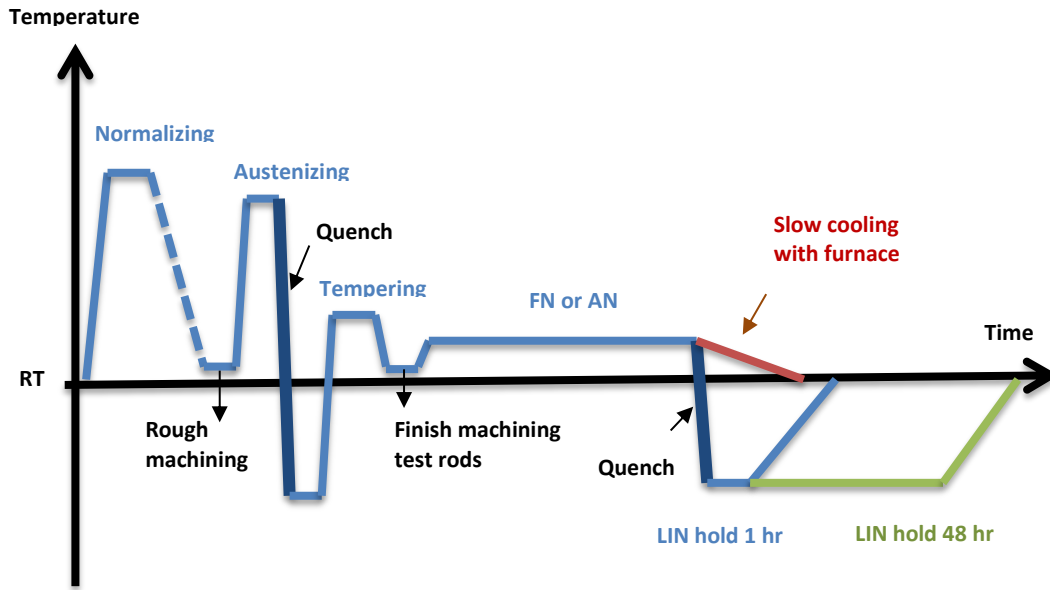


Figure 2 Thermal processing sequences

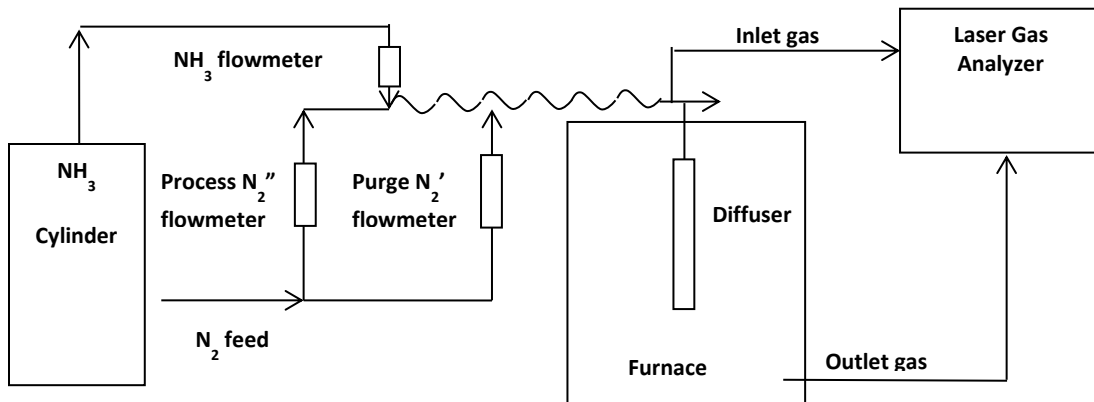


Figure 3 Atmosphere nitriding apparatus

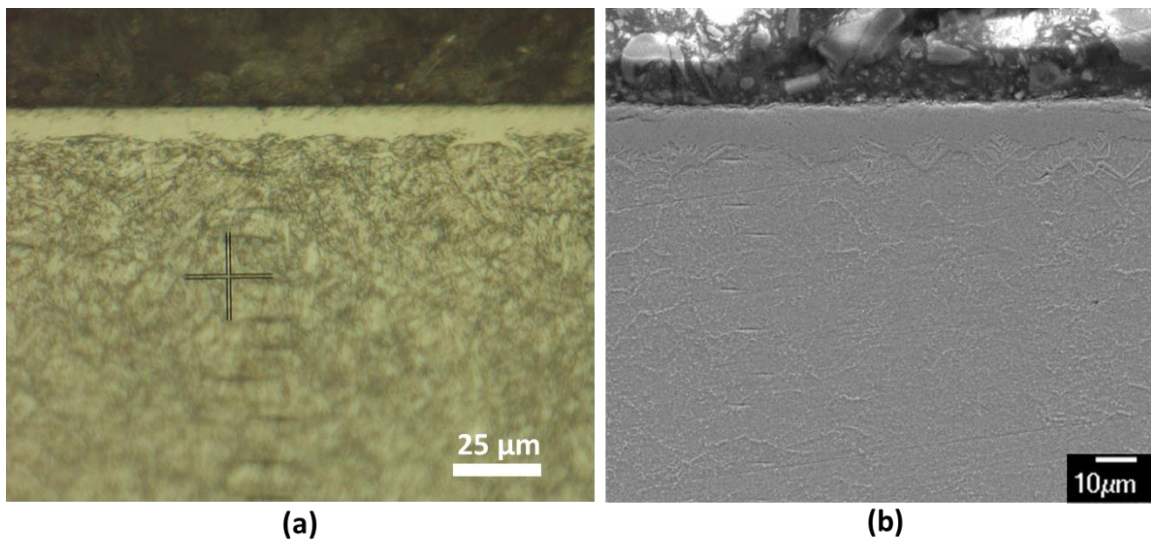
Three different configurations of samples were used: (1) a rod shape to measure dimensional change after nitriding, (2) a disk shape for evaluating microstructure and

hardness, and (3) flat thin coupons to measure weight gain after nitriding. Nitrided disks were etched in 2% Nital. OM ZEISS IM35, SEM JEOL JSM-7000F, Oxford energy dispersive x-ray spectroscopy and JEOL Superprobe JXA-8900R were used for microstructure and concentration profile analysis, while microhardness profiling was carried out on Shimadzu HMV-2000. The dimensional stability of liquid nitrogen quenched and soaked components has been reported in reference [12].

3. Results

1.1 Microstructure and nitrogen concentration profile

Figure 4 shows the optical and SEM micrographs of samples processed along three different paths. After the conventional ferritic nitriding (figure 4(a) and (b)), the hardened case is composed of compound layer and diffusion zone. The austenitic nitriding results in three layers (figure 4(c) to 4(f)), the top, “white” or compound nitride layer, the middle transition layer, that appears dark on the samples cooled with the furnace but bright on the samples quenched in liquid nitrogen, and the inner diffusion zone. The white layer thickness increases from 10 μm to 30 μm as the nitriding temperature is increased from the ferritic to the austenitic range, indicating that the nitrogen flux into the metal core is larger due to the larger diffusion rate at elevated temperature.



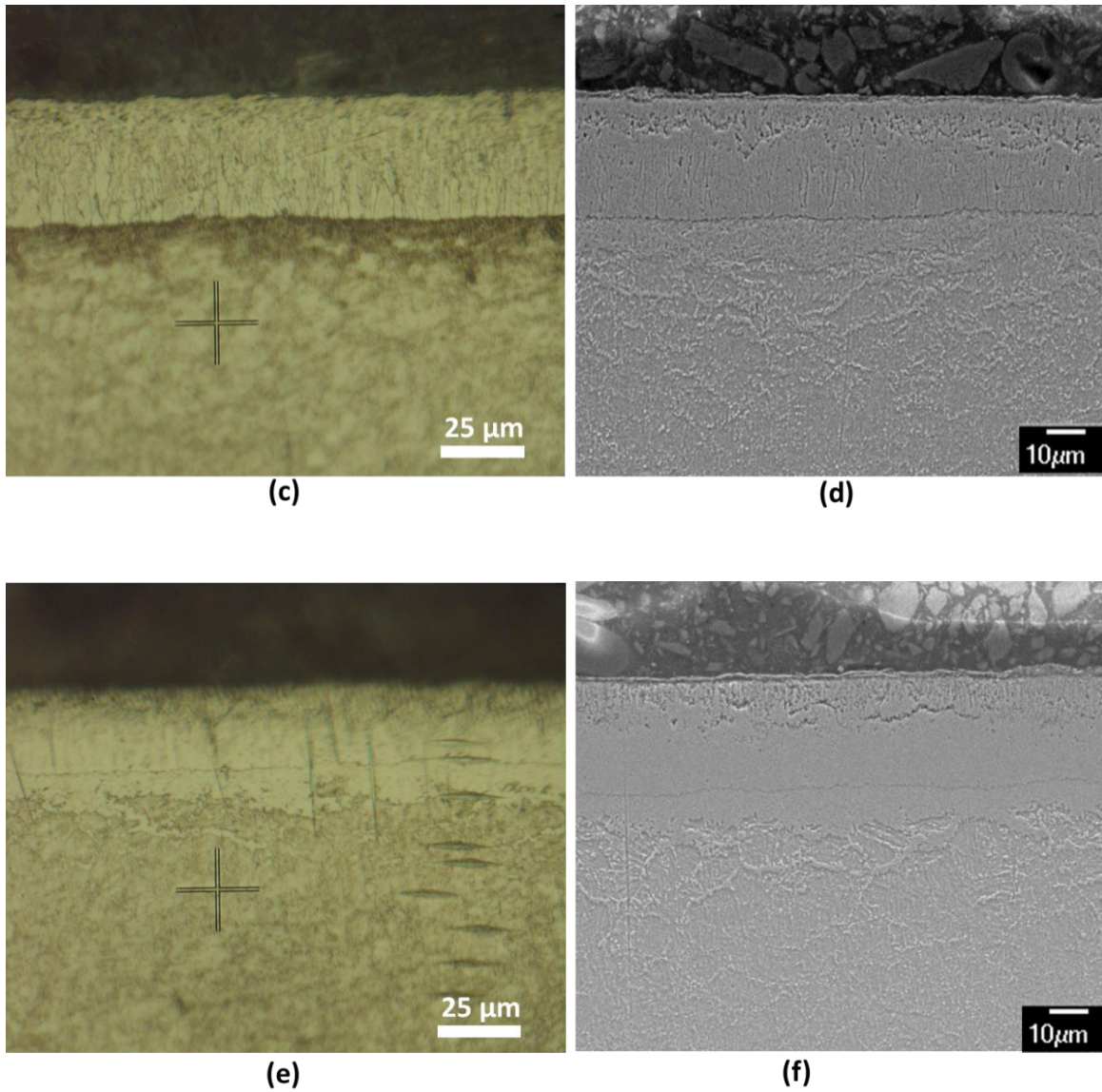


Figure 4: Optical and secondary images of cross sections of ferritic and austenitic nitrided samples. (a and b): Ferritic nitriding and cooling with furnace. (c and d): Austenitic nitriding and cooling with furnace. (e and f): Austenitic nitriding and LIN soaking 1 hr. Etched in 2% Nital.

The nitrogen concentration profiles for the FN and AN, both concluded with the slow furnace cooling, as well as the profiles for AN then quenched and soaked in LIN for 1 hour are presented in figure 5. As expected, the nitrogen profiles of AN samples are significantly broader than for the FN treatment.

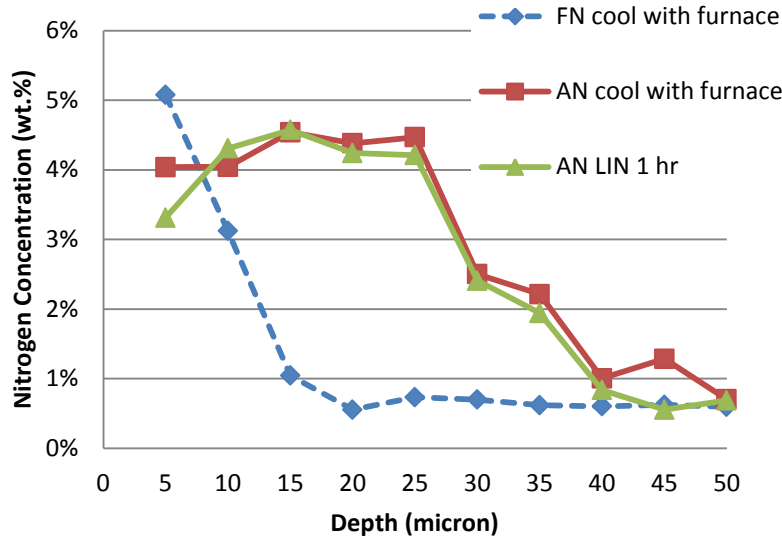


Figure 5 Nitrogen concentration profiles for ferritic nitriding (FN) and cooling with furnace, austenitic nitriding (AN) and cooling with furnace, as well as austenitic nitriding (AN) and quenched in LIN bath;

Figure 6 illustrates that three major phases dominates three layers respectively at 610°C. The outmost white layer, whose concentration is between 4 wt.%-4.5 wt.%, comprises of mostly ϵ and minor austenite. The transition layer, the second layer seen in figure 4 (c-f), whose concentration is from 2 wt.%-2.3 wt.% dominated by N-austenite. Figure 4 and 5 confirms that the cooling method has an insignificant effect on redistribution of nitrogen concentration. But microstructure of transition layer is modified by cooling rates. Appearing darker after etching in figure 4(c) (slow cooling) and brighter in 4(e) (fast cooling), the transition layer responds to the cooling rate change by replacing equilibrium-favored braunite [13] with a more etch-resistant N-austenite. Due to decreased M_s temperature by nitrogen atoms, after cooling in liquid nitrogen and short storage time, the austenite stabilized. The dark transition layers were reported to comprise ferrite, ϵ and γ' [2] based on XRD examination.

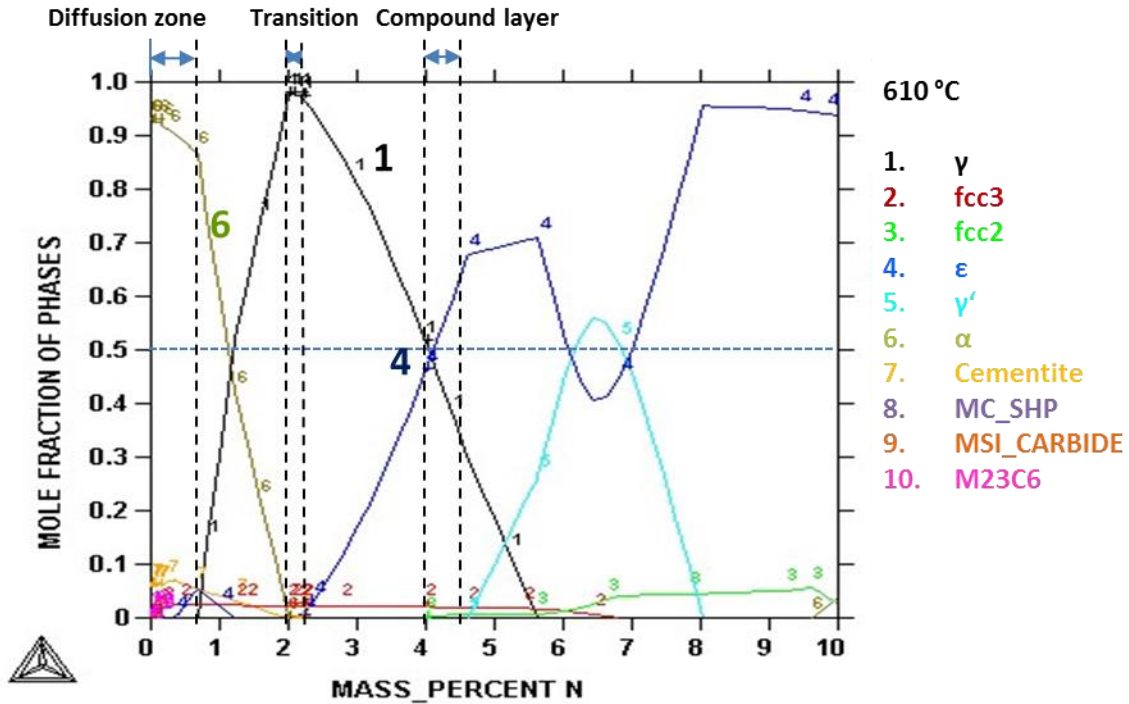


Figure 6 Mole fraction of phases vs. mass percent of nitrogen at 610°C, generated by Thermo-Calc.

1.2 Hardness profiles

Effect of finish-cooling methods on microhardness profiles is presented in figure 7 for the three AN disks: (a) slow cooled with furnace, (b) fast cooled in LIN bath and held there (soaked) for 1 hour, as well as (c) fast cooled in LIN and soaked for 48 hours. Typically, hardness within diffusion zones is higher for the LIN quenched and soaked samples, and the effect scales with the soaking time indicates that, apart from the expected athermal martensitic transformation, an isothermal martensitic transformation [14-16] or age-hardening may be operating. The low hardness between the surface and inner core peak is due to the austenite stabilization. The more nitrogen atoms, the harder the martensitic transformation, thus when nitrogen concentration decreases, with prolonged time, austenite starts to transform into martensite and increases the hardness at inner core part. Therefore, due to the isothermal martensitic transformation, it is expected that the desired continuous hardness profile could be achieved with longer soaking time in liquid nitrogen.

A more detailed transmission electron microscopy will be required to interpret the data. Although the subject falls outside the scope of the present study, it should be mentioned that a large number of references exist on so-called “deep” or multi-hour cryogenic soaking treatments of martensitic steels, producing significant improvements of wear resistance while displaying only a mild increase in hardness. This effect has been attributed to the precipitation of submicron carbides taking place during LIN bath soaking [17].

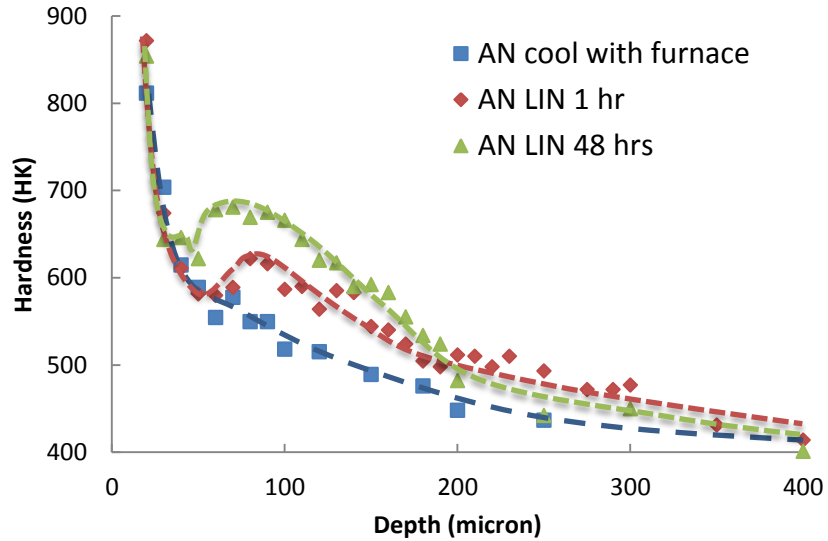


Figure 7 Hardness profiles of austenitic nitrated samples

1.3 Nitrogen flux

Although frequently overlooked, nitrogen flux control is important for optimizing nitriding parameters. Table 2 presents the flux values measured from weight gain of thin coupons and calculated from concentration profiles in figure 5. The following equations are used in which: J – flux, t – time, A – surface area, and $C(x)$ – concentration at depth x .

$$J = \frac{\text{weight gain}}{A \cdot t} \quad 27$$

$$J = \frac{\int_0^{x=C_0} f(x)}{A \cdot t} \quad 28$$

A reasonable agreement between the results of the two methods indicates their potential parity in the industrial practice. Of note, the AN treatment brings about a 2.5-times higher nitrogen uptake than the conventional FN treatment which confirms the starting assumptions.

Table 2 Average Nitrogen Flux for 4 Hour Nitriding at 525°C (FN) and 610°C (AN)

	Weight gain (g)	Flux (g/cm ² /s) from wt. gain	Flux (g/cm ² /s) from conc. profile
FN	1.89E-02	5.75E-08	8.69E-08
AN	4.80E-02	1.06E-07	1.50E-07

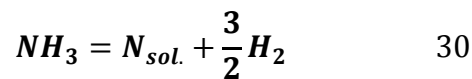
4. Discussion

4.1 Nitrogen diluted ammonia atmosphere

Nitriding potential is defined by

$$K_N = \frac{P_{NH_3}}{P_{H_2}^{1.5}} \quad 29$$

out of nitriding reaction



giving the equilibrium constant

$$K = a_N \frac{P_{H_2}^{1.5}}{P_{NH_3}} \quad 31$$

nitrogen activity is

$$a_N = K \cdot K_N \quad 32$$

In the atmosphere of molecule nitrogen diluted ammonia, nitrogen acts in counter effects [9]. The presence of nitrogen lowers the partial pressure of NH₃ and H₂ simultaneous thus increases nitriding potential, however, the dilution for the whole reaction acts like

pressure reduction, thus based on Le Chatelier's rule, it promotes the equilibrium to the dissociation side, thus reduces nitriding potential. In general, the dilution of ammonia increases the nitriding potential, as shown in figure 8, however, the nitrogen availability at metal surface is reduced. Therefore, the process for this kind of atmosphere is not only controlled by nitriding potential, nitrogen availability as well should be taken into account. The same investigation has been reported by Michalski [10] and Zimadars [18]. In nitrogen diluted ammonia atmosphere, nitriding potential is not able to unequivocally describe the boundary condition of the process. The utilization of nitrogen availability as a parameter creates more possibility for atmosphere controlling [10]. The investigation in reference [18] claimed in the nitrogen oxinitriding atmosphere, the layer growth rate depends on ammonia percentage in the process gas.

In reference [19], nitrogen availability of the nitriding atmosphere (m_{N_2}) ties the ammonia dissociation rate (α) with the flow rate of the input atmosphere (F_{in}) liters/minute in by the equation

$$m_{N_2} = \frac{F_{in} \alpha}{1.62 - \alpha} \quad 33$$

In this study, nitrogen flux has been calculated in table 2 as nitrogen availability using weight gain measurements and integration of nitrogen concentration profiles.

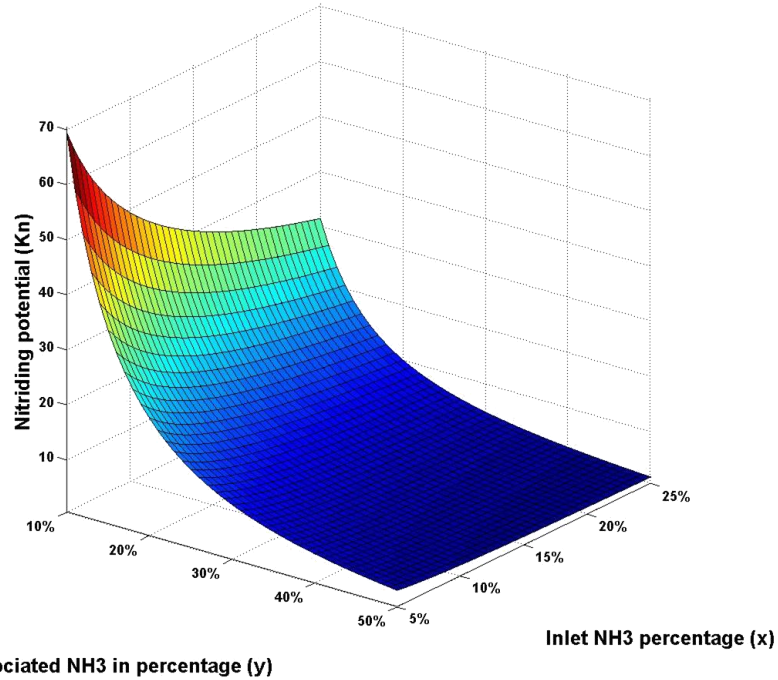


Figure 8 Diagram for nitriding potential K_N as a function of inlet NH_3 percentage x and NH_3 dissociate rate y .

In figure 9, the decreasing of nitriding potential is shown during the process, the average of the nitriding process is about 1.8, correlating to the diagram in figure 10 which is showing the relationship between nitriding potential and surface nitrogen concentration, the corresponding surface concentration is located at 9 wt.%. However, the measured surface nitrogen concentration is between 4%-4.5%, which indicates that the equilibrium between nitriding atmosphere and metal surface may not be reached yet at the period of this study. Even though generally, the nitrogen content in the compound layer close to the surface is significantly lower than the content corresponding to local equilibrium with the imposed nitriding potential, attributed to the competition between the relative slow kinetics of ammonia dissociation, the desorption of molecular nitrogen gas from the surface and solid state diffusion into bulk metal [20, 21], the intrinsic non-equilibrium character of nitrogen diluted ammonia atmosphere [9] makes the surface equilibrium hard to achieve.

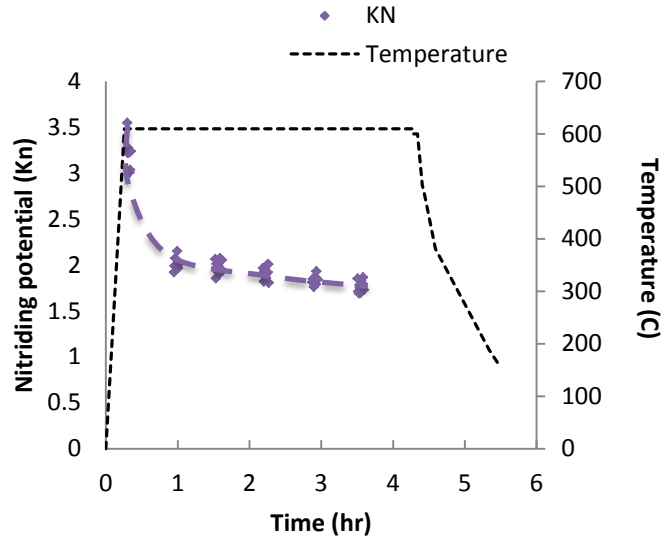


Figure 9 Measured nitriding potential and temperature during the AN process.

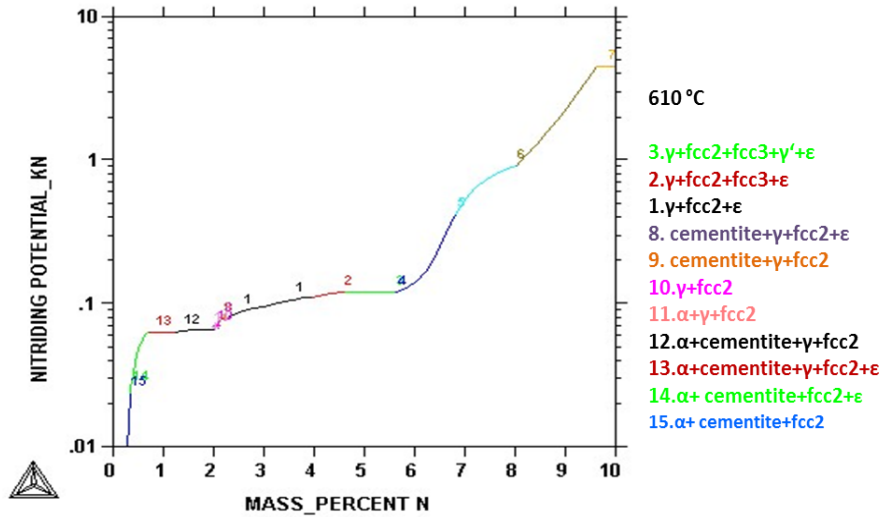


Figure 10 Diagram of nitriding potential as a function of nitrogen mass concentration, generated by ThermCalc.

4.2 Kinetics of layers growth

The diffusion controlled layer growth kinetics is express as parabolic relationship,

$$x_i = k_i \sqrt{t} \quad 34$$

x_i is the thickness of i phase layer, k_i is the growth rate constant of i and t is the time.

If local equilibrium prevails all phase interfaces and between nitriding medium and metal surface under isothermal condition, the horizontal lines in figure 10 are interfaces between different layers, since nitriding potential is projected by nitrogen activity (equation 6). The surface concentration and concentration at both sides of interfaces can be determined.

As mentioned earlier the surface equilibrium is not achieved, thus to control the thickness of each layer and determine the equilibrium state at interfaces, more experiments are needed under the same atmosphere but with different processing time. However, if local-equilibrium has been assumed at solid/solid interfaces in the cases of AN samples, the nitrogen concentration at the front end of each layer is fixed during the process. Once quasi-equilibrium [21] is built up in the system, the nitrogen activity on both sides of interfaces are equal, therefore the boundary conditions at each interface are accessible from nitrogen concentration profile, as shown in figure 11.

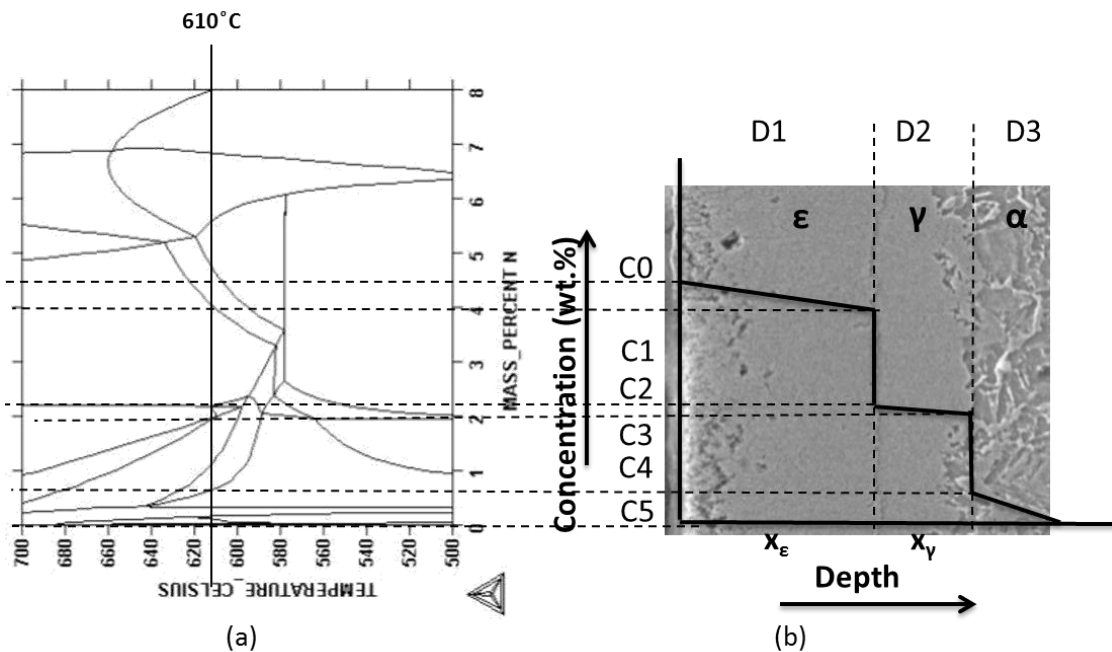


Figure 11 Fe-N isopleth (a); and concentration/depth diagram for growth of nitride layers imposed with SEM image for AN LIN 1hr sample (b).

Measured nitrogen flux can be utilized as solid/gas interface boundary condition. The analytic solution for diffusion in steel with flux boundary condition is not available, therefore the governing Fick's second law need to be solved by a set of finite difference equations. For planar geometry and one dimensional diffusion problem, the following equation [22] can be used:

$$C_i^{t+\Delta t} = \frac{\Delta t}{(\Delta x)^2} \left[D_{\varepsilon i}^t \left(C_{i-1}^t - 2C_i^t \left(\frac{(\Delta x)^2}{D_{\varepsilon i}^t \Delta t} - 2 \right) + C_{i+1}^t \right) + \frac{(D_{\varepsilon(i+1)}^t - D_{\varepsilon(i-1)}^t)(C_{i+1}^t - C_{i-1}^t)}{4} \right] \quad 35$$

Where C and $D\varepsilon$ are carbon concentration and diffusion coefficient in ε , corresponding to particular location (node i) and time t , respectively. Δx is space increment between the nodes, and Δt is time increment.

When $C = C1$, the corresponding x is the desired x_ε shown in figure 11(b).

The kinetics of layers growth can be determined by migration of interface.

$$v^{\gamma/\alpha} = \frac{J^\gamma - J^\alpha}{C3 - C4} = \frac{1}{(C3 - C4)} \left[D_\alpha \left(\frac{\partial C^\alpha}{\partial x} \right) - D_\gamma \left(\frac{\partial C^\gamma}{\partial x} \right) \right] \quad 36$$

Since the interfaces are assumed to be local equilibrium, the austenite layer follows the parabolic growth using equation 8. Kirkaldy's solution [23] of Fick's partial derivative equation is utilized.

$$C^\gamma(y, t) = A^\gamma + B^\gamma \operatorname{erf} \left(\frac{y}{2\sqrt{D_\gamma t}} \right) \quad 37$$

$$C^\alpha(y, t) = A^\alpha - B^\alpha \operatorname{erfc} \left(\frac{y}{2\sqrt{D_\alpha t}} \right) \quad 38$$

where y is the depth below ε layer.

At quasi-equilibrium state, the constant concentrations at ε/γ and γ/α interfaces under isothermal condition are applied. A_γ , B_γ , A_α , B_α are determined by these boundary conditions,

$$C^\gamma(0, t) = C2 \quad 39$$

$$C^\gamma(x_\gamma, t) = C3 \quad 40$$

$$C^\alpha(x_\gamma, t) = C4 \quad 41$$

$$C^\alpha(\infty, t) = C5 \quad 42$$

Then the above error functions can be derived as

$$C^\gamma(y, t) = C2 + (C3 - C2) \frac{\operatorname{erf}\left(\frac{y}{2\sqrt{D_\gamma t}}\right)}{\operatorname{erf}\left(\frac{k}{2\sqrt{D_\gamma t}}\right)} \quad 43$$

$$C^\alpha(y, t) = C5 - (C5 - C4) \frac{\operatorname{erfc}\left(\frac{y}{2\sqrt{D_\alpha t}}\right)}{\operatorname{erfc}\left(\frac{k}{2\sqrt{D_\alpha t}}\right)} \quad 44$$

Apply equation 8, 14 and 15 to equation 17-18,

The migration rate of γ/α interface can be written as

$$v_{\gamma/\alpha} = \frac{dx_\gamma}{dt} = \frac{x_\gamma}{2} \frac{1}{\sqrt{t}} = \frac{1}{C3 - C4} \left[\frac{\sqrt{D_\alpha} (C5 - C4) \exp\left(-\frac{k_\gamma^2}{4D_\alpha}\right)}{\sqrt{\pi t} \operatorname{erfc}\left(\frac{k_\gamma}{2\sqrt{D_\alpha}}\right)} - \frac{\sqrt{D_\gamma} (C3 - C2) \exp\left(-\frac{k_\gamma^2}{4D_\gamma}\right)}{\sqrt{\pi t} \operatorname{erfc}\left(\frac{k_\gamma}{2\sqrt{D_\gamma}}\right)} \right] \quad 45$$

The flux balance at γ/α interface is

$$\frac{x_\gamma}{2} = \frac{1}{C3 - C4} \left[\frac{\sqrt{D_\alpha} (C5 - C4) \exp\left(-\frac{k_\gamma^2}{4D_\alpha}\right)}{\sqrt{\pi} \operatorname{erfc}\left(\frac{k_\gamma}{2\sqrt{D_\alpha}}\right)} - \frac{\sqrt{D_\gamma} (C3 - C2) \exp\left(-\frac{k_\gamma^2}{4D_\gamma}\right)}{\sqrt{\pi} \operatorname{erfc}\left(\frac{k_\gamma}{2\sqrt{D_\gamma}}\right)} \right] \quad 46$$

If two of three major parameters, diffusion coefficients, growth rate constant of each layer, and the depth of austenite layer are measured, the other parameter can be solved from above interface flux balance equation. Further experiments carried out under the same processing condition but with different times are needed to validate the proposed model.

It is noted that the thickness of compound layer is much thicker than the middle sublayer, this is due to the larger nitrogen diffusivity in ε [24] than in γ [25] as well as larger homogeneity range of ε than γ , resulting in larger nitrogen flux in ε . Meanwhile, it is

illustrated that the thickness of austenite layer is following parabolic growth, however, the top compound layer is determined by the nitrogen flux from atmosphere to metal surface. If the nitrogen flux from atmosphere is excessive, it does not take the part in the growth kinetics of inner layers, the growth of compound layer would exceed to the growth of austenite layer and diffusion zone. Therefore, to control the layer thickness by control of nitrogen flux in each layer, boost and diffuse scheme analogue to that in low pressure carburizing can be employed.

5. Conclusion

At subcritical temperature, the gas nitriding of low-alloy AISI 4140 steel in nitrogen diluted ammonia atmosphere increases the rate of nitrogen absorption from nitriding atmosphere 2.5 times and the thickness of nitrided case from 10 micron to 40 micron as compared to the conventional ferritic nitriding. A transitional, nitrogen-austenite sublayer forms between the conventional, hard compound layer and soft diffusion zone during the subcritical austenitic nitriding.

The local equilibrium between nitriding medium and metal load surface has not built up yet during the period in this experiment. The intrinsic character of nitrogen diluted ammonia atmosphere makes nitriding potential not sufficiently represents the nitriding capability. Therefore, if quasi-equilibrium (the local equilibrium only at solid interfaces) is assume in the system, the layer growth kinetics can be controlled by the nitrogen flux from the atmosphere into metal surface and the interfaces migration. Based on parabolic growth of diffusion controlled layers, a mathematic model has been derived. Once two of three major components, diffusion coefficient, growth rate constant and layer depth, are measured, the other one is accessible from the mathematical calculation. The excessive nitrogen atoms constitute to the growth of top compound layer, as suggested, boost and diffuse conditions are beneficial to control the thickness of each layer.

Liquid nitrogen quenching and soaking increases the hardness of the diffusion layers in the subcritically nitrided steel. Due to the nitrogen stabilized retained austenite, the hardness peak appears at inner part of diffusion zone. The hardness increase is

proportional to the soaking time suggesting cryogenic aging and isothermal martensitic transformation as the operating mechanisms.

Future work should examine phases present in the transition layer after cryogenic soaking, evaluate wear and mechanical properties of subcritically nitrided components, determine the experimental equilibrium state then correlate it with thermodynamic predictions, and validate the proposed model.

Acknowledgements

This work has been financed and administrated by Air Products and Chemicals, Inc. The authors would like to thank Mr. John Green of Air Products for the help in experimentation. The continuous support from Center for Heat Treating Excellence at Worcester Polytechnic Institute and Thermo-Calc Software are gratefully acknowledged.

References

- [1] N.I. Kardonina, A.S. Yurovskikh and A. S. Kolpakov, 2011, "Transformations in the Fe – N System," *Metal Science and Heat Treatment*, **52**(9) pp. 457-467.
- [2] M. Fattah, F. M., 2010, "Comparison of Ferritic and Austenitic Plasma Nitriding and Nitrocarburizing Behavior of AISI 4140 Low Alloy Steel," *Materials & Design*, **31**(8) pp. 3915-3921.
- [3] Yasumaru, N., 1992, "Formation of Austenite and Martensite in Surface Layer of Pure Iron with Ion Nitriding," *Materials Transactions, JIM*, **33**(1) pp. 7-10.
- [4] M.J. Van Genderen, A. Böttger and E.J. Mittemeijer, 1997, "Formation of A " Iron Nitride in FeN Martensite: Nitrogen Vacancies, Iron-Atom Displacements, and Misfit-Strain Energy," *Metallurgical and Materials Transactions.A, Physical Metallurgy and Materials Science*, **28**(1) pp. 63-77.

- [5] V.G. Gavdijuk, V.M. Nadutov and K. Ullakko, 1991, "Low Temperature Ageing of Fe-N Martensite," *Scripta Metallurgica Et Materialia*, **25**(4) pp. 905-910.
- [6] Gavriljuk, V. G., 2006, "Austenite and Martensite in Nitrogen-, Carbon- and Hydrogen-Containing Iron Alloys: Similarities and Differences," *Materials Science & Engineering, A, Structural Materials : Properties, Microstructure and Processing*, **438-440**pp. 75-79.
- [7] Sorokin, Y. V., and Minkevich, A. N., 1966, "Nitriding Steel in a Mixture of Nitrogen and Ammonia," *MiTOM*, **5**pp. 49-52.
- [8] Minkevich, A. N., 1965, "Thermochemical Treatment of Metals and Alloys," *Mashinostroenie*, pp. 331.
- [9] Maldzinski, L., and Tacikowski, J., 2006, "Concept of an Economical and Ecological Process of Gas Nitriding of Steel," *Journal of Heat Treatment and Materials*, **61**(6) pp. 1-7.
- [10] Michalski, J., 2012, "Using Nitrogen Availability as a Nitriding Process Parameter," *Industrial Heating*.
- [11] Bell, T., 1968, "Martensite Transformation Start Temperature in Iron-Nitrogen Alloys," *The Journal of the Iron and Steel Institute*, **206**(10) pp. 1017-1021.
- [12] Wei, Y., Zurecki, Z., and Sisson Jr., R. D., 2012, "Thermodynamic model-assisted evaluation of phase transformations in subcritical austenitic nitriding," *Materials Science and Technology (MS&T) 2012. Pittsburgh, PA*, pp. 180.

- [13] Totten, G.E., 2006, "Steel heat treatment handbook. 2nd edition," Taylor and Francis Group, UK, .
- [14] Laughlin, D. E., and et al., 2008, "Thermally activated martensite: its relationship to non-thermally activated (athermal) martensite," ICOMAT 2008, Santa Fe, USA, .
- [15] Lobodyuk, V. A., and Estrin, E. I., 2005, "Isothermal Martensitic Transformations," Physics-Uspekhi, **48**(7) pp. 713-732.
- [16] Zhao, J. C., and Notis, M. R., 1995, "Continuous Cooling Transformation Kinetics Versus Isothermal Transformation Kinetics of Steels: A Phenomenological Rationalization of Experimental Observations," Materials Science and Engineering, **R15**pp. 135-208.
- [17] Das, D., and et al, 2009, "Influence of Varied Cryotreatment on the Wear Behavior of AISI D2 Steel," Wear, **266**pp. 297-309.
- [18] Zimdars, H., 1987, "Technologische Grundlagen Fur Die Erzeugung Nitridhaltiger Schichten in stickstoffangereicherten Nitrieratmosphären," Dissertation Bergakademie Freiberg, pp. 37-39.
- [19] Michalski, J., 2011, "Characteristics and calculations of atmospheres for controlled gas nitriding of steel," Instytut Mechaniki Precyzyjnej, Warszawa, .
- [20] Somers, M. A. J., and Christiansen, T., 2005, "Kinetics of Microstructure Evolution during Gaseous Thermochemical Surface Treatment," Journal of Phase Equilibria and Diffusion, **26**(5) pp. 520-528.

- [21] Ratajski, J., 2004, "Model of Growth Kinetics of Nitrided Layer in the Binary Fe-N System," International Journal of Materials Research and Advanced Techniques (Z. Metallkd.), **95**(9) pp. 823-828.
- [22] Karabelchtchikova, O., 2007, "Fundamentals of Mass Transfer in Gas Carburizing," Dissertation, Worcester Polytechnic Institute.
- [23] Kirkaldy, J. S., 1958, "Diffusion in Multicomponent Metallic System: I. Phenomenological Theory for Substitutional Solid Solution Alloys," Canadian Journal of Physicals, **36**(7) pp. 899-906.
- [24] Sun, Y., and Bell, T., 1997, "Computer Prediction of Threshold Nitriding Potential Curves," Heat Treatment of Metals, **24**pp. 43-49.
- [25] Straumal, B. B., Vershinin, N. F., Friesel, M., 2001, "Ionic Nitriding of Austenitic and Ferritic Steel with the Aid of a High Aperture Hall Current Accelerator," Defect and Diffusion Forum, **194-199**pp. 1457-1462.

Paper #2: Subcritical temperature austenitic nitriding and cryogenic treatment on low alloy steel (*published in Proceedings of Materials Science and Technology (MS&T) 2012, Pittsburgh, PA, October, 2012*)

¹Y. Wei, ²Z. Zurecki, ¹R.D. Sisson, Jr.

¹Center for Heat Treating Excellence, Worcester Polytechnic Institute, Worcester, MA, USA

²Metals Processing Center of Excellence, Air Products & Chemicals, Inc., Allentown, PA, USA

Key words: austenitic nitriding, subcritical temperature, thermodynamics, cryogenic, simulation

Abstract

Conventional nitriding of low-alloy steels is a multi-hour surface hardening process carried out at ferritic temperatures and concluding a complete heat treatment cycle: normalizing, austenitizing, martensitic quenching and tempering. An alternative, subcritical-temperature austenitic nitriding process is evaluated with the purpose of accelerating the treatment and optimizing the hardness and toughness of nitrided layers while minimizing the distortion of steel parts treated. The alternative process involves cryogenic nitrogen quenching as well as aging. This paper presents results of experimental work on AISI 4140 steels, examining the interplay between the nitriding and cooling conditions and phase transformations in both ferritic (525°C) and subcritical, nitrogen-austenitic (610°C) processes. Thermodynamic models, used to design process conditions, are applied also in the microstructural interpretation of nitrided layers, examined via SEM, EPMA and EDS. Kinetics of interstitial diffusion and phase transformation-based dimensional control of nitrided parts are also presented.

2. Introduction

During the recent decades, gas nitriding has become increasingly popular as a surface hardening method used in the steel processing industry. Conventionally, gas nitriding of

low-alloy steels (ferritic-phase nitriding) takes place in the temperature range of 495-565 °C, shown as lower shading area in Figure 1. Rapid quenching is not required, and this prevents large dimensional distortions, normally produced by the classic, carbon austenite-to-martensite phase transformation. However, due to the limited nitrogen solubility in ferrite [1] and low diffusion rates at low process temperatures, the nitrogen hardened layer is relatively shallow, even for the treatments lasting many hours or days. Also, the nitrogen concentration rapidly decreases from the surface to the core which results in an undesired, sharp hardness and stress gradient. In this paper, a modified method is explored for accelerating nitriding treatment and optimizing the hardness and toughness of the core and the surface layers, while assuring minimum distortion of the parts treated. The method involves increasing the nitriding temperature to the sub-critical temperature: above the eutectoidal transformation temperature in the Fe-N system but below the corresponding temperature in the Fe-C system, shown as top shading area in Figure 1, combined with quenching and further cooling to cryogenic temperatures. The purpose of the latter is to promote the transformation of the nitrogen-formed austenite into nitrogen-formed martensite. The core of the parts treated according to the evaluated method is expected to retain its original microstructure and properties, whereas the surface layer may comprise the conventional, hard compound layer (γ' -Fe₄N and ϵ -Fe₂₋₃N) and, an additional, somewhat softer transition layer of N-martensite with a possible fraction of retained N-austenite. This work aims at verifying if the described method can reduce typically sharp hardness and stress gradients between the compound layer and the core without causing part distortion. Fe-N austenite has been investigated by several authors. Fattah [2] compared corrosion of steel after plasma ferritic- and austenitic-nitriding followed with a slow cooling. Yasumaru [3] examined the effects of nitriding at three different temperatures and water quenching on pure iron. Microstructural evolution during aging and tempering of cryogenically quenched Fe-N martensite was analyzed using elemental, carbon-free iron as the starting material [2, 4-6]. There is debate [7-9] on the nitrogen and carbon precipitation in the Fe-C-N martensite during aging and tempering, however only Cheng [10] reported on tempering of low-alloyed steel and transformation of FeNiN martensite. Considering the martensite transformation starting point (Ms), nitrogen stabilizes austenite more effectively than carbon. Reference [5]

reported Ms to be only 120K for Fe-2.75 wt.%N alloy. When nitrogen content exceeds 2.2 wt.%, the N-austenite is stable at room temperature due to its Ms point located below the room temperature [3]. Bell [11] proposed the relationship between Ms and N-concentration as $M_s (\text{ }^\circ\text{C}) = 533 - 228NC$ (wt.%). In this view, a post-nitriding treatment involving cryogenic soaking appears to be advisable for transforming austenite to martensite. References published to date offer little on the physical metallurgy of Fe-N and Fe-N-C austenite formed in the popular structural steels during the subcritical temperature nitriding and their transformation products in the subsequent thermal treatments. Thus, the further examination of this area is technologically justified.

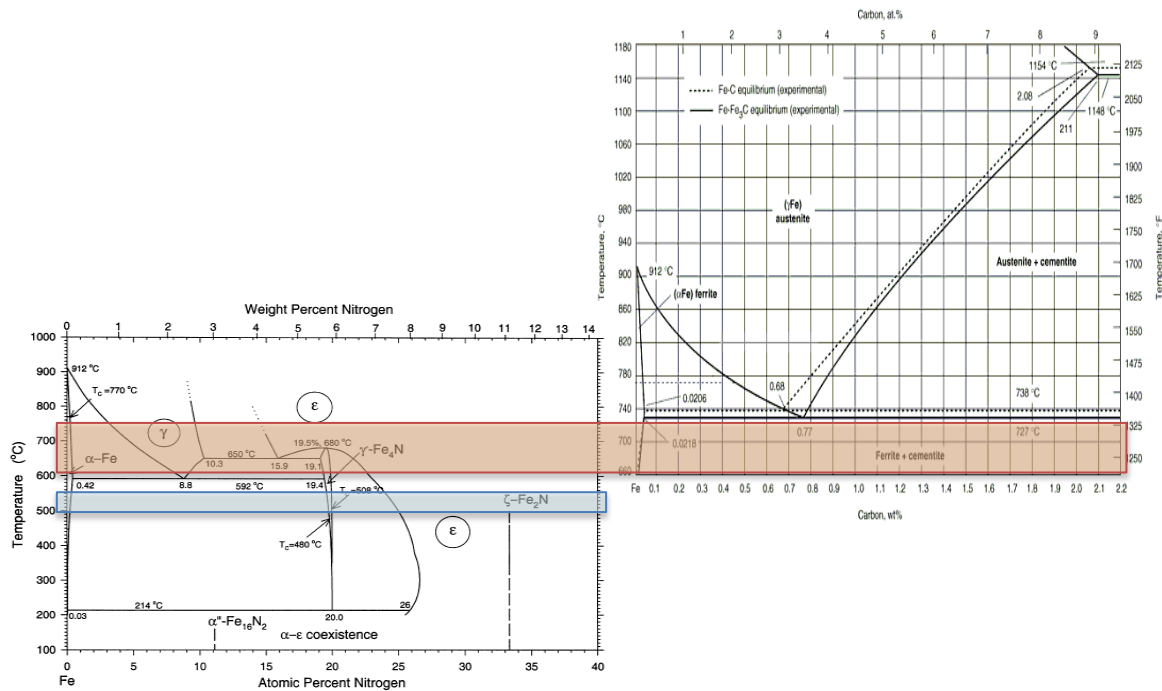


Fig. 1: Temperature ranges for ferritic and subcritical austenitic nitriding

3. Experimental

AISI 4140 steel, characterized by high hardenability, was selected as the test materials. The composition of 4140 is listed in Table I.

Table I: Composition of Low-alloy Steel Tested

		C	Cr	Fe	Mn	Mo	P	S	Si
AISI 4140	minimum	0.38	0.8	Bal.	0.75	0.15	0	0	0.15
	maximum	0.43	1.1	Bal.	1	0.25	0.035	0.04	0.35

Material was processed in the sequence illustrated in Figure 39: normalizing, rough machining, austenitizing, oil and LIN quenching, tempering and oil quenching, finish machining, nitriding, and finish cooling of nitrified samples in three different ways. Material was processed in the sequence illustrated in Figure 2: normalizing, rough machining, austenitizing, oil and LIN quenching, tempering and oil quenching, finish machining, nitriding, and finish cooling of nitrified samples in three different ways. Ferritic nitriding at 525 °C and austenitic nitriding at 610 °C lasted 4 hours in N₂-diluted 25% NH₃ atmosphere. The three finish cooling paths examined were: (a) slow cooling inside furnace, (b) fast cooling in liquid nitrogen bath, LIN (-195°C) and holding for 1 hour, as well as (c) fast cooling in LIN combined with holding for 48 hours. Figure 3 shows the atmosphere nitriding apparatus used.

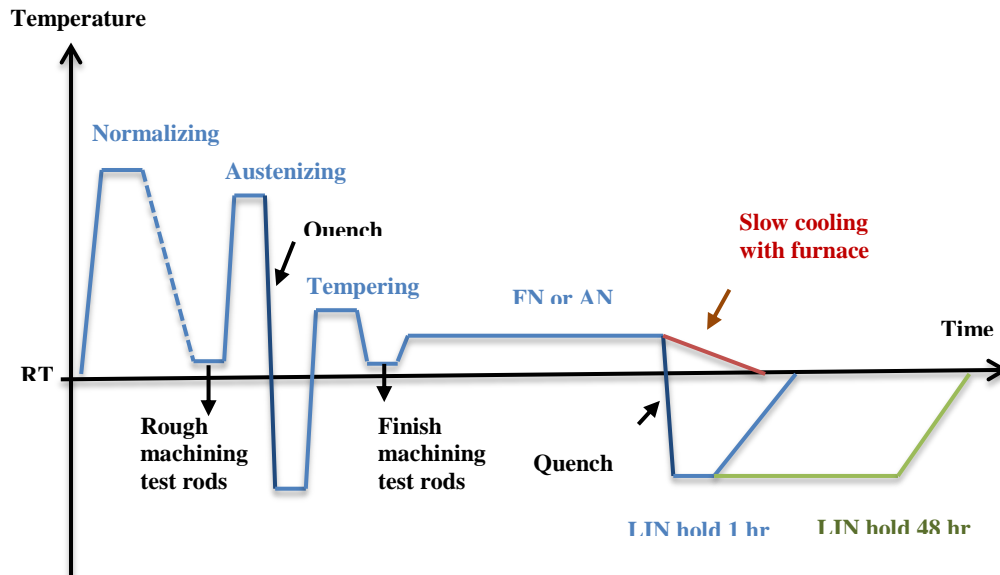


Fig. 2: Thermal processing sequence

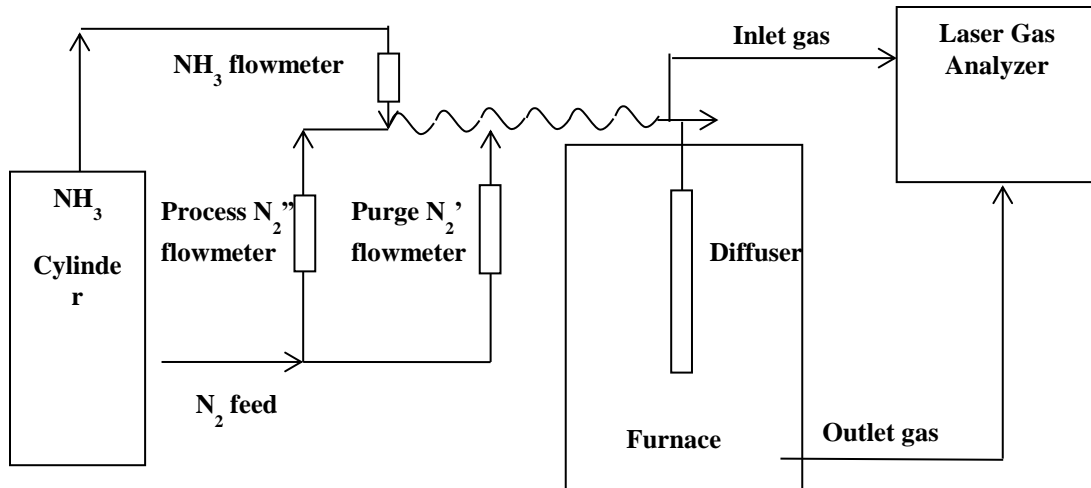


Fig. 3: Atmosphere nitriding apparatus

Three different configurations of samples were used: (i) a rod shape to measure dimensional change after nitriding, (ii) a disk shape for evaluating microstructure and hardness, and (iii) flat coupons to measure weight gain after nitriding. Nitrided disks (ii) were etched in 2% Nital. OM ZEISS IM35, SEM JEOL JSM-7000F, Oxford energy dispersive x-ray spectroscope and JEOL Superprobe JXA-8900R were used for microstructure and concentration profile analysis, while microhardness profiling was carried out on Shimadzu HMV-2000.

4. Results and Discussion

4.1 Microstructure and Nitrogen Distribution

Figure 4 shows the optical and SEM micrographs of samples processed along three different paths. After the conventional ferritic nitriding (FN), the hardened case is composed of compound layer and diffusion zone. The austenitic nitriding (AN) results in three layers, the top, “white” or compound nitride layer, the middle transition layer, that appears dark on the samples cooled with the furnace but bright on the samples quenched in liquid nitrogen (LIN), and the inner diffusion zone. The white layer thickness increases from 10 μm to 30 μm as the nitriding temperature is increased from the ferritic to the

austenitic range, indicating that the N flux into the metal core is larger due to the temperature raise and larger solubility of N in austenite. The nitrogen concentration profiles for the FN and the AN, both concluded with the slow furnace cooling, as well as the profile for AN and quenched in LIN are presented in Figure 5 left. As expected, the N profiles of the two AN samples are the same and significantly broader than for the FN treatment. At 610°C, the maximum N concentration observed, 4-5 wt. %, corresponds to the region consisting of mostly ϵ , with minor N-austenite and γ' , as shown in Figure 5 right. The transition layer, i.e. the 2nd layer seen in Figure 6, dominates in the N-concentration region between about 1 and 4 wt%. This range shown in Figure 5 right is dominated by N-austenite. Figure 6 confirms that the cooling method has an insignificant effect on redistribution of nitrogen and pre-existing carbon, and minor variations can be attributed to experimental errors. The microstructure of transition layer is modified by cooling rates, though. Appearing darker after etching in Figure 4b (slow cooling) and brighter in 4c (fast cooling), the transition layer responds to the cooling rate change by replacing equilibrium-favored braunite [12] with a more etch-resistant mixture of N-martensite and N-austenite. The dark transition layers were reported to comprise ferrite, ϵ and γ' [2] based on XRD examination.

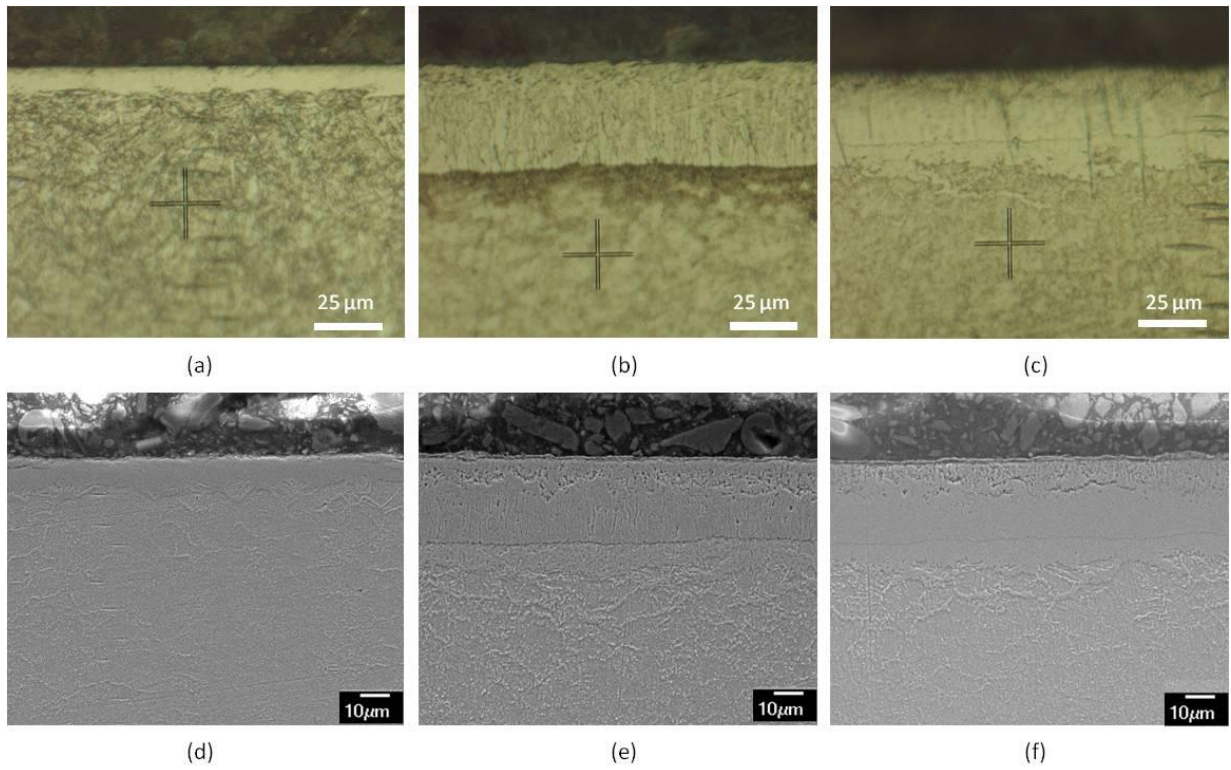
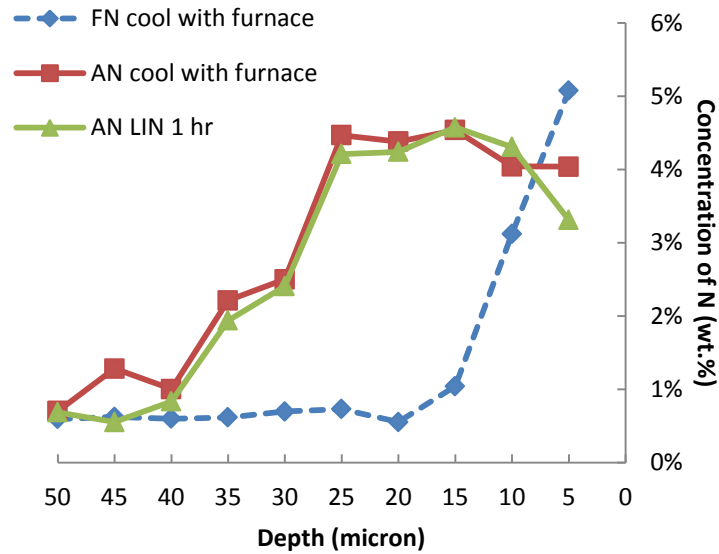
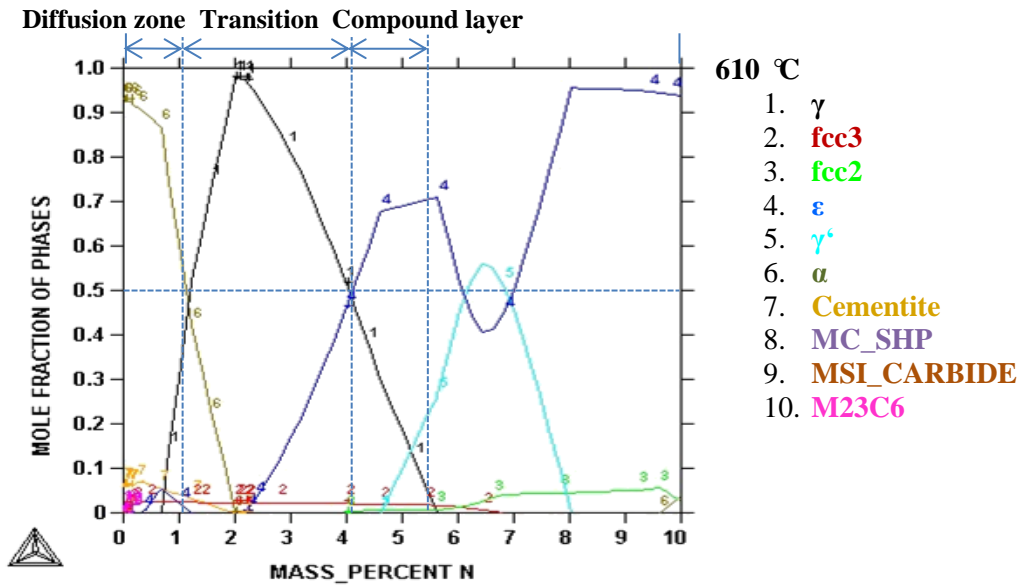


Fig. 4: Optical and secondary images of cross sections of ferritic and austenitic nitrided samples. (a and d): Ferritic nitriding and cooling with furnace. (b and e): Austenitic nitriding and cooling with furnace. (c and f): Austenitic nitriding and LIN quenching. Etched in 2% Nital.



(a)



(b)

Fig. 5, (a), Nitrogen concentration profiles for ferritic nitriding (FN) and cooling with furnace, austenitic nitriding (AN) and cooling with furnace, as well as austenitic nitriding (AN) and quenched in LIN bath; (b), Mole fraction of phases vs. mass percent of nitrogen at 610°C, Thermo-Calc.

Higher temperatures and larger solubility in austenite accelerate nitrogen flux from atmosphere into steel, but it's interesting to note that the present AN treatments produced a relatively thick white layer and thin transition layer. The effect is a likely result of a comparatively low nitrogen diffusion coefficient in the austenitic phase, lower than for the ferrite and nitrides, Figure 7 [13-16]. Thus, once the N-austenite is formed beneath the white layer, an effective diffusion barrier is created. Nitrogen builds up in the growing white layer, and the expansion of transition layer slows.

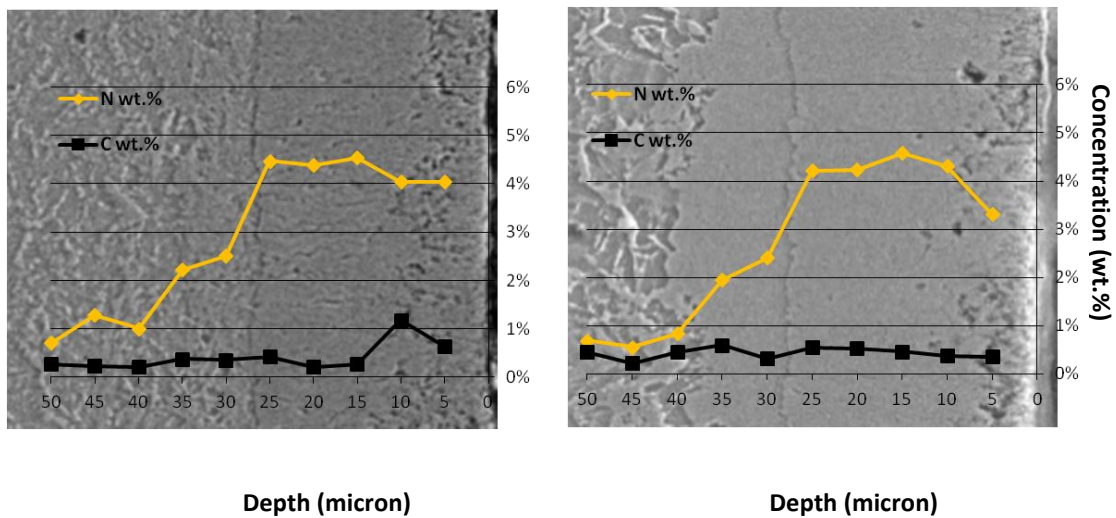


Fig. 6: Nitrogen and carbon concentration in AN samples (a) cooled with furnace, and (b) quenched in LIN, superimposed on the corresponding SEM images.

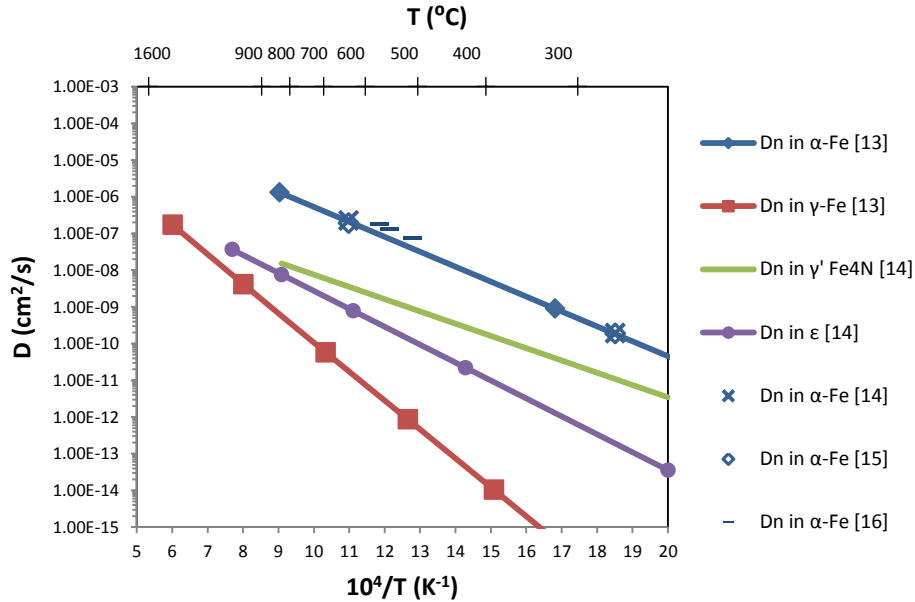


Fig. 7: Diffusion coefficient of nitrogen in different phases.

Compound layers are undesired in certain engineering applications. An additional investigation was carried out on control and dissolution of compound layers by the simultaneous modification of nitriding potential (K_n) and nitrogen flux using inert gas dilution of ammonia. Results will be reported in the future.

4.2 Hardness Profiles

Effect of finish-cooling method on microhardness profile is presented in Figure 8 for the three AN disks: (a) slow cooled with furnace, (b) fast cooled in LIN bath and held there (soaked) for 1 hour, as well as (c) fast cooled in LIN and soaked for 48 hours. Typically, hardness within the transition and diffusion zones is higher for the LIN quenched and soaked samples, and the effect scales with the soaking time indicating, that apart from the expected athermal martensitic transformation, an isothermal martensitic transformation [17-19] or age-hardening may be operating. A more detailed transmission electron microscopy will be required to interpret the data. Although the subject falls outside the scope of the present study, it should be mentioned that a large number of references exist on so-called “deep” or multi-hour cryogenic soaking treatments of martensitic steels, producing significant improvements of wear resistance while displaying only a mild

increase in hardness. This effect has been attributed to the precipitation of submicron carbides taking place during LIN bath soaking [20].

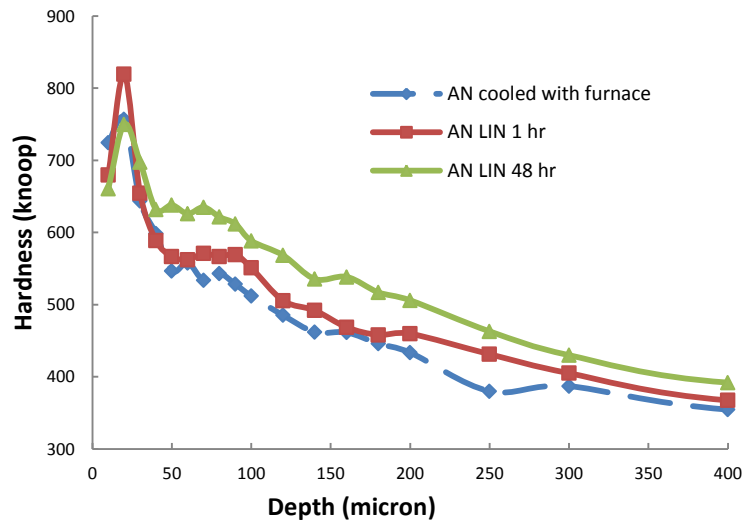


Fig. 8: Hardness profiles of austenitic nitrated samples

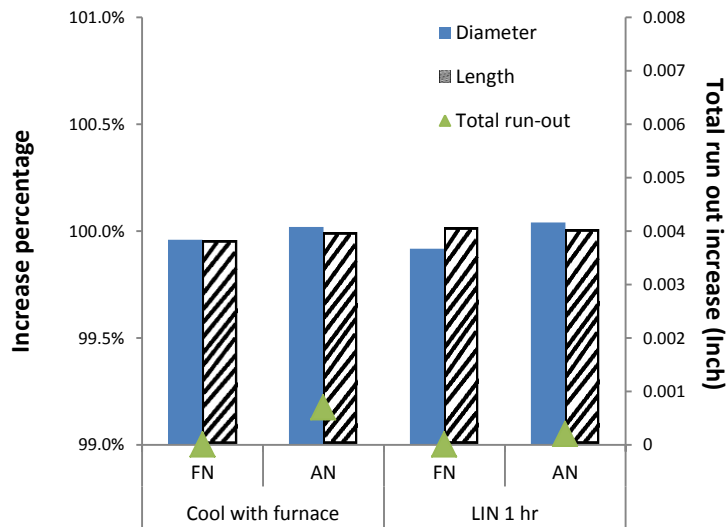


Fig. 9: Diameter and length changes, as well as total run-out increase of ferritic and austenitic nitrated rods (i).

4.3 Nitrogen Flux

Although frequently overlooked, N flux control is important for optimizing nitriding parameters. Table II presents the flux values measured from weight gain of coupons (iii) and calculated from concentration profiles, Figure 5, left. The following equations are used in which: J – flux, t – time, A – surface area, and C(x) – concentration at depth x.

$$J = \frac{\text{weight gain}}{A \cdot t} \quad (1)$$

$$J = \frac{\int_0^{x=C_0} f(x)}{A \cdot t} \quad (2)$$

A reasonable agreement between the results of the two methods indicates their potential parity in the industrial QC practice. Of note, the subcritical AN treatment brings about a 2.5-times higher nitrogen uptake than the conventional FN treatment which confirms the starting assumptions.

Table II: Average Nitrogen Flux for 4 Hour Nitriding at 525°C (FN) and 610°C (AN)

	Weight gain (g)	Flux (g/cm ² /s) from wt. gain	Flux (g/cm ² /s) from conc. profile
FN	1.89E-02	5.75E-08	8.69E-08
AN	4.80E-02	1.06E-07	1.50E-07

4.4 Dimensional Stability

A minimum-distortion nitriding of low-alloy steels can be achieved by limiting the processing temperature to below the eutectoidal transformation temperature in their respective Fe-C-M systems, where: C – carbon, and M - metallic alloying additions, as well as assuring uniform heating, cooling and atmosphere flow-field [21]. Dimensional stability of subcritically nitrided and differently cooled AISI 4140 rods (i), Φ 6.35 mm x L 101.6 mm, ground to R_a 0.4 μm, was evaluated and compared to that resulting from the conventional ferritic nitriding using two cooling methods. Treatment resultant changes in the rod diameter, length, and total run-out were considered. Shown in Figure 9, the results prove that, overall, the stability of rods nitrided at 610°C and cooled in LIN bath is about the same as for the conventionally nitrided rods. Total run-out increased only in the

case of the slow cooled AN specimens, probably due to a partial decomposition of N-austenite into a soft braunite phase.

5. Conclusions

1. Subcritical temperature austenitic nitriding of low-alloy AISI 4140 steel increases the rate of nitrogen absorption from nitriding atmosphere and the thickness of nitrided case as compared to the conventional ferritic nitriding.
2. A transitional, nitrogen-austenite sublayer forms between the conventional, hard compound layer and soft diffusion zone during the subcritical austenitic nitriding. Its thickness and the thickness of compound layer can be controlled through measurement of nitrogen flux, dilution of undissociated NH_3 atmosphere with N_2 , adjusting nitriding potential, and applying proper boosting-diffusing conditions.
3. Liquid nitrogen quenching and soaking increases the hardness of the transition and diffusion layers in the subcritically nitrided steel. The hardness increase is proportional to the soaking time suggesting cryogenic aging and isothermal martensitic transformation as the operating mechanisms.
4. Dimensional change and distortion of the subcritically nitrided and liquid nitrogen quenched/soaked parts are in the same range as after the conventional ferritic nitriding. Slow cooling with furnace may result in nonlinear deformations, however.
5. Future work should examine phases present in the transition layer after cryogenic soaking, evaluate wear properties of subcritically nitrided surfaces, and correlate nitrogen flux from nitriding atmosphere to the extent of ammonia dissociation and dilution with inert gases.

Acknowledgements

This work has been financed and supported by Air Products and Chemicals, Inc. Computational contributions of the CHTE at Worcester Polytechnic Institute must be also acknowledged. The authors would like to thank Mr. John Green of Air Products for the help in experimentation.

References

1. N. I. Kardonina, A. S. Yurovskikh and A. S. Kolpakov, 2011, "Transformations in the Fe – N System," *Metal Science and Heat Treatment*, 52(9) (2011), 457-467.
2. M. Fattah, "Comparison of Ferritic and Austenitic Plasma Nitriding and Nitrocarburizing Behavior of AISI 4140 Low Alloy Steel," *Materials & Design*, 31(8) (2010), 3915-3921.
3. N. Yasumaru, "Formation of Austenite and Martensite in Surface Layer of Pure Iron with Ion Nitriding," *Materials Transactions, JIM*, 33(1) (1992), 7-10.
4. M. J. Van Genderen, A. Böttger and E.J. Mittemeijer, "Formation of α " Iron Nitride in FeN Martensite: Nitrogen Vacancies, Iron-Atom Displacements, and Misfit-Strain Energy," *Metallurgical and Materials Transactions. A, Physical Metallurgy and Materials Science*, 28(1) (1997), 63-77.
5. V. G. Gavdijuk, V. M. Nadutov and K. Ullakko, "Low Temperature Ageing of Fe-N Martensite," *Scripta Metallurgica Et Materialia*, 25(4) (1991), 905-910.
6. V. G. Gavriljuk, "Austenite and Martensite in Nitrogen-, Carbon- and Hydrogen-Containing Iron Alloys: Similarities and Differences," *Materials Science & Engineering. A, Structural Materials : Properties, Microstructure and Processing*, 438-440 (2006), 75-79.
7. A. Böttger et al., "Tempering of iron-carbon-nitrogen martensites: (re)distribution of interstitial atoms " *Materials Science Forum*, 318-320 (1999), 103-108.

8. Liu Cheng, A. Böttger and E. J. Mittemeijer, "Tempering of Iron-Carbon-Nitrogen Martensites," *Metallurgical Transactions. A, Physical Metallurgy and Materials Science*, 23(4) (1992), 1129-1145.
9. P. Ferguson, K. H. Jack, *Scripta Metallurgica*, 18 (1984), 1189.
10. Liu Cheng, A. Böttger and E. J. Mittemeijer, "The Tempering of FeNiN Martensite," *Metallurgical Transactions.A, Physical Metallurgy and Materials Science*, 22(9) (1991), 1945-1956.
11. T. Bell, "Martensite Transformation Start Temperature in Iron-Nitrogen Alloys," *The Journal of the Iron and Steel Institute*, 206(10) (1968), 1017-1021.
12. George, Totten, *Steel heat treatment handbook. 2nd ed* (UK: Taylor and Francis Group, 2006).
13. B. B. Straumal, N. F. Vershinin and M. Friesel, et al, "Ionic nitriding of austenitic and ferritic steel with the aid of a high aperture Hall current accelerator", *Defect and Diffusion Forum*, 194-199 (2001), 1457-1462.
14. Y. Sun, T. Bell, "Computer prediction of threshold nitriding potential curves", *Heat Treatment of Metals*, 24 (1997), 43-49.
15. Traugott E. Fischer, "Materials science for engineering students", *Academic Press*, (2009), 195.
16. M. Weller, *Material Science Forum*, 366-368 (2001), 95-137.
17. D. E. Laughlin et al., "Thermally activated martensite: its relationship to non-thermally activated (athermal) martensite" (paper presented at ICOMAT, Santa Fe, USA, 2008).
18. V. A. Lobodyuk, E. I. Estrin, "Isothermal martensitic transformations", *Physics-uspekhi*, 48(7) (2005), 713-732.
19. J. C. Zhao, M. R. Notis, "Continuous cooling transformation kinetics versus isothermal transformation kinetics of steels: a phenomenological rationalization of experimental observations", *Materials Science and Engineering*, R15 (1995), 135-208.

20. D. Das et al., "Influence of varied cryotreatment on the wear behavior of AISI D2 steel", *Wear*, 266 (2009) 297-309.
21. D. Pye, "Distortion during nitriding", *Industrial Heating*, Jan. 7th, 2011

Paper #3: Process Optimization for Industrial Practices of Plasma Activated Nitrogen-Hydrocarbons Atmosphere Carburizing *(to be submitted to International Heat Treatment and Surface Engineering)*

Yingying Wei¹, Zbigniew Zurecki², Kai Kang², Richard D. Sisson, Jr.¹

¹Worcester Polytechnic Institute, Worcester, MA 01609, USA

²Air Products and Chemicals, Inc. Allentown, PA 18195, USA

Abstract

Problems with intergranular oxidation (IGO), energy efficiency and carbon footprint of conventional endothermic atmosphere (CO-H₂-N₂) carburizing is forcing heat treating and manufacturing companies to move toward increasingly capital- and operating-cost expensive, low-pressure (vacuum furnace) carburizing methods. In response, a new activated and alternate carburizing method (A2A carburizing) has recently been developed, bridging the endothermic atmosphere and vacuum processes, where a plasma-activated, oxygen-free, non-equilibrium nitrogen-hydrocarbon gas blend is utilized. The optimization of industrial A2A carburizing processes involves improvement of case uniformity of parts as a function of position in the charge as well as on different sides of the parts. Connected to the optimization, a computational fluid dynamics (CFD) study is conducted for examination of gas flow field inside the furnace and trays holding steel parts treated. To mitigate soot in the atmosphere and minimize the poorly carburized contact area between parts, effects of different combinations of nitrogen-hydrocarbons mixture on soot formation in atmosphere, deposition on metal surface and graphite growth at carburizing temperature are investigated. A mixture of N₂-0.4% C₃H₈-1% CH₄ mixture has been proven to be able to provide a well carburizing hardened case with less soot in atmosphere, less coke deposition on metal surface, as well as minimized marginally carburized contact zone. A soot formation mechanism for non-equilibrium atmosphere in A2A carburizing is proposed.

1. Introduction

To accelerate the process, merge the merits of gas carburizing and vacuum carburizing, eliminate intergranular oxides, reduce capital/operational cost and promote usage of a more safe and environmental friendly atmosphere, a plasma activation and alternate atmosphere heat treatment technology (A2A technology) has been introduced by Air Products and Chemicals, Inc.[1] Different from conventional plasma heat treating processes [2], in which loading parts performance as one electrode, this technology adapts cold plasma discharge to activate the inlet gas and promote the hydrocarbon dissociation in the atmosphere. During recent years, a series of gas stream-activating, cold-plasma injectors have been developed at Air Products. A high-voltage/low-amperage, low power (below 2 KW) DC or AC electric discharge between electrodes on the plasma injector ionizes, partially dissociates and converts the gas molecules on their way into the furnace [1]. The low thermal energy activates hydrocarbons to ions, radicals and various low chain byproducts [3-6], and prevents complete dissociation of hydrocarbons into carbon and hydrogen only.

The plasma injector can be easily retrofitted to various types of the conventional, radiant tube or electrically heated and 1-atm pressure furnaces in order to carry out carburizing, carbonitriding, neutral carbon annealing, as well as nitrocarburizing operations falling into a relatively low temperature range [7]. So far, this technology has been lab tested on the carburizing of low-alloy and stainless steels [7], low-and high-temperature nitriding of carbon, alloy and stainless steels [8]. It has been proven to be effective to eliminate intergranular oxides, accelerate the process, and at the same time reduce cost. Application of A2A technology onto industrial scale furnace is more challenging, requires dynamic in-situ atmosphere control and more uniform gas stream. In this paper, a computational fluid dynamic study is presented to improve the carburizing uniformity by modification of the loading configuration.

A propensity for sooting on the steel surface continues to be an unresolved issue in non-equilibrium carburizing operations. Several investigations performed by Grabke [9-13] provide a good understanding of thermodynamic, kinetics and mechanisms of coke deposition for equilibrium atmosphere. Many investigations about soot/coke formation in equilibrium or hydrocarbon non-equilibrium atmosphere are reported at the temperature

lower than practical carburizing temperature [14-20], its formation and deposition at temperature above 900°C has seldom been reported. In this study, a series of nitrogen-hydrocarbons blend tests at 930°C is implemented to alleviate the soot particles in the atmosphere as well as on metal surface. The mechanism of soot formation and deposition is proposed.

2. Experimental methods

2.1 Industrial practices

Industrial practices have been done at one industrial site. The onsite integral quench furnace (IQF) schematic is demonstrated in figure 1. Gas stream flows in from the top inlet, after being stirred by a 4-blade fan, it circulates around the muffle and flows into the heating chamber through the three columns of bottom vents, on top of where is 4 stacks of trays with components loaded.

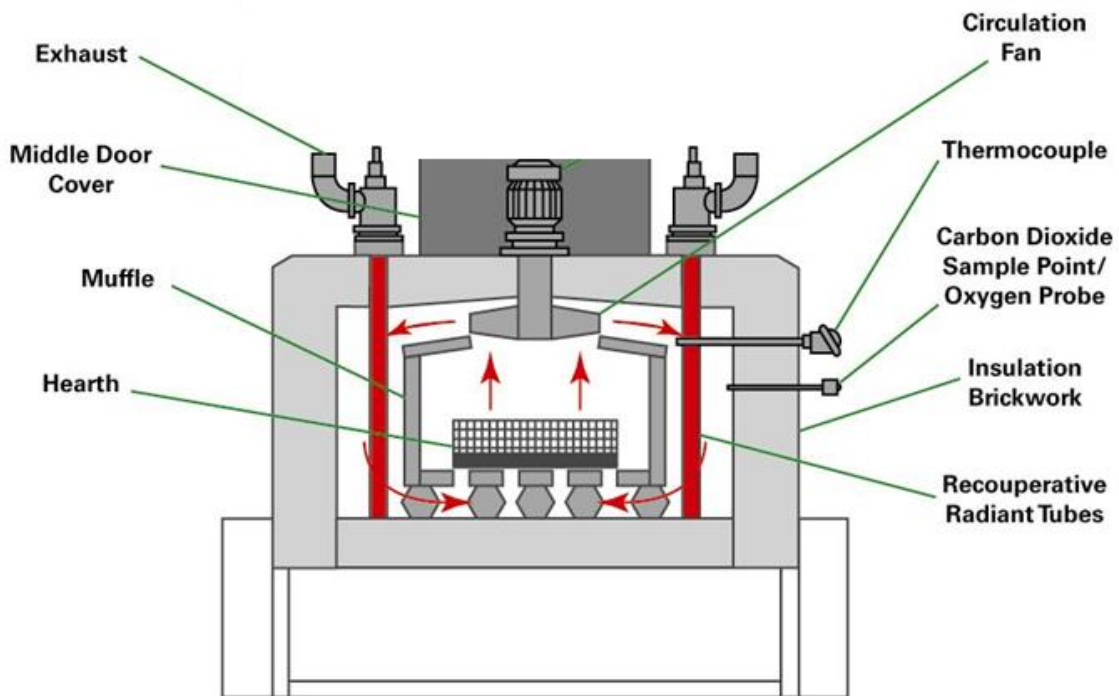


Figure 1 Schematic of industrial integral quench furnace, Ipsen design [21]

Shown in Figure 2, the cold plasma injector is mounted at the inlet of the furnace, individually controlled by a 110V/30A AC power supply. Gas are pre-mixed upstream

and fed into the integral quench furnace through the plasma injector. H₂, CO, CO₂, CH₄, C₃H₈ in the furnace are monitored by probe gas analyzers.

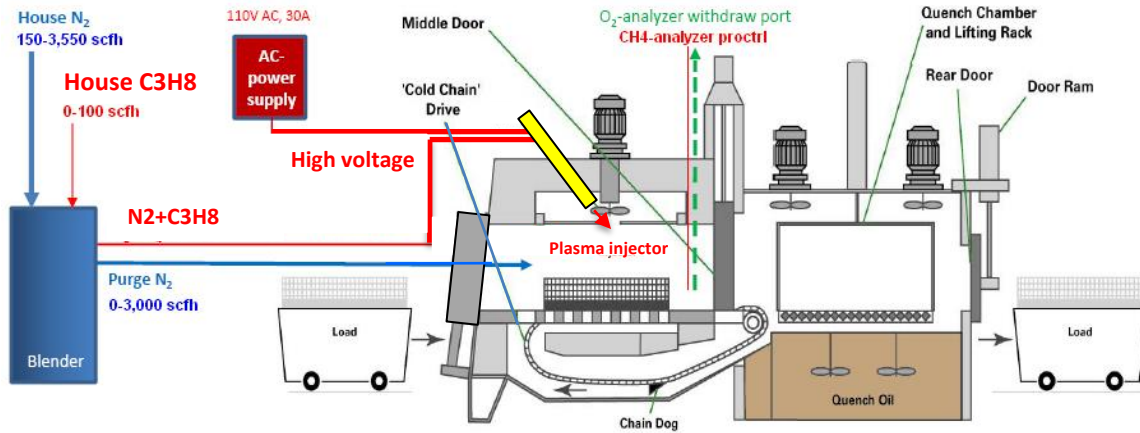


Figure 2 Retrofit of industrial integral quench furnace, Ipsen design [21]

Four tests, T1-T4, have been done at 930 °C with plasma activated nitrogen-propane atmosphere. First three tests are implemented with the same traditional loading configuration as demonstrated in figure 3(a), but with different boost and diffuse schemes, trying to optimize the process efficiency, hardened case depth and surface quality. In such loading configuration, normal basket trays are used. Test samples and dummy parts are shoveled into trays and shaken for uniform distribution.

Nevertheless, the last test is taking carburizing with a new loading configuration as shown in figure 3(b), with a center channel in each tray and an entire solid top sheet metal cover. Two ends of the channel in each tray are also covered with solid metal panels. Width of three bottom channels is the same as floor center vents, but the width of top channel is $\frac{3}{4}$ of three bottom ones.



(a)



(b)

Figure 3 Pictures of conventional loading (a); and center channel configuration loading (b)

Upon charging the components into furnace, the temperature in the heating chamber drops from 930°C to 730°C , and oxygen level increases to 600 ppm due to the open of chamber door. To consume the residual oxygen in the furnace, propane is purged at a

base amount level. When temperature and oxygen level recovers, pre-mixed blend gas is purged into furnace and following the designed boost and diffuse steps.

16MnCr5 DIN steel is used as test material, its composition is list in table 1.

Table 1 Composition of 16MnCr5 DIN steel

	C	Fe	Cr	Mn	Mo	Ni	Si	Al	Cu
wt. %	0.16	Bal.	0.95	1.15	Max. 0.08	Max. 0.30	Max. 0.40	Max. 0.035	Max. 0.30

On carburized test samples, OM ZEISS IM35 and Shimadzu HMV-2000 are utilized for optical micrographs and microhardness profiles.

2.2 Nitrogen-hydrocarbons blend tests for A2A carburizing

Five different combinations of CH₄ and C₃H₈ with balanced nitrogen, listed in table 2, are used to test the soot formation both in atmosphere and on metal surface. A semi-industrial lab scale furnace manufactured by Applied Test Systems, with 18” depth x 15” width x 12” height is used. Gas blends are premixed at upstream of furnace inlet then blow into furnace through plasma injector. During the process, a filter is used at the furnace outlet for measurement of soot deposition rate, which indicates the soot amount in the atmosphere. Boost time for weight gain measurements on coupons is set to be the same, 60 minutes for each condition. While boost time for soot deposition rate measurements is set to be different, allowing enough deposits to be measureable by microbalance. Gas composition CO, CO₂, CH₄ is monitored by Siemens Tri Gas Ultramat 23, C₃H₈ is measured by Siemens Ultramas 22, O₂, H₂ and dew point are measured by Alpha Omega trace O₂ series 3000, Cosa/Xentaur dew point XPDM and Thermco binary gas thermal conductivity analyzer 6900 series, respectively. Percentage of each composition is taken from average of readings over the period at processing temperature.

Table 2 Conditions for nitrogen - hydrocarbons blend tests

conditions	Inlet		Condition			
	C3H8 (%)	CH4 (%)	Total flow (scfh)	Temperature (°C)	Boost time (min)	
					Filter	Weight
1	1.8	4	200	930	20	60
2	1.8	0			20	
3	0.4	4			40	
4	0.4	1			90	
5	0.4	0			187	

Polished AISI 8620 (table 3) disk coupons with 0.05 micron surface finish are used in condition 1, 3, 4 and 5. Two coupons are used in condition 1, 3 and 5. One is used for weight gain measurements, and the other one is partially covered by a square steel bar to mimic the situation when parts are touching each other. In condition 4, to investigate the correlation between grain boundary and soot deposition, another coupon with additional pre-etching step by 2% nital is also employed. After carburizing at 930 °C, coupons are cooled with furnace in nitrogen atmosphere, preventing deposited soot convert to a solid thin film during oil quench.

Table 3 Composition of AISI 8620

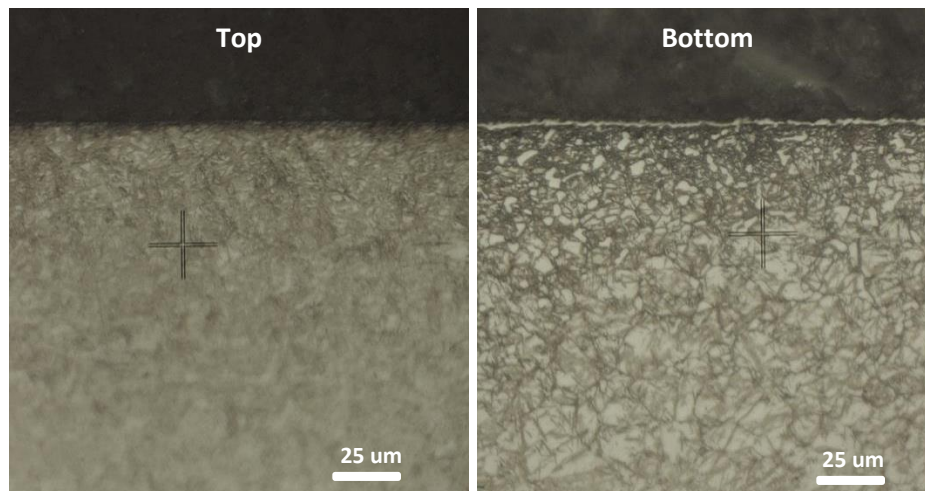
	C	Cr	Fe	Mn	Mo	Ni	P	S	Si
8620	0.18 – 0.23	0.40 – 0.60	Bal.	0.70 – 0.90	0.15 – 0.25	0.40 – 0.70	0 – 0.035	0 – 0.040	0.15 – 0.30

A tape test is used to visually compare the amount of soot deposition on coupon surface from each condition. Weight gain is measured after washing the coupons with acetone. OM ZEISS IM35, SEM JEOL JSM-5910LV and EDS Thermo Noran System Six (NSS) equipped with a silicon drift detector (SDD) are used for microstructure analysis.

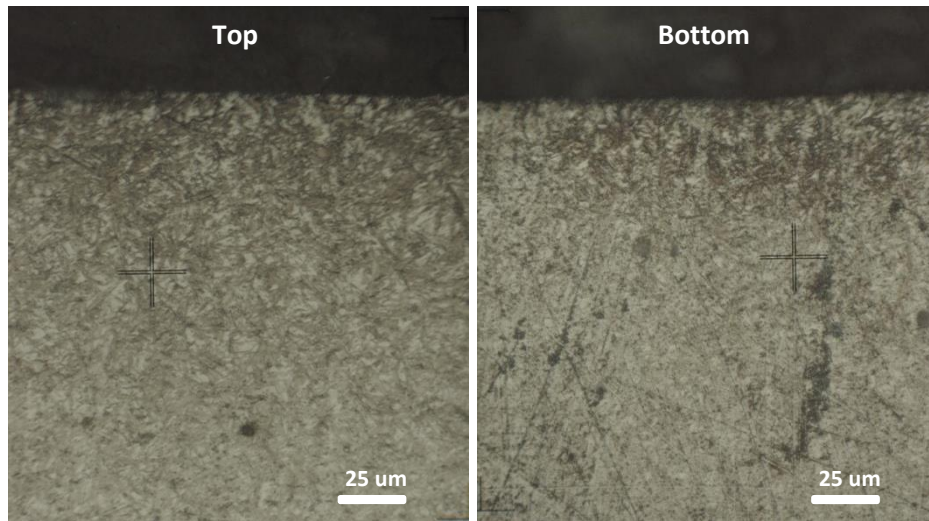
3. Results

3.1 Microstructure and hardness for different loading configurations

Figure 4(a) presents the optical images of top and bottom sides on the part from bottom tray in T3. It is observed that less carburizing at top side and over carburizing at bottom side. At bottom side, carbides and large grains of retained austenite are found at surface and in near surface layer respectively. It is because that high carbon content in boundary layer enhances the flux from atmosphere to metal surface, exceeds the diffusion rate inside the metal. Austenite is over saturated with carbon and forms carbides. This over saturation suppresses martensite transformation during quench and leaves large amount of austenite. However, demonstrated in figure 4(b), uniform carburizing is achieved between top and bottom sides on the part, which is from bottom tray of T4. Fine martensite is uniformly distributed over the hardened case. Meanwhile, no intergranular oxide is observed in all of images.



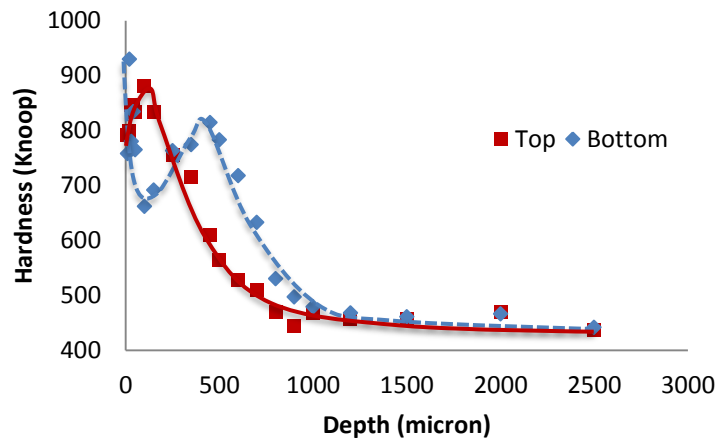
(a)



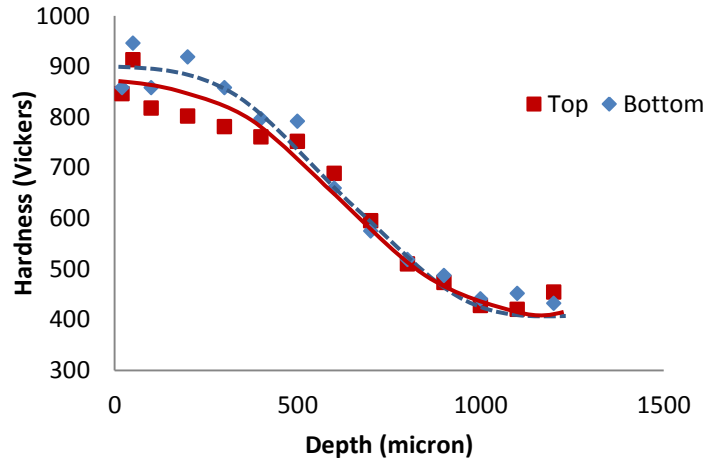
(b)

Figure 4 Optical microscopic images of top and bottom sides on the part in bottom tray from (a) T3; and (b) T4

Corresponding to microscope images, hardness profiles on each side are shown in figure 5. On the part from T3, there is less case depth on top side comparing to bottom side, meanwhile, a hardness drop is shown at near surface due to large amount of austenite. As illustrated in figure 5(b), same case depth are achieved on both sides of the sample from T4, absence of hardness drop at surface on bottom side is due to uniformly distributed fine martensite.



(a)



(b)

Figure 5 Hardness profiles of top and bottom sides on the part in bottom tray from (a) T3; and (b) T4

Top chart of figure 6 shows the average hardness of all parts within one tray from T1 to T4. Large deviations over four trays are shown from T1 to T3. Hardness range is from HRC 52 to 56 for T1, and 52-58, 55-60 for T2 and T3, respectively. Not only the average hardness of trays deviates, so does hardness of components within one tray, which is shown in bottom chart of figure 6. Compare to T4, the standard deviation value in each tray from all T1-T3 is relatively higher and heavily vary among trays which is illustrating very non-uniform carburizing. In these tests, the conventional dense “shovel-loading” is applied. In T4 when the center channel configuration is utilized, narrow range of average hardness among trays is observed in top chart of figure 6, the deviation in each tray is smaller than the corresponding values from T1-T3, meanwhile, the variation of standard deviation among trays is limited, illustrating the uniform carburizing.

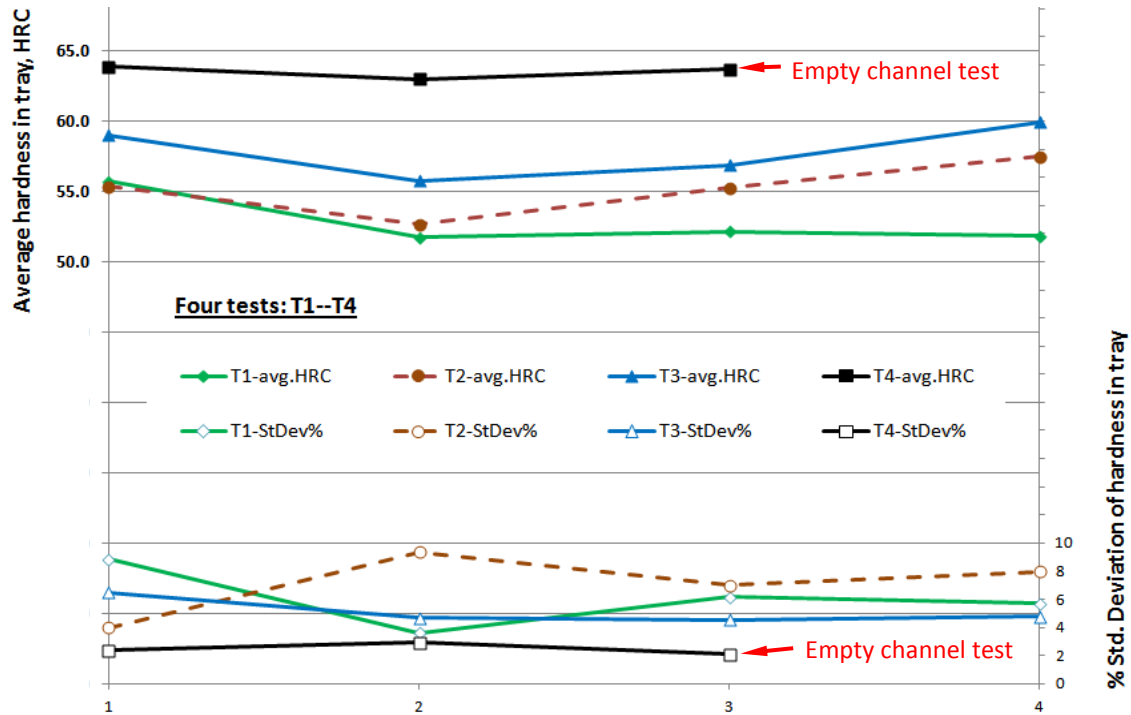


Figure 6 Average hardness (top chart) in each tray; and standard deviation among parts (bottom chart) in each tray from four industrial practices, tray 1 to tray 4 is from bottom to top

3.2 Microstructure and hardness of contacted area

To keep efficiency the same as endo-gas carburizing, in industrial tests, test samples are highly dense, shovel loaded in trays, the same way as conventional atmosphere carburizing. Therefore, it is inevitable that parts touch each other, leading to pale contact area on carburized parts, as shown in figure 7. Around the contact area, a dark perimeter is shown up and the rest of the surface appears grey.

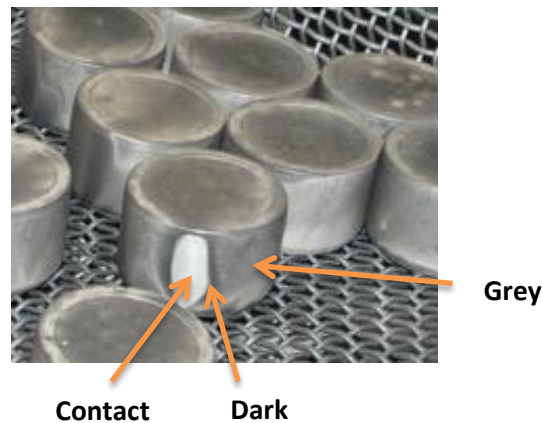


Figure 7 Photograph of as-quenched part being touched during A2A carburizing

Illustrated in figure 8(a), the contact area is barely carburized, with very shallow case shown in hardness profile (figure 9), comparing to the similar case depth of dark perimeter and grey area in the same hardness profile. However, the as quenched condition at grey area (figure 8(f)) appears rough microstructure with scattered cementite on surface and large austenite grain in near surface sub-layer, which is corresponding to the hardness drop at near surface in hardness profile. Thus, pale contact area is soft, marginally carburized, the dark areas, next to contact spot were properly carburized, and the most exposed to gas atmosphere grey areas were somewhat over carburized due to the fact that the furnace atmosphere was set to be over carburizing by the process controller. Carburizing was acceptable outside the contact area, with minor portions, hardness drop near surface, that could be corrected by the subsequent tempering treatment.

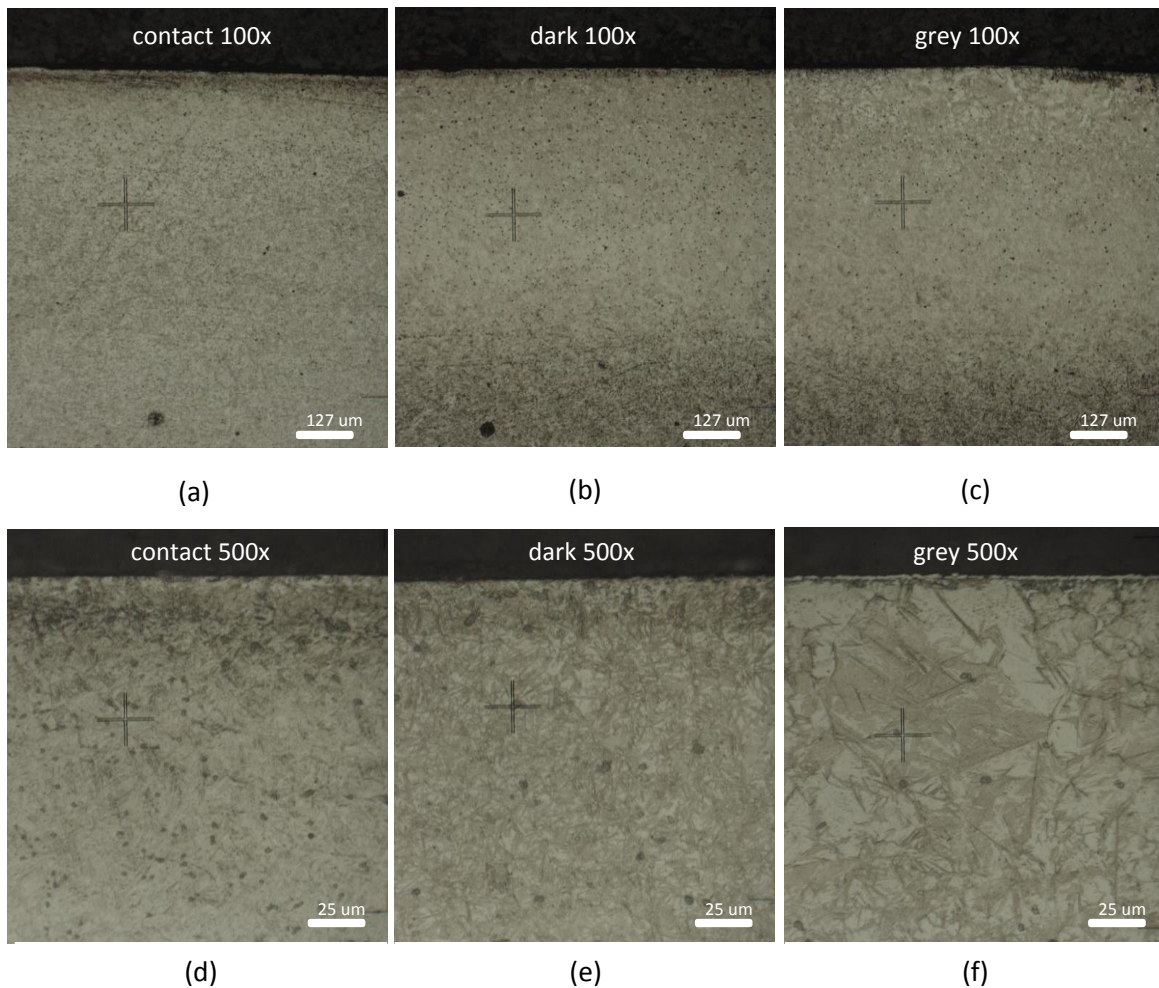


Figure 8 Optical micrographic images of contact (a) and (d), dark (b) and (e), as well as grey (c) and (f) areas on the as-quenched part being touched during A2A carburizing

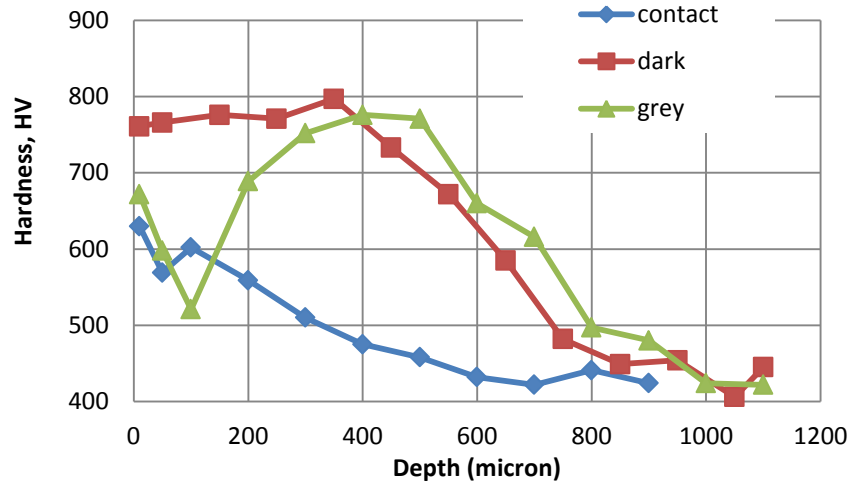


Figure 9 Hardness profiles of contact, dark and grey areas on the as-quenched part being touched during A2A carburizing

3.3 Soot formation in atmosphere and deposition on metal surface

Figure 10 compares the soot deposition rate on filter from nitrogen-hydrocarbons blend tests, which illustrates that soot in the atmosphere is increasing with propane, while when the propane percentage is fixed, it increases with methane. Besides condition 5, the carbon fluxes in condition 1-4 are very close. Condition 5 is poorly carburized with very low flux. Condition 3 and 4 is appearing as the optimized ones, with less soot in the atmosphere and enough carbon flux on the coupon.

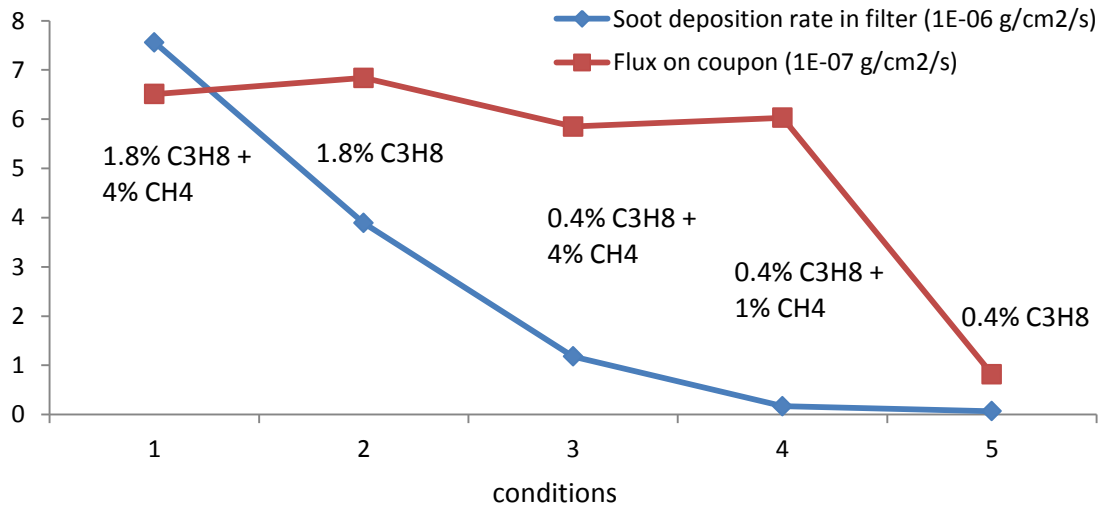


Figure 10 Measured soot deposition rate in filter and flux on coupons for five conditions

In figure 11(a) it is observed that dark soot on the tape in condition 1, 3, 4 and 5, no matter how much flux it is. However, the soot severity on metal surface cannot be associated to the soot amount in the atmosphere.

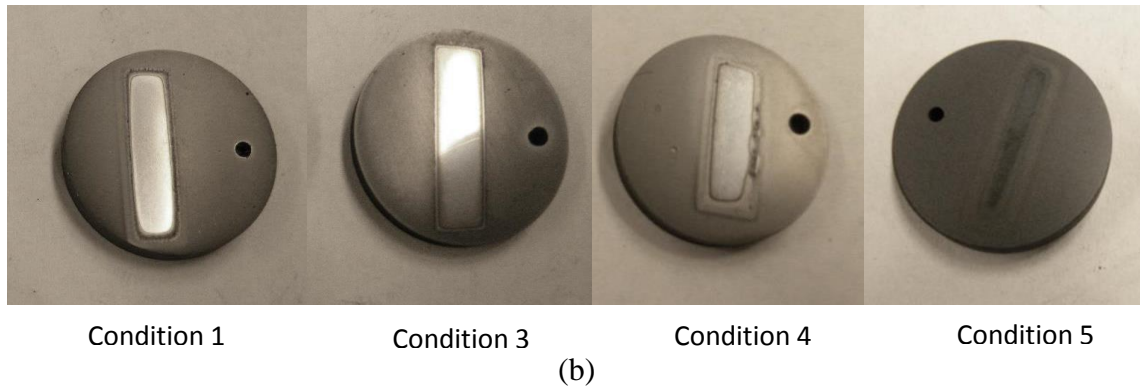
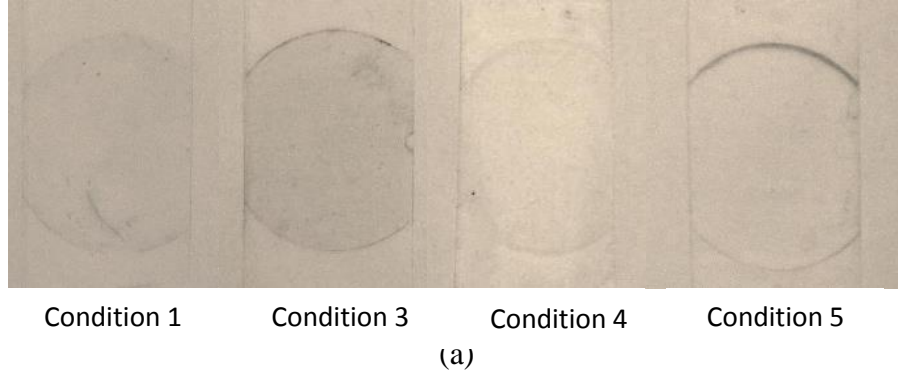


Figure 11 Pictures of soot on tape (a); and contact area (b) of coupons from condition 3, 1, 4, and 5 (left to right)

Analogue to chemical vapor deposition [22], at high temperature and one atmosphere pressure, the deposition is a mass transportation limited process, rather than surface reaction limited process. The deposition rate of pyrolytic soot is determined by gas mass transfer coefficient h_g .

$$h_g = \frac{D_g}{\delta}$$

where D_g is the diffusion coefficient in boundary layer, δ is boundary layer thickness. Theoretically, D_g is proportional to

$$D_g \propto \frac{T^{3/2}}{P}$$

where temperature T and pressure P are fixed in this set of experiments, then D_g is the same in different conditions.

Boundary layer thickness is proportional to

$$\delta \propto \left(\frac{\mu x}{\rho U}\right)^{1/2}$$

in which μ is gas viscosity, ρ is gas density, x is the location and U is the gas velocity. In conditions of blend test, x and U are constant, then the boundary is affected by gas viscosity and density.

Therefore, in the blend tests conditions, the pyrolytic soot deposition rate on metal surface is determined by

$$h_g \propto \left(\frac{\rho}{\mu}\right)^{1/2}$$

The more soot nucleation in the atmosphere does not necessary leads to more soot deposition on the metal surface.

However, correlating figure 11(a) and (b), the more soot deposits on the metal surface, the less penetration depth it is in the narrow gap between contact parts.

Therefore, the best combination of results has been achieved in condition 4, with enough carbon flux on coupon, but less soot in atmosphere and on metal surface, therefore largest penetration depth within contact zone.

3.4 Graphite filaments growth on metal surface

Graphite filaments are observed on metal surface, which appear as bright spots in figure 12(a). There are large amount of filaments as seen in the optical image from condition 1. For condition 3, 4 and 5, only sporadic filaments are shown.

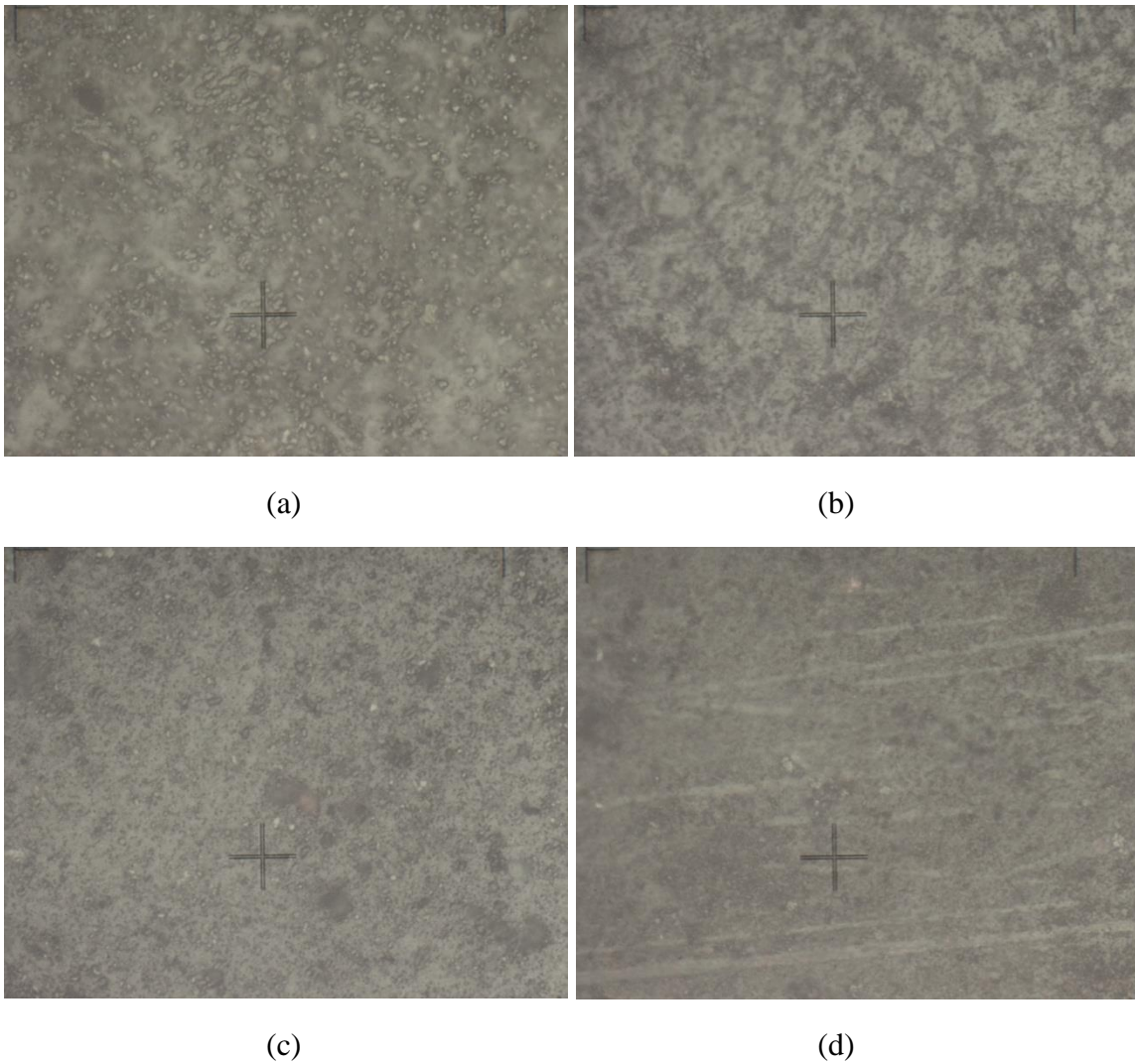
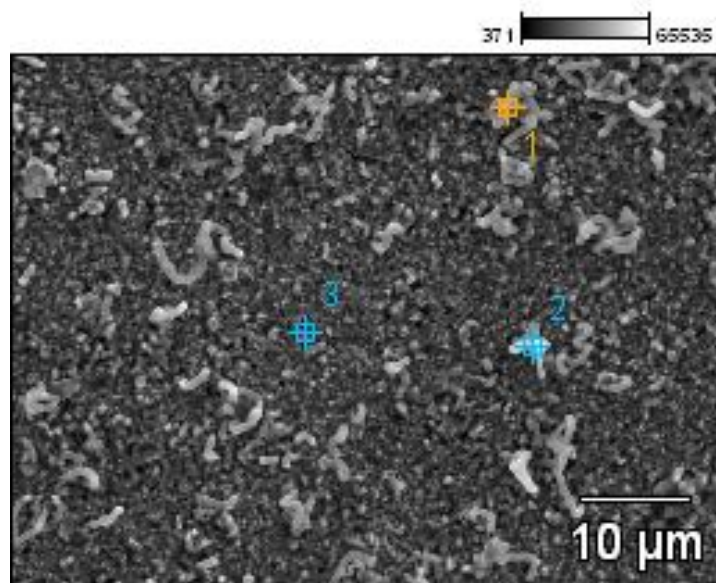
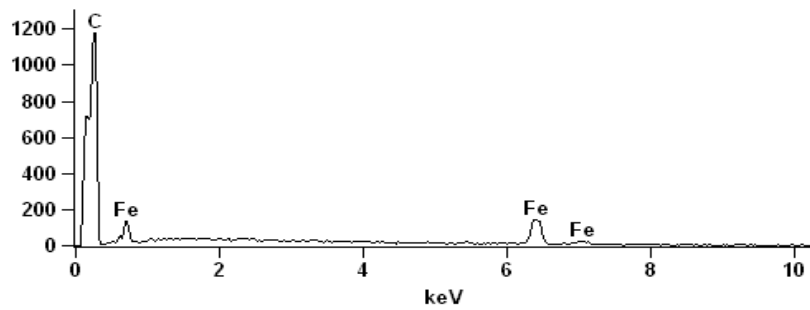


Figure 12 Optical microscopic images of flat surface of coupons from condition 1 (a), condition 3 (b), condition 4 (c) and condition 5 (d), washed with acetone.

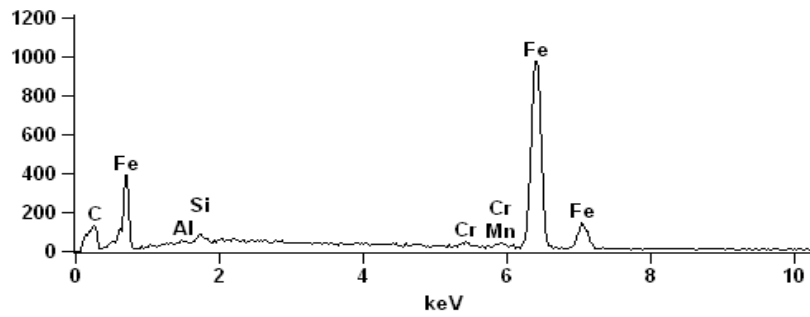
Surface morphology after carburizing is also investigated. EDS results of condition 4 in figure 13 demonstrated very different morphologies between pre-etched and non-pre-etched coupons. On the former one, carbon fibers grows out of surface with ~100 nm diameter, however, on the latter one, backscatter electron image shows only carbides particles. It is the etched grain boundary serves as active sites, promotes the catalytic dissociative adsorption and dehydrogenation of hydrocarbons, and results in growth of carbon filaments.



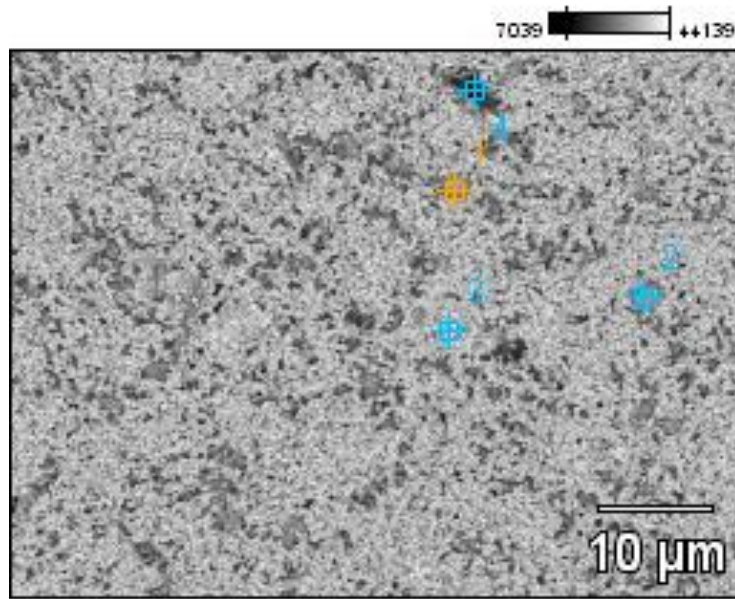
Full scale counts: 1174 71655 8620 sooted surface(1)_pt1



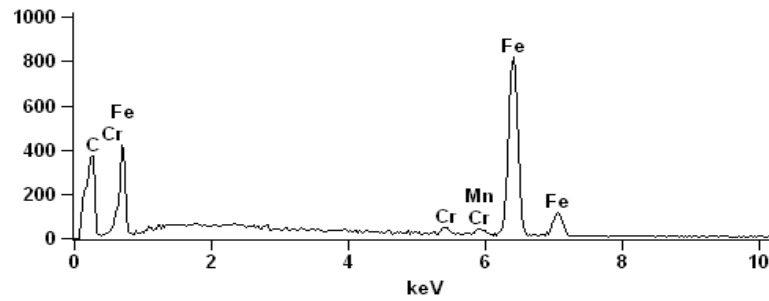
Full scale counts: 977 71655 8620 sooted surface(1)_pt3



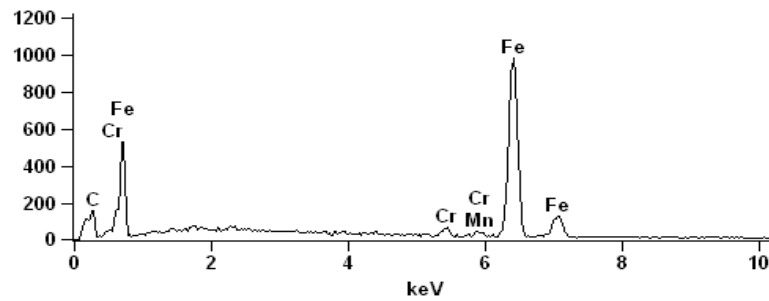
(a)



Full scale counts: 818 71655 8620 cleaned surface(1)_pt1



Full scale counts: 979 71655 8620 cleaned surface(1)_pt3



(b)

Figure 13 EDS results of pre-etched surface (a); and non-pre-etched surface (b) of coupon from condition 4

4. Discussion

4.1 Computational fluid dynamic study of gas flow

A computational fluid dynamic study is used to demonstrate the gas flow pattern within the furnace for different loading configurations. Geometry used in CFD for industrial integral quench furnace is demonstrated in figure 14. After stirring by the fan and flowing around the muffler, gas stream flows into the hot chamber through 3 columns by 10 rows of bottom vents. Charging trays are stacked on top of middle 8 rows of vents. To maximize production efficiency, traditionally, components are densely packed in trays. Demonstrated in fluid dynamic prediction of gas velocity at longitudinal cross section in figure 15(a), it is showing that the velocity vectors through trays are very slow compare to the other parts within the furnace. The slow gas velocity leads to thick boundary layer at the near surface thus results in slow diffusion within it. Meanwhile, in figure 15(b), the gas velocity vectors at lateral cross section prefer spreading out of the charging tray to going through them. Therefore, less carbon resource and non-uniform gas stream are provided to the parts in trays, leading to slow carburizing rate and non-uniform carburizing effect between top and bottom sides on components, and average hardness deviations among trays.

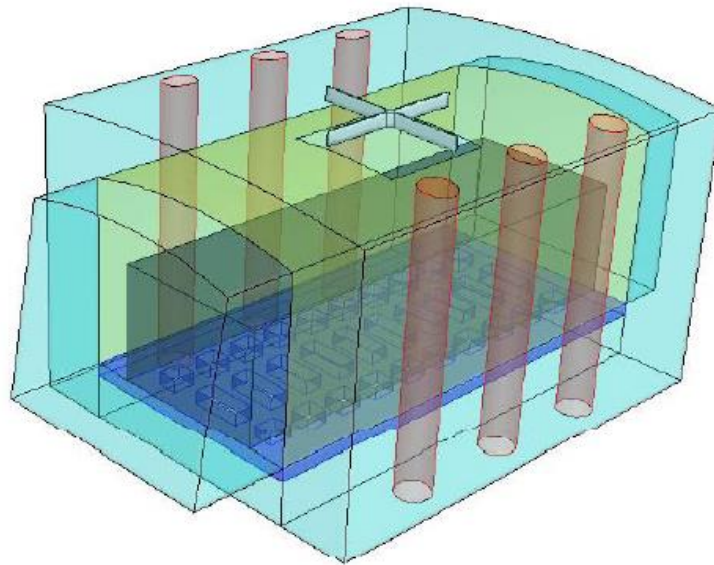
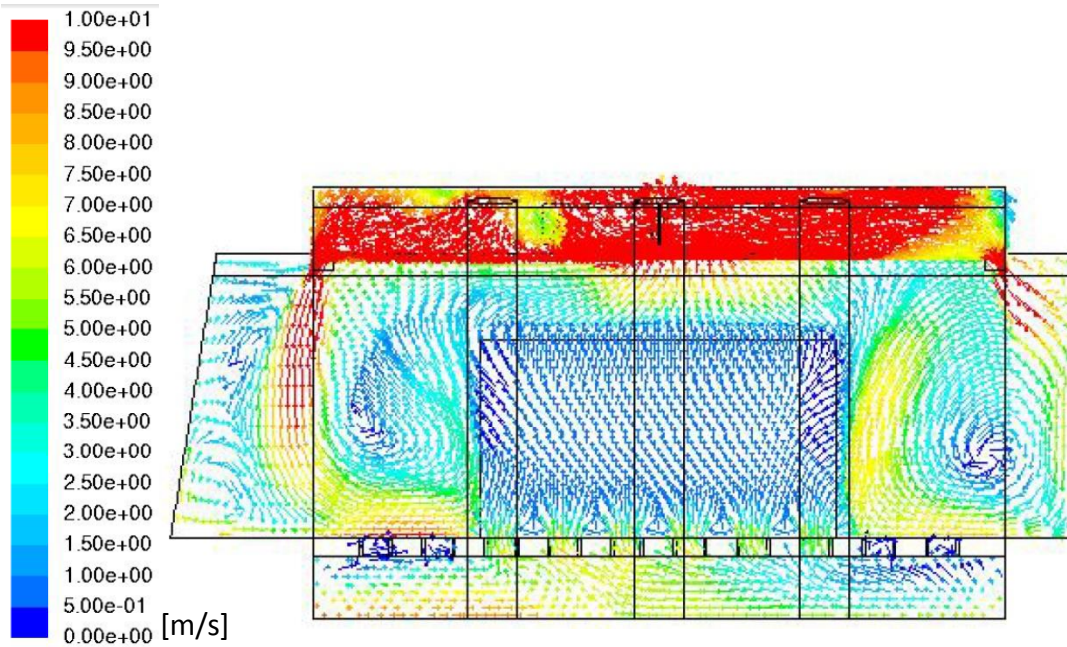
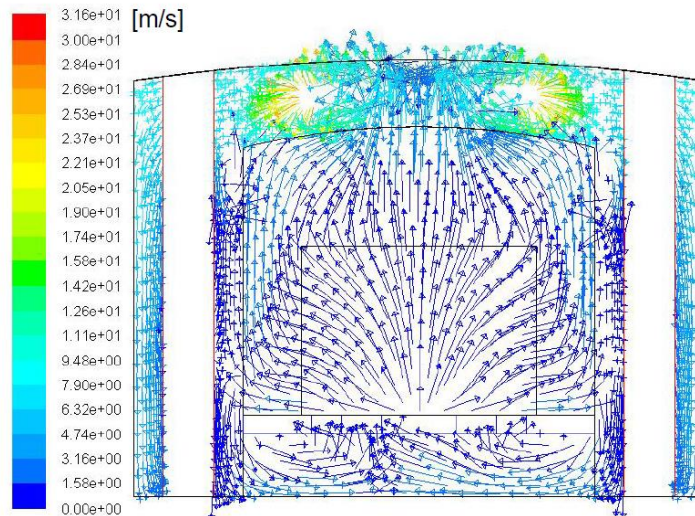


Figure 14 Geometry of industrial integral quench furnace used in CFD modeling



(a)



(b)

Figure 15 Computational fluid dynamic model showing gas velocity vectors through trays (200scfh, 1.5% C3H8), (a) cross sectional; (b) lateral; assuming homogeneous resistance throughout the tray volume, horizontal resistance as 60% packed, vertical resistance as 80% packed

To have more gas stream introduce into trays, the center channel design is considered. Two ends of each channel are covered by solid stainless steel sheet, as well as the top of the channel in top tray. Different configurations of this design are listed in table 4. Mass flow per unit metal at the open side borders of the corresponding tray in each model are

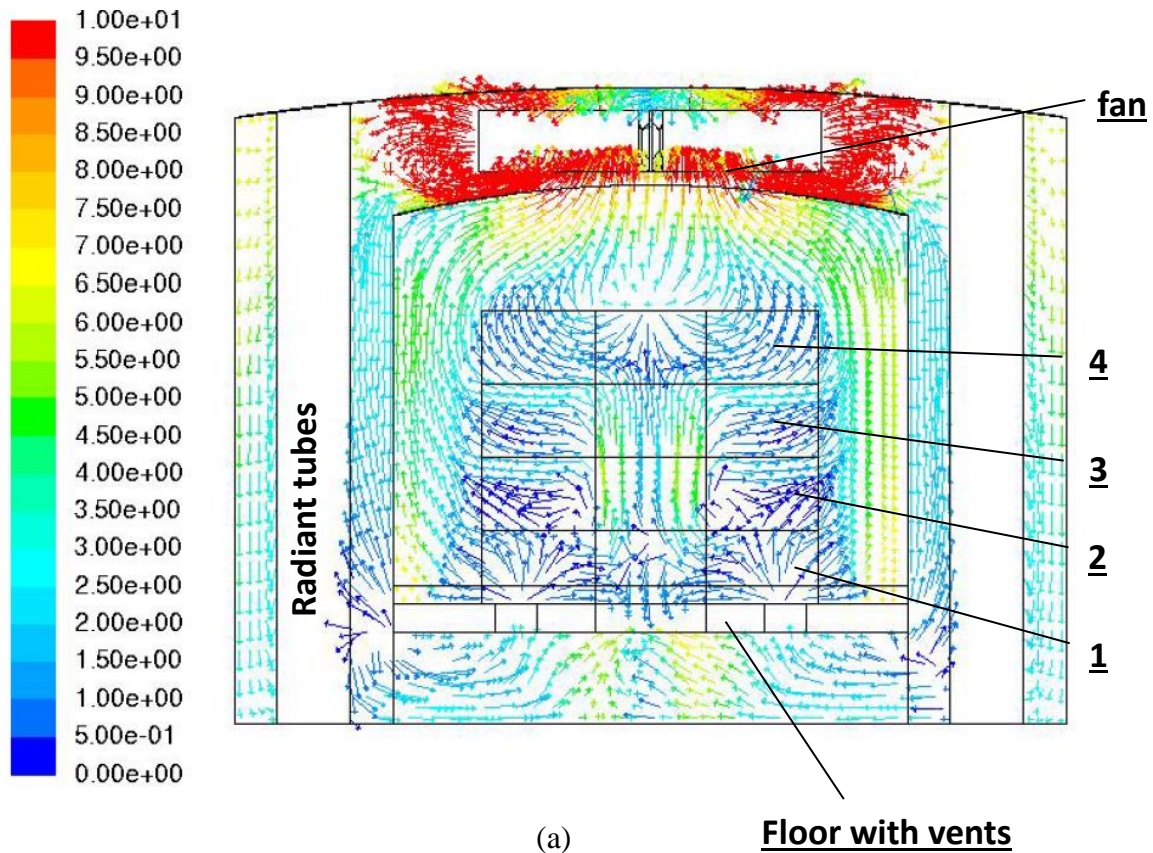
calculated from CFD simulation, from tray 1 to tray 4 are the trays from bottom to top respectively.

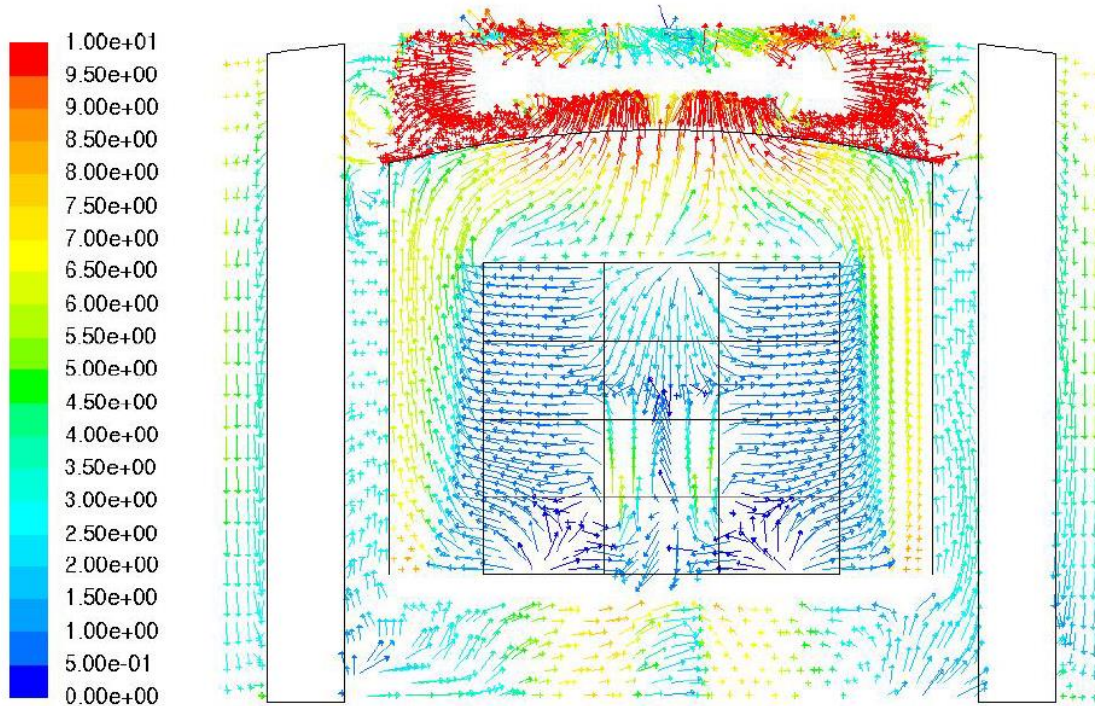
Table 4 Conditions of four center channel loading configurations

	Model 1 trays				Model 2 trays				Model 3 trays				Model 4 trays			
	1	2	3	4	1	2	3	4	1	2	3	4	1	2	3	4
Center channel width	a*				a				a				a		0.5a	
Packing height	Full				2/3 full		Full		Full				Full			
Top tray full metal cover	No				No				Yes				Yes			

* a equals to the width of middle column vents.

In model 1 and model 2 (figure 16(a)), most inflow from center vents escapes from top tray, most inflow from side vents escapes from bottom tray. Mass flow per unit metal difference between first 2 models is limited.





(b)

Figure 16 CFD simulation of center channel configuration model 2(a), and model 3 (b), showing gas velocity vectors (m/s)

However, with the introduction of entire top tray metal sheet cover in model 3, shown in figure 16(b), gas stream from the center vents flows into the center channel, forced by the top metal sheet cover, the part that escapes out from the top tray flows horizontally through each tray to achieve the uniform carburizing.

In table 5, uniformity of mass flow per unit metal in model 3 is largely improved with top metal sheet cover. In model 4, the channel in top tray is narrowed to $\frac{1}{2}$ width of channels in other tray, mass flow per unit metal at top tray is even further decreased, over corrected the improvement in model 3. Therefore, an intermediate design with $\frac{3}{4}$ width channel is utilized in industrial practice T4. In consequence, average hardness deviation among trays and hardness non-uniformity between parts top and bottom sides are improved as described in section 3.1, due to more uniform mass flow over trays and horizontal gas stream through each tray.

Table 5 Mass flow (kg/s) per kg-metal through trays of different center channel loading configurations calculated from CFD simulation

Gas kg/s per kg-metal	Model 1	Model 2	Model 3	Model 4
Tray 1	3.80E-04	3.30E-04	4.80E-04	5.00E-04
Tray 2	2.67E-04	4.00E-04	3.67E-04	3.84E-04
Tray 3	3.00E-04	7.41E-04	4.34E-04	4.46E-04
Tray 4	9.07E-04	8.74E-04	5.54E-04	3.77E-04

4.2 Mechanism of soot formation and deposition

In hydrocarbon atmosphere, a sequence of complex polymerization processes is involved, resulting in a variety of high molecular weight products [19], which is considered as polycyclic aromatic hydrocarbons (PAH). PAH may condense into liquid drops, even at high temperature, and deposits as tar, or maybe further carbonized in the gas to originate soot [23] in the form of spherical particles consisting of small crystallites [19].

In A2A carburizing, to preserve the advantages of vacuum carburizing but still keep production efficiency as in gas carburizing, components are inevitably touching each other, leading to the poorly carburized contact area (figure 7). In figure 17, gas flow in the crevice between two parts is stagnant, which increases the boundary layer thickness, lowers the diffusion of carbon resource from atmosphere to metal surface, slows down the carburizing rate and therefore results in less carburizing area. At the same time, a large amount of soot and tar are easily generated in the non-equilibrium atmosphere, deposit in the crevice area, and act as diffusion barrier for further diffusion of carbon source. Thus, soot control in atmosphere is an effective method to minimize the poorly carburized contact area and improve the carburizing evenness.

However, different from catalytic soot formation on top of cementite [14, 24] when austenite solubility has been reached, it is observed that soot forms at flow stagnant areas, and deposit on the dark perimeter where cementite is not formed, as shown in figure 8(e). It is speculated that it is pyrolytic carbon that will deposit on metal with or without the formation of cementite. This kind of carbon layer in vacuum carburizing has been reported to be fine crystalline graphite [25] and active hydrocarbons of different saturation degree [26, 27], which can constitute an additional carbon source [25-27].

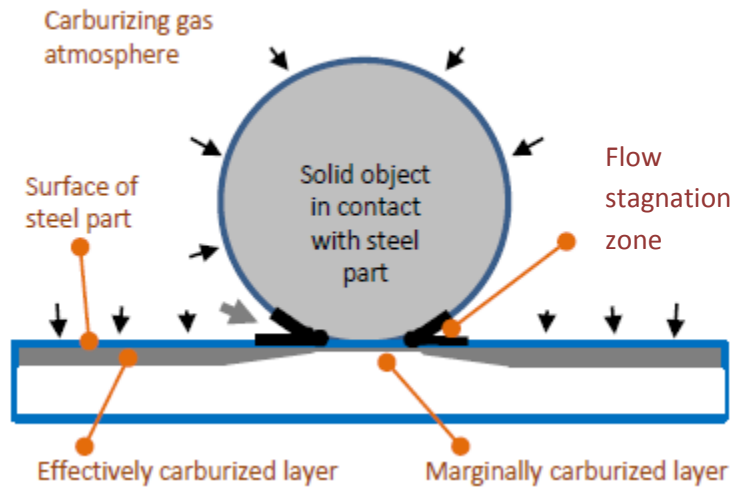


Figure 17 schematic of contacted area

To from less soot in atmosphere and on metal surface, but still keep adequate carburizing capability, a blend of nitrogen-methane-propane is taken, since propane and methane are relatively less expensive and available onsite at most of the heat treating shops. In table 6, it is showing more tendencies for decomposition and soot for propane due to more negative Gibbs free energy. Thus blend with methane gives more possibility to mitigate the soot but still provide carburizing ability under plasma activation.

Table 6 Gibbs free energy of CH₄ and C₃H₈ for one carbon atom formation at 927°C and 1atm

Reaction	ΔG (KJ/mol)
$CH_4 = C_{graphite} + 2H_2$	-23.11
$1/3C_3H_8 = C_{graphite} + 4/3H_2$	-67.13

Results of nitrogen-methane-propane blend tests are listed in table 7. Surface carbon concentration is calculated from offline software CarbTool©. Correlation of surface concentration and volume fraction of cementite in figure 18 indicates that in conditions from 1-4, cementite are formed at the surface as dispersed islands as shown in figure 13(b), with only a few volume percentage if local equilibrium has been reached. But in condition 5, the surface concentration is very low so it is still in the austenite region, thus,

no cementite is formed on surface. However, in figure 11(a), soot is observed on every tape regardless of the cementite formation.

Table 7 Calculated surface carbon concentration from flux on coupon for nitrogen-hydrocarbons blend tests

conditions	Inlet C3H8 (%)	Inlet CH4 (%)	Flux on coupon (10^{-7} g/cm ² /s)	Calculated surface carbon concentration (wt.%)
1	1.8	4	6.51	1.36
2	1.8	0	6.84	1.40
3	0.4	4	5.85	1.27
4	0.4	1	6.03	1.30
5	0.4	0	0.82	0.41

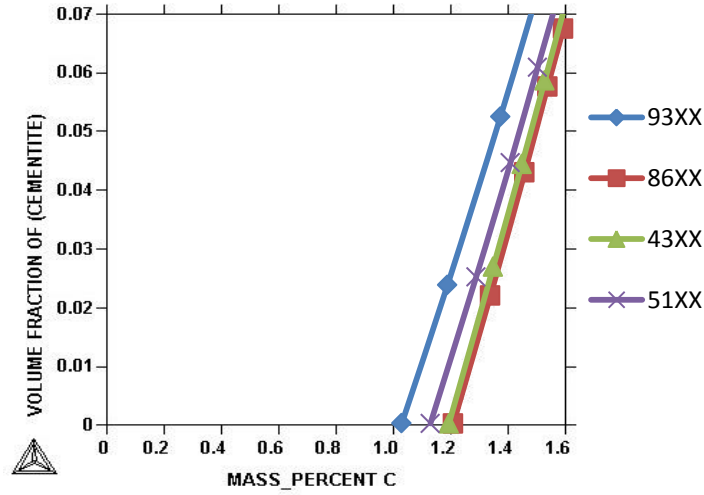


Figure 18 Volume fraction of cementite on AISI 93xx, 86xx, 51xx, 43xx at 930 °C and 1 atmosphere

Therefore, if soot or tar precipitates in the atmosphere, it will diffuse through the boundary and deposit on the metal surface, the deposition rate is affected by several factors as discussed in section 3.3. This type of soot can be removed with tape if the parts are cooled with furnace as the experimental condition, however, it will become a sticky layer attached on the surface when parts are quenched in oil, and leave the dark sooty areas. Atmosphere composition control is able to alleviate the pyrolytic soot or tar in the atmosphere (figure 10), increase the carburizing penetration depth into the contact area

(figure 11), minimize the marginally carburized area and thus improves the process quality.

In consequence, the following mechanism is proposed in figure 19. In non-equilibrium atmosphere at practical carburizing temperature, soot particles and PAH clusters precipitate easily from the gas phase just like snowflakes and would be easy to condensate on metal surface as a pyrolytic soot layer. The graphitic crystalline soot constitutes carbon resource. If the metal surface can absorb carbon fast enough, like many low-carbon steels, the carburizing is uninterrupted. When carbon atoms supersaturate in austenite matrix, and activity of carbon is larger enough to stabilize carbides, precipitates form at the grain boundary. Carbides and cementite is claimed to be catalytic to carbon deposition by many researchers [9, 10, 14, 17, 20]. When there are suitable nucleation sites are available, as shown in figure 13(a), the etched grain boundary, graphite nucleates and increases carbon activity larger than 1, then cementite becomes unstable and starts to decompose. The decomposed carbon atoms attach to the graphite plane and metal atoms migrate through graphite by gradient to the tip of the filament, agglomerating to the clusters and particles which act as catalysts for further carbon deposition [12], therefore elongate the graphite filaments. This type of carbon deposition of filaments has been reported as the major fraction of any catalytic carbon deposition [14-19], and on iron base alloys surface, it prefers forming in higher carbon hydrocarbons to forming in methane [20]. In consequence, in figure 12(a) without any active sites on metal surface, a large amount of carbon filaments is investigated on the surface of coupon from condition 1, which has much more propane than conditions 3-5; however, on the surface of coupons from conditions 3-5, only scattered bright spots are observed. When the grain boundary is etched before carburizing, the dissociative adsorption and dehydrogenation of hydrocarbons is promoted, providing active sites for graphite nucleation and filaments growth as shown in figure 13(a). But in figure 13(b), without active sites, only isolated carbides are observed in backscatter electron microscope image.

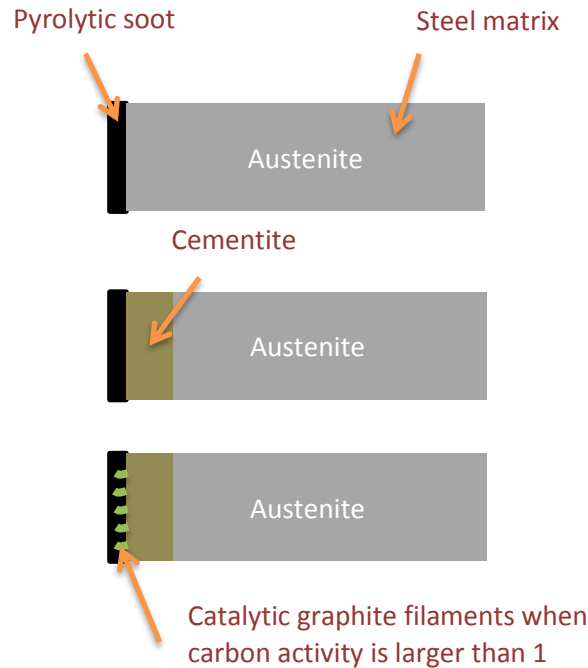


Figure 19 mechanism of soot deposition on metal surface and graphite filaments growth

5. Conclusion

A cold plasma injector has been developed and tested for activated nitrogen-methane/propane, one pressure atmosphere carburizing. It has been proven to be effective to eliminate intergranular oxides and promote carburizing process. The first industrial scale demonstrations confirmed its utility on retrofitting into industrial integral quench furnace. The boost-diffuse scheme is used as in low pressure carburizing furnace. The CFD study assisted center channel configuration modification improves the gas stream uniformity, therefore reduces the hardness deviation among stacked trays as well as carburizing unevenness between two sides on the components.

When the carbon source is excessive in the atmosphere, the soot formation mechanism is proposed in three steps: 1) soot particles and PAH formation in atmosphere; 2) pyrolytic soot deposition on metal surface, depending on the gas composition, hydrocarbons and hydrogen concentration ratio; 3) graphite filaments growth, depending on the conditions described above.

The nitrogen-hydrocarbons blend tests illustrate that in the condition with 0.4% propane and 1% methane, the optimized results has been achieved. In this condition, sufficient carbon flux has been obtained, but with least soot deposition on metal surface and in atmosphere. Meanwhile graphite filaments grown on metal surface are investigated, its formation is associated with hydrocarbons type, cementite/carbides formation and surface catalytic sites. Therefore, soot mitigation in atmosphere and on metal surface can be achieved by control of the gas composition. The carbon filaments elimination can be obtained by control of cementite formation and surface condition.

Acknowledgement

The authors would like to thank Mr. John Green for laboratory supports, Mr. Guido Plicht for industrial practices implementation and Air Products and Chemicals, Inc for funding, managing and permitting to publish this work. The continuous support from Center for Heat Treating Excellence at Worcester Polytechnic Institute is grateful acknowledged.

References

- [1] Wang, X., Zurecki, Z., and Sisson Jr., R. D., 2012, "*Development of Nitrogen-Hydrocarbon Atmospheric Carburizing and Process Control Methods*," Journal of Materials Engineering and Performance, DOI: 10.1007/s11665-012-0294-0.
- [2] YAGITA, K., and OHKI, C., 2010, "*Plasma Nitriding Treatment of High Alloy Steel for Bearing Components*," NTN TECHNICAL REVIEW, Vol.78, pp. 33-40.
- [3] Zhaoa, G., and et al., 2006, "*Methane Conversion in Pulsed Corona Discharge Reactors*," Chemical Engineering Journal, Vol.125, pp. 67-79.
- [4] Kado, S., and et al., 2004, "*Diagnosis of Atmospheric Pressure Low Temperature Plasma and Application to High Efficient Methane Conversion*," Catalysis Today, Vol.89, pp. 47-55.
- [5] Li, X., and et al., 2004, "*Methane Conversion to C2 Hydrocarbons and Hydrogen in Atmospheric Non-Thermal Plasmas Generated by Different Electric Discharge Techniques*," Catalysis Today, Vol.98, pp. 617-624.

- [6] Indarto, A., and et al., 2006, "Effect of Additive Gases on Methane Conversion using Gliding Arc Discharge," *Energy*, Vol.31, pp. 2986-2995.
- [7] Zurecki, Z., and Wang, X., 2009, "*Atmosphere carburizing using electric discharge-activated nitrogen-natural gas mixtures*," Proceedings of Heat Treating Conference and Exposition 2009, Indianapolis, IN.
- [8] Wang, X., 2011, "*Activated Atmosphere Case Hardening of Steels*," Dissertation, Worcester Polytechnic Institute .
- [9] Grabke, H. J., 1998, "*Thermodynamics, Mechanisms and Kinetics of Metal Dusting*," *Materials and Corrosion*, Vol.49, pp. 303-308.
- [10] Grabke, H.J., and Schütze, M., 2007, "*Corrosion by Carbon and Nitrogen - Metal Dusting, Carburisation and Nitridation*," Woodhead Publishing, pp. 331.
- [11] Grabke, H. J., and Muller-Lorenz, E. M., 1995, "*Effect of Sulfur on the Stability of Cementite*," *Steel Research*, Vol.66(6), pp. 254-258.
- [12] Grabke, H. J., 2002, "*Carburization, Carbide Formation, Metal Dusting, Coking*," *MATERIALI IN TEHNOLOGIJE*, Vol.36(6), pp. 297-305.
- [13] Wei, Q., Pippel, E., Woltersdorf, J., 1999, "*Microprocesses of Coke Formation in Metal Dusting*," *Materials and Corrosion*, Vol.50, pp. 628-633.
- [14] Young, D. J., and Zhang, J., 2012, "*Metal Dusting: Catastrophic Corrosion by Carbon*," *Journal of Minerals, Metals, and Materials Society*, Vol.64(12), pp. 1461-1469.
- [15] Horsley, G. W., and Cairns, J. A., 1984, "*The Inhibition of Carbon Deposition on Stainless Steel by Prior Selective Oxidation*," *Applications of Surface Science*, Vol.18, pp. 273-286.
- [16] Zhang, J., Boddington, K., and Young, D. J., 2008, "*Oxidation, Carburisation and Metal Dusting of 304 Stainless Steel in CO/CO₂ and CO/H₂/H₂O Gas Mixtures*," *Corrosion Science*, Vol.50, pp. 3107-3115.
- [17] Bonnet, F., Ropital, F., Berthier, Y., 2003, "*Filamentous Carbon Formation Caused by Catalytic Metal Particles from Iron Oxide*," *Materials and Corrosion*, Vol.54(11), pp. 870-880.

- [18] Toh, C. H., Munroe, P. R., Young, D. J., 2003, "*High Temperature Carbon Corrosion in Solid Oxide Fuel Cells*," *Materials at High Temperatures*, Vol.20(2), pp. 129-136.
- [19] Figueiredo, J. L., 1999, "*Reactivity of Coke Deposited on Metal Surfaces*," *Materials and Corrosion*, Vol.50, pp. 696-699.
- [20] Brown, A. M., and Hill, M. P., 1983, "*The characterization of carbon deposit morphologies using in situ scanning electron microscopy*," ACS Symposium Series, American Chemical Society: Washington, DC, pp. 193-222.
- [21] Ipsen, Inc., [Http://Www.Ipsenusa.Com/Index.Php](http://www.ipsenusa.com/index.php) .
- [22] Martin, P.M., 2010, "*Handbooks of deposition technologies for films and coatings (Third edition)*," Elsevier Inc., pp. 912-314.
- [23] Trimm, D.L., 1982, "*Progress in catalyst deactivation*," Martinus Nijhoff Publishers, The Hague .
- [24] Kula, P., 2005, "*Vacuum Carburizing—process Optimization*," *Journal of Materials Processing Technology*, Vol.164, pp. 876-881.
- [25] Gorockiewics, R., and Lapinski, A., 2010, "*Structure of the Carbon Layer Deposited on the Steel Surface After Low Pressure Carburizing*," *Vacuum*, 85, pp. 429-433.
- [26] Gorockiewicz, R., 2006, *Inżynieria Materiałowa*, 5(152), pp. 981-984.
- [27] Kula, P., Siniarski, D., Pietrasik, R., 2006, *Inżynieria Materiałowa*, 5(152), pp. 1092-1096.

Paper #4: Modeling of carbon distribution during atmosphere and low pressure carburizing processes (*published in Journal of Materials Engineering and Performance, Vol.22(1), 2013, DOI:10.1007/s11665-012-0353-6*)

Y. Wei, L. Zhang, R.D. Sisson, Jr.,

Center for Heat Treating Excellence, Worcester Polytechnic Institute, Worcester, MA, USA

yingyingwei@wpi.edu

(Submitted June 15, 2012)

(Footnote to go above the author info and special issue footnotes): This paper is an updated version of the 2011 HTS-Bodycote Best Paper in Heat Treating, which won the award under the title “Intelligent Heat Treating: Simulation of Carburization Process.” The ASM Heat Treating Society established the Best Paper in Heat Treating Award in 1997 to recognize a paper that represents advancement in heat-treating technology, promotes heat treating in a substantial way, or represents a clear advancement in managing the business of heat treating. The award, endowed by Bodycote Thermal Process-North America, is open to all students, in full time or part-time education, at universities (or their equivalent) or colleges. It also is open to those students who have graduated within the past three years and whose paper describes work completed while an undergraduate or post graduate student. The subject matter of the paper is required to cover any aspect of research or development applied to the fields of heat treatment, surface engineering, hot isostatic pressing (hip), metallurgical coatings, testing, or materials processing, including any production process, information technology, or relevant management or business issues.

Footnote: This article is an invited paper selected from presentations at the 26th ASM Heat Treating Society Conference, held October 31 through November 2, 2011, in Cincinnati, Ohio, and has been expanded from the original presentation.

Abstract

Heat treaters need an effective simulation tool to predict the carburization performance of a variety of steels. The tool is needed not only to predict the carbon profile but also to optimize the process in terms of the cycle time and the total cost. CarbTool© has been developed to meet these needs for gas and vacuum carburization. In this paper,

CarbTool© predictions were compared with industrial experimental results for three types of steels (AISI 8620, 5120, 4320), heat treated by both gas and vacuum carburizing processes. Based on the agreement of model predictions and experimental results, it is found that CarbTool© could be used to predict the carbon concentration profile for a variety of alloys in both gas and vacuum carburizing processes.

Keywords: Simulation, Gas carburizing, Vacuum carburizing, CarbTool©

1. Introduction

Carburizing media are divided into three kinds: liquid, solid carbonaceous compounds, and atmospheric. In both gas and vacuum carburization processes, the steel part is subjected to an atmosphere with high carbon potential.

The optimization of the industrial carburizing parameters is typically pursued by a trial and error method. In addition to being time consuming and expensive, this approach yields suboptimal results at best [1]. In this paper, effective gas and vacuum carburizing models are presented. The models may also be used to optimize the processes.

1.1 CarbTool© – Carburizing Simulation Tool

A simulation program has been developed by CHTE (Center for Heat Treatment Excellence) for the calculation of the carbon concentration profile during the gas and vacuum carburizing processes.

The solution algorithm used in CarbTool© is based on the finite difference method (FDM), and the code is developed using Microsoft Visual C++ in Window OS. The tool has been built on the concept of the carbon flux at the surface between the gas and steel is to be specified by the user. The outputs of CarbTool© are the carbon concentration distribution profile inside the steel part and the surface carbon concentration profile as a function of time.

Users input parameters about the carburization process, such as carburization temperature, carburizing time, and carbon potential or carbon flux. After a quick simulation the carbon profile along the distance below the surface can be plotted with the case depth labeled according to a user defined value.

CarbTool© has two modules – Gas carburizing and vacuum carburizing. The functions for each module are listed below:

1) Gas Carburization: variable operating temperature, constant mass transfer coefficient, variable carbon potential, single boost-diffuse process, data export of carbon profile at certain interval and final time, effective case depth indication at 0.35 wt.% carbon or other user defined condition.

2) Vacuum Carburization: variable operating temperature, constant flux process design, cementite transformation indication, cyclic and non-cyclic boost-diffuse process design, data export of carbon profile at certain interval and final time, effective case depth indication at 0.35 wt.% carbon or other user defined condition.

1.2 Gas Carburizing Model

Gas carburizing is a complex phenomenon which involves three distinct stages [3]: 1) carbon transport from the atmosphere to the steel surface, 2) surface reductive chemical reactions, and 3) diffusion of the absorbed carbon atoms towards the bulk of the steel down the chemical potential gradient. Total carbon transfer from the atmosphere to the steel is thus determined by the limiting process, which kinetically becomes the rate controlling stage of carburizing. Figure 1 shows the mechanisms of carbon transfer during carburizing and the primary control parameters: the mass transfer coefficient (cm/s) (β) defining carbon atoms flux ($\text{g/cm}^2/\text{s}$) (J) from the atmosphere to the steel surface and the coefficient of carbon diffusion in steel (D) at Austenizing temperatures [2].

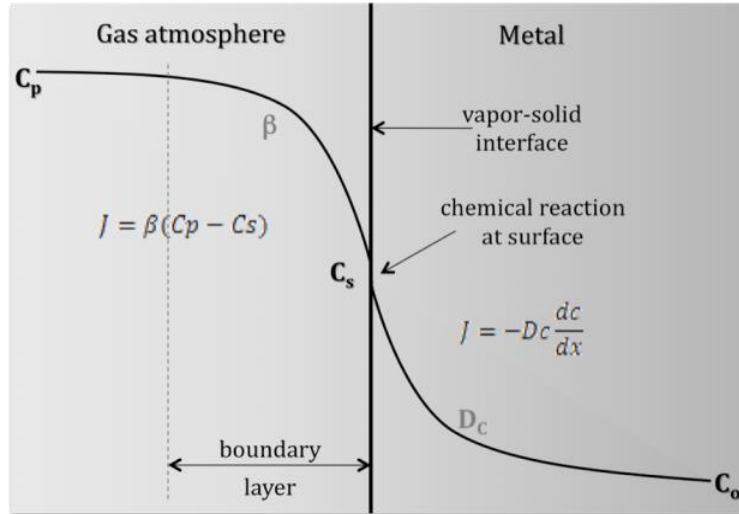


Fig. 1 Schematic of gas carburization process [2].

It appears that the carbon transport mechanism is well understood, however, experimental results have shown that actual carbon concentration curves often deviate from the predicted ones for different carburizing atmospheres. This suggests that knowledge of carbon potential and carburizing time are not sufficient for the process control, and requires a more complete understanding of β and D as a function of the process parameters for the successful control of the gas carburizing process [2].

The mass transfer coefficient in the gas phase is an important parameter especially in the initial stage of carburizing. It determines the thickness of the boundary gas layer at the gas-solid interface and defines the maximum flux of carbon atoms from the surface towards the bulk of specimen. It is very sensitive to atmosphere composition, gas flow parameters, temperature, etc. Many mass transfer models have been investigated by several authors [4-8]. Munts and Baskakov [4] measured β ranging from $2 \cdot 10^{-5}$ to $2 \cdot 10^{-4}$ cm/s at 800-1000 °C. β values varied with carburizing temperature and C_p in the atmosphere. However, once C_p approaches the near-solubility limit in Austenite with carbon content greater than 0.5 wt. %, the value of β becomes consistent with temperature and has little relation with gas compositions [4].

The carbon potential of the carburizing atmosphere is set as boundary condition to define the physical problem. The mass balance of the steel is

$$\beta(C_p - C_s) = -D_c \frac{dc}{dx} \quad (1)$$

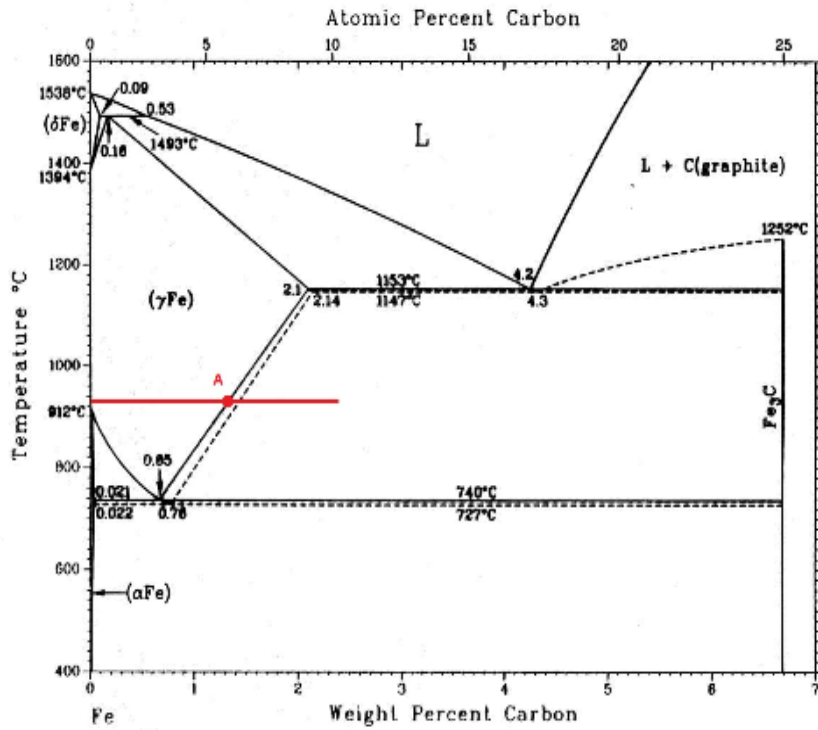
1.3 Vacuum Carburization Model

In vacuum carburizing, a small quantity of hydrocarbon gas (i.e. C_2H_2 , C_6H_{12}) is added to a vacuum furnace. The addition reacts in the atmosphere and may never reach equilibrium. Also, in some cases soot may form. Therefore, the mass balance boundary condition is not applicable for this process. However, a constant surface flux can be used. It is assumed that the amount of carbon produced by the surface reactions is equal to the mass flow rate for diffusion described by Fick's first law.

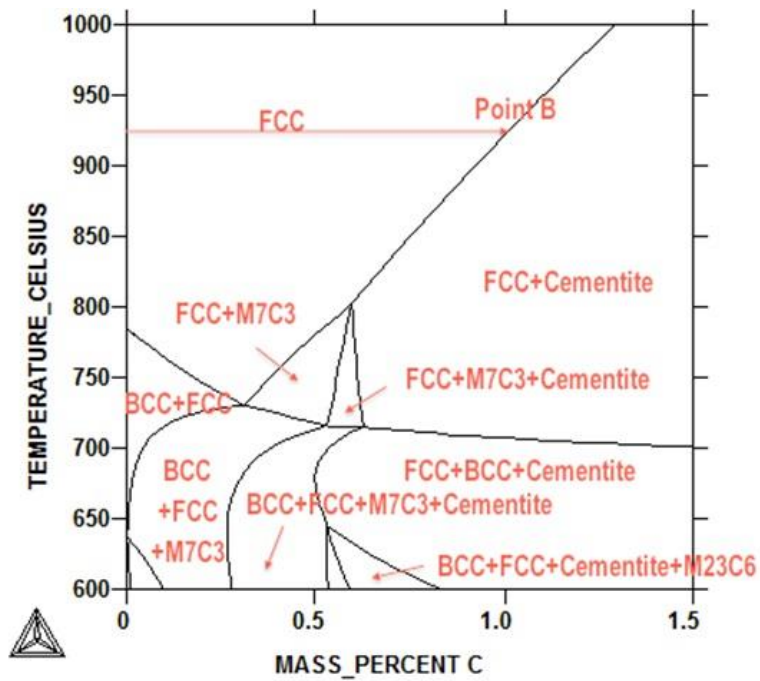
$$J|_{x=0} = -D|_{x=0} \cdot \frac{dC}{dx}|_{x=0} \quad (2)$$

where $x=0$ at the gas-steel surface.

During vacuum carburizing, depends on the decomposition rate of hydrocarbon additions, the surface carbon concentration can reach the Austenite solubility limit quickly and easily due to the high carbon flux and then form carbides. In plain carbon steel, cementite will start forming at 1.3 wt.% carbon (point A) at 925 °C, as shown in Figure 2 (a). On 93 series alloy steel, the saturation point is reached at 1.03 wt.% carbon (point B) at the same temperature due to the alloy compositions, mostly because of Cr, which facilitates carbides formation, as shown in Figure 2 (b).



(a)



(b)

Fig. 2 Fe-Fe₃C phase diagram (a) and 93xx isopleth diagram (b).

Current commercial carburization simulation software does not consider the formation of carbides on the steel surface [10]. When surface carbon concentration of 93xx steel is plotted as a function of time during carburizing process, the surface carbon concentration will increase beyond the solubility limit, as seen in Figure 3. But in reality, the steel will start to form cementite at 1.03 wt.% carbon (as seen in Figure 4). Therefore in simulation it is necessary to consider the maximum solubility of carbon in Austenite, otherwise, the formation of carbides will not be considered, carburizing model calculation after formation of carbides will be affected, and finally lead to a discrepant result. CarbTool© indicates at which carbon concentration cementite will start to form, and shows the cementite volume fraction along with increasing total carbon content. In this case, cementite formation in processes can be controlled.

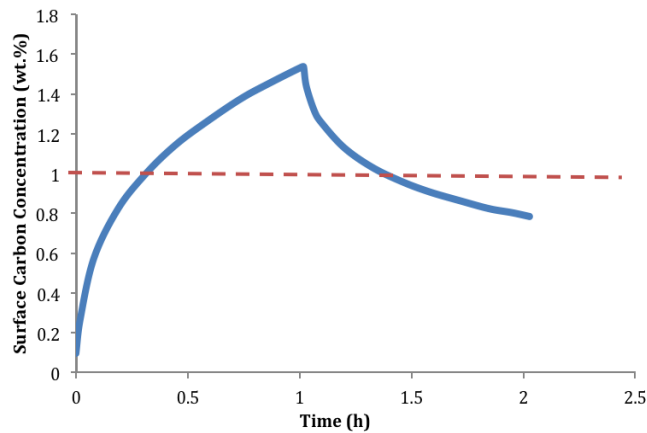


Fig. 3 Output of carbon concentration as the function of time of single boost and diffuse vacuum carburizing

To determine the Austenite maximum carbon solubility, ThermoCalc was utilized to draw the diagram of mole fraction of cementite for alloys. The diagram for 93xx, 86xx, 51xx, 43xx and 10xx was drawn and presented in Figure 4. As seen in Figure 4, the carbon solubility of 93xx is the least, approximately at 1.0 wt. % carbon, while the limits of other alloys are larger, which is corresponding to the decreasing Cr percentage in the alloys.

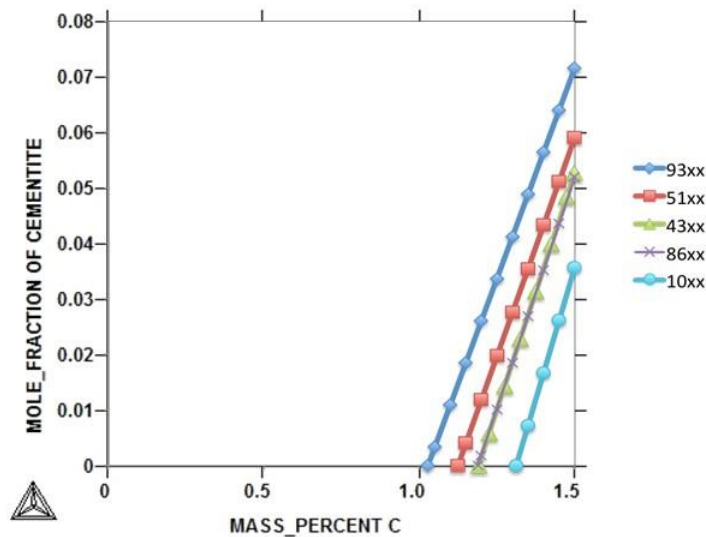


Fig. 4 Mole fraction diagram of AISI 93xx, 86xx, 51xx, 43xx and 10xx.

2. Experimental Procedure

In a current case, comparable carbon profiles for a series of steels are required for fatigue testing. These profiles need to be achieved by gas carburizing in endothermic gas as well as vacuum carburizing in cyclohexane. The modeling was used to design and revise the process parameters to achieve the same surface carbon concentration and effective case depth.

Three materials listed in Table 1 were chosen, which need to obtain the same carbon distribution after both gas and vacuum carburizing.

Table 1 Chemical Composition (wt %) of alloys at room temperature

	C	Cr	Fe	Mn	Mo	Ni	P	S	Si
8620	0.18 – 0.23	0.40 – 0.60	Bal.	0.70 – 0.90	0.15 – 0.25	0.40 – 0.70	0 – 0.035	0 – 0.040	0.15 – 0.30
5120	0.17 – 0.22	0.70 – 0.90	Bal.	0.70 – 0.90	0	0	0 – 0.035	0 – 0.040	0.15 – 0.30
4320H	0.17 – 0.23	0.35 – 0.65	Bal.	0.40 – 0.70	0.20 – 0.30	1.55 – 2.00	0 – 0.035	0 – 0.040	0.15 – 0.30

The objective of carbon profiles is to achieve the surface carbon to 0.80 ± 0.05 wt. % for 8620 and 5120, 0.70 ± 0.05 wt.% for 4320, as well as effective case depth to $0.035''$

(0.889mm) at C=0.35 wt. %, for both gas carburizing and vacuum carburizing. Rod specimen with 76.2 mm length and 9.525 mm diameter was used. Figure 5 shows the geometry of the specimen. Gas carburizing and vacuum carburizing process parameters are designed by CarbTool©.

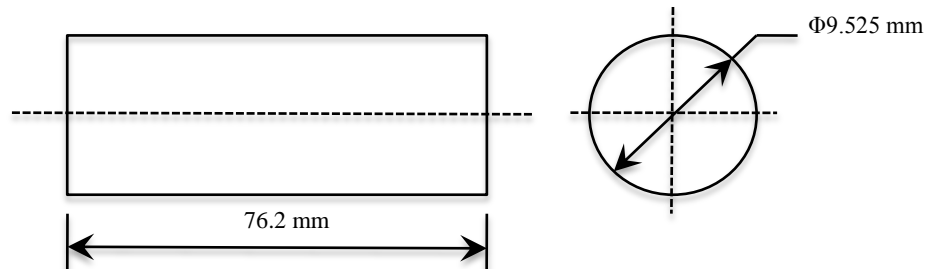


Fig. 5 Geometry of sample

Test samples were gas carburized in an industrial furnace using a boost and diffuse method. The heat treating process is to heat up to 1700 °F and hold in endothermic gas at a higher carbon potential, then hold it at the same temperature at a lower carbon potential as transition step, the diffuse step keeps samples at 1550 °F at the lower carbon potential, and followed by quench to room temperature. Figure 6 presents the process schematic. Listed in Table 2 are detailed process parameters for gas carburizing.

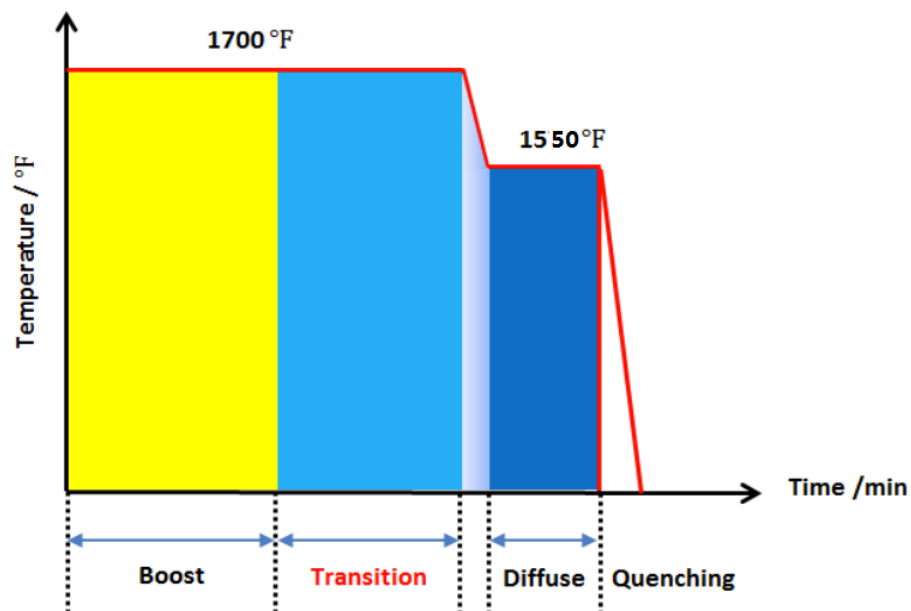


Fig. 6 Process schematic of gas carburizing

Table 2 Process parameters for gas carburizing

Steel	Carbon potential (%)	Time (min)	Carbon potential (%)	Time (min)	Carbon potential (%)	Time (min)
8620	1.10	175	0.85	75	0.85	30
5120	1.10	180	0.85	75	0.85	30
4320	1.10	156	0.70	90	0.70	30

The steps for vacuum carburizing is consisting of two boost-diffuse cycles at 1700 °F, followed by a transition cooling to lower the temperature and hold at 1575 °F, then quenched to room temperature, as presented in Figure 7. Table 3 is the process parameters for vacuum carburizing.

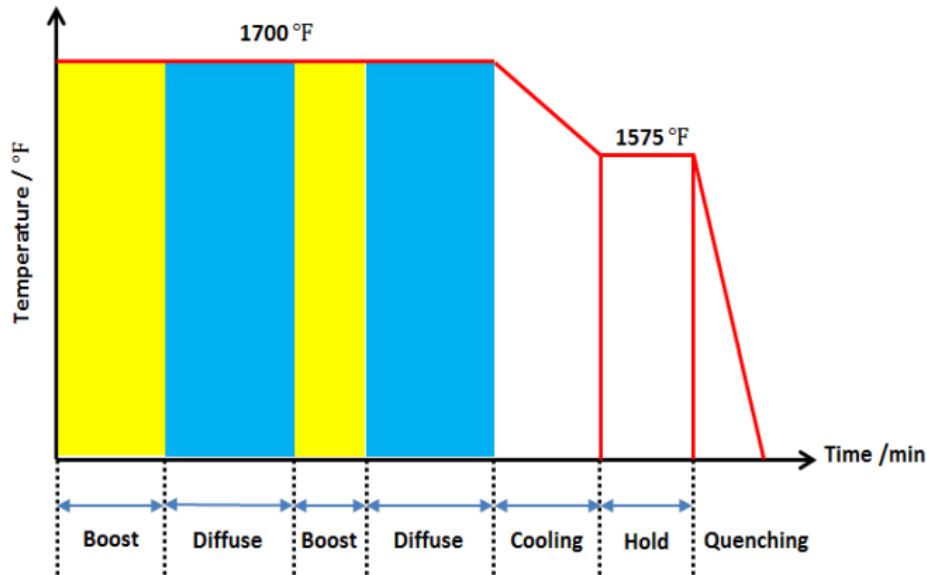


Fig. 7 Process schematic of vacuum carburizing

Table 3 Process parameters for vacuum carburizing

	Carbon flux (g/cm ² /s)	1st Boost (min)	1st Diffuse (min)	2nd Boost (min)	2nd Diffuse (min)	Cooling (min)	Hold (min)
8620	7.42E-07	66	59	0.0	0.0	60	20
5120	5.36E-07	91	57	0.0	0.0	65	20
4320	1.09E-06	28	60	11	72	35	20

Optical Emission Spectrometer (OES) was performed to measure the carbon-depth profiles of carburized parts.

3. Results and discussion

3.1 Gas Carburizing in endothermic gas

CarbTool© was used to simulate the process. For different materials, carbon potential and process time are set separately.

Figure 8 and Figure 9 presented the simulation results. Figure 8 presents the surface carbon concentration as a function of process time. CarbTool© also provides simulation results of carbon profiles after boost and diffuse steps, as shown in Figure 9,

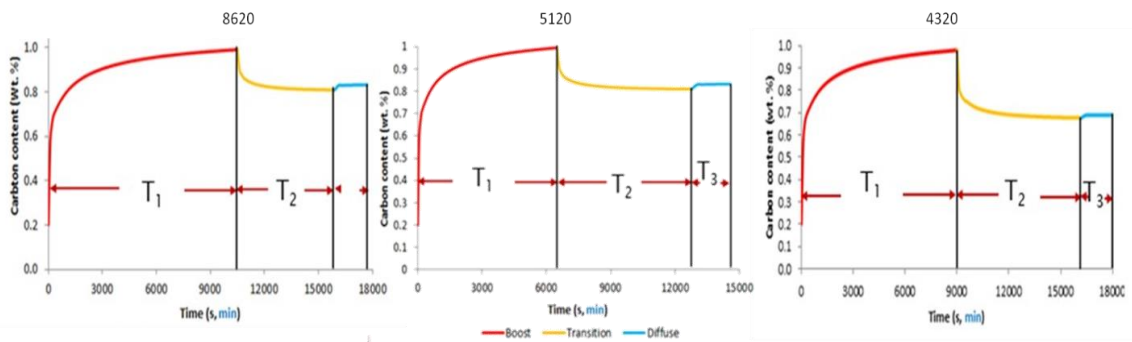


Fig. 8 Surface carbon concentration changes along with carburizing time on 8620, 5120 and 4320.

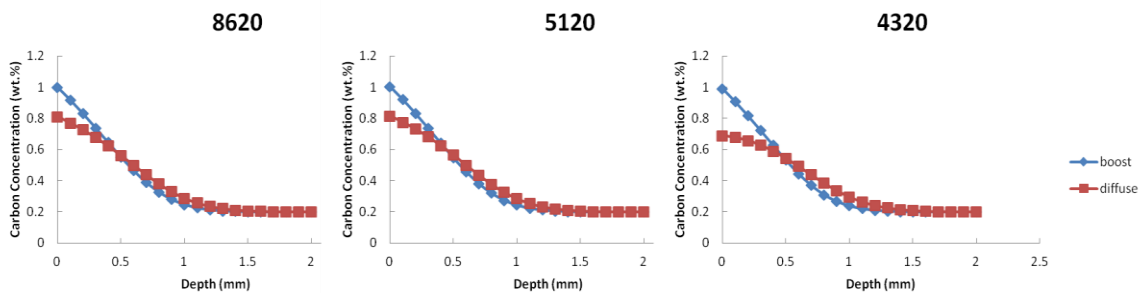


Fig. 9 Carbon profiles after boost step and diffuse step on 8620, 5120 and 4320.

The simulation was calculated by inputting parameters of boost-diffuse cycles. Figure 10 presents the experimental results and model predictions from CarbTool©. Experimental results of all three alloys, the surface carbon concentration and effective case depth, meet the specification within the range, as listed in table 4.

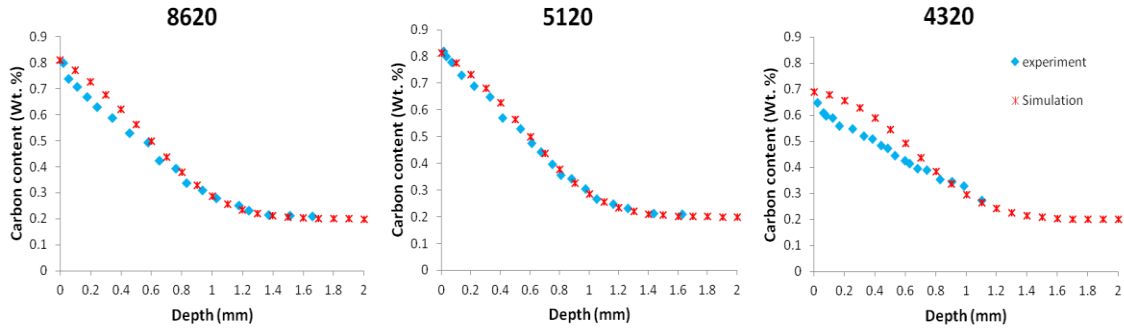


Fig. 10 Comparison between experimental and predicted carbon profiles from gas carburizing of 8620, 5120 and 4320.

Table 4 Gas carburizing results comparison between experiments and prediction

		8620	5120	4320
Surface Carbon (wt.%)	Target	0.8±0.05		0.7±0.05
	Experiment	0.80	0.82	0.65
	Simulation	0.83	0.83	0.69
Effective Case Depth (mm)	Target	0.889±0.05		
	Experiment	0.82	0.84	0.87
	Simulation	0.89	0.89	0.89

3.2 Vacuum Carburizing in Cyclohexane (C₆H₁₂)

As mentioned earlier, flux is the boundary condition in vacuum carburizing model, which is the counterpart of carbon potential in gas carburizing model. Flux was calculated based on directed integration of carbon profiles from industrial experience data, which is similar but not identical to the vacuum carburizing process preceded in this experiment. The equation below was used,

$$J = \frac{\int_0^{x=C_0} f(x)}{A \cdot t} \quad (3)$$

In which, x is depth, f(x) is the carbon concentration as a function of depth, C₀ is initial carbon content in bulk material, A is surface area, t is total boost time.

The calculated flux was input into CarbTool©; other carburizing parameters (temperature, time and dimension) were kept the same with industry process. Experimental and predicted carbon profiles were compared in Figure 11. This is minor

discrepancy between experimental result and prediction. During the process, flux is not a constant. It changes with variable factors, alloy compositions, furnace construction, pressure, different cycle combinations and etc. Thus, the calculated flux from different process design will provide a roughly range of how much carbon will diffuse into the surface of steel. At the same temperature and within the same boost stage, with the carbon accumulation at the surface of steels, flux changes with carbon content. In despite of the same total boost process time, the different cycle combinations will lead to different final carbon concentration profiles. Therefore, in practical vacuum carburizing process design, experience flux data could be used as a reference to predict the rough carbon profile. Desired carbon-depth profiles could be achieved by subtly adjusting the process parameters.

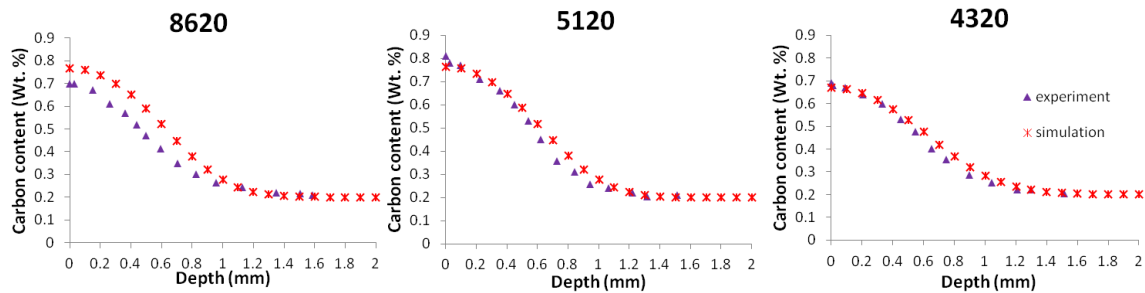


Fig. 11 Comparison between experimental and predicted carbon profiles from vacuum carburizing of 8620, 5120 and 4320.

3.3 Gas carburizing and vacuum carburizing results comparison

The experimental carbon profiles from both gas carburizing and vacuum carburizing are compared in Figure 12. These two processes generated comparable carbon-depth profiles.

4. Conclusion

The modeling tool, CarbTool©, was used to predict both gas and vacuum carburizing. It is very effective in creating carburized case with comparable carbon distribution. These effective models saved time and money over a variety of experimental trials. Carburization modeling will assist heat treaters to better understand the effects of process parameters on the diffusion process, distribution of carbon concentration, and effective case depth, as well as give engineers the possibility of optimizing the material, process

and design for achieving the optimum performance.

Acknowledgments

The support of the Center for Heat Treating Excellence (CHTE) at Worcester Polytechnic Institute and the member companies is gratefully acknowledged. The author would thank Timken Inc. for providing the raw materials and supporting in this work. The carburization heat treatments were administrated by Mr. Ben Bernard and Mr. Ralph Poor of Surface Combustion, Inc. Their support through facilities and experimental work is greatly appreciated.

References

- [1] Sahay, S.S., "Cost Model Based Optimisation of Carburising Operation", *Surf. Eng.*, 2004, Vol. 20 No. 5, pp. 379.
- [2] Karabelchtchikova, O., "Fundamentals of Mass Transfer in Gas Carburizing", Ph.D. Dissertation, Worcester Polytechnic Institute, 2007.
- [3] Karabelchtchikova, O., "Carburization Process Modeling and Sensitivity Analysis using Numerical Simulation", *MS&T '06: Materials Science and Technology 2006 Conference and Exhibition*, 2007.
- [4] Munts, V.A. et al, "Rate of Carburizing of Steel", *Met. Sci. Heat Treat.* Vol. 22, No. 5-6 (1980), pp. 358-360.
- [5] Stolar, P. et al, "Kinetics of Transfer of Carbon from Carburising and Carbonitriding Atmospheres", *Metallic Materials*, Vol. 22, No. 5(1984), pp. 348-353.
- [6] Rimmer, K. et al, "Surface Reaction Rate in Gas Carburizing", *Haerterei-Technische Mitteilungen*, Vol. 30, No. 3(1975), pp. 152-160.
- [7].Raic, K. T. "Control of Gas Carburizing by Diagram Method." *Scand. J Metall.*, Vol. 22(1993), pp. 50-54.

[8] Munts, V. A. et al, "Mass Exchange in Carburization and Decarburization of Steel" *Met. Sci. Heat Treat.* Vol. 25, No. 1-2(1983), pp. 98-102.

[9] American society for metals, *Metals Handbook, Volume 8: Metallography, Structures and Phase Diagrams. 8th Edition*, 1973, pp. 236,275,276

[10] Kula, P. et al, "Vacuum carburizing - process optimization", *13th International Scientific Conference on Achievement in Mechanical and Materials Engineering*, 2005, Poland.

Paper #5: Intelligent Heat Treating: Simulation of Carburization Process
(published in Proceedings of the 26th ASM Heat Treating Society Conference, Cincinnati, OH, Nov 2011, pp. 91-98)

Y. Wei, G. Wang, R.D. Sisson, Jr.,

Center for Heat Treating Excellence, Worcester Polytechnic Institute, Worcester, MA, USA

yingyingwei@wpi.edu

B. Bernard, R. Poor

Surface Combustion, Inc. Maumme, OH, USA

Keywords: Modeling, Gas carburizing, Vacuum carburizing, CarbTool©

Abstract

Heat treaters need an effective simulation tool to predict the carburization performance of a variety of steels. The tool is needed not only to predict the carbon profile but also to optimize the process in terms of the cycle time and the cost. CarbTool© has been developed to meet these needs for gas and vacuum carburization. In this paper, CarbTool© predictions were compared with industrial experimental results of four types of steels, heat treated by both gas and vacuum carburizing processes. Based on the excellent agreement of model predictions and experimental results, CarbTool© may be used to predict the carbon concentration profile for a variety of alloys in both gas and vacuum carburizing processes.

Introduction

Carburizing media are divided into three kinds: liquid, solid carbonaceous compounds, and atmospheric. In both gas and vacuum carburization processes, the steel part is subjected to an atmosphere with high carbon potential.

The optimization of the industrial carburizing parameters is typically pursued by a trial and error method. In addition to being time consuming and expensive, this approach yields suboptimal results at best [1]. In this paper, effective gas and vacuum carburizing models are presented. The models may also be used to optimize the processes.

Carburizing Modeling

In this section carburization models for gas carburizing and vacuum carburizing processes developed at CHTE (Center for Heat Treatment Excellence) are presented and discussed.

CarbTool© – Carburizing Simulation Tool

A simulation program has been developed by CHTE for the calculation of the carbon concentration profile during the carburizing processes.

The solution algorithm used in CarbTool© is based on the finite difference method (FDM), and the code is developed using Microsoft Visual C++ in Window OS. The tool has been built so that the carbon flux at the surface between the gas and steel is to be specified by the user [2]. The outputs of CarbTool© are the carbon concentration distribution profile inside the steel part and the surface carbon concentration profile as a function of time.

Users input parameters about the carburization process, such as carburization temperature, carburizing time, and carbon potential or carbon flux. After a quick simulation the carbon profile along the distance below the surface can be plotted with the case depth labeled according to a user defined value.

CarbTool© has two modules – Gas carburizing and vacuum carburizing. The functions for each module are listed below:

1) Gas Carburization

Variable operating temperature;

Constant mass transfer coefficient;

Variable carbon potential;

Single boost-diffuse process;

Data export of carbon profile at certain interval and final time;

Effective case depth indication at 0.35 wt.% carbon or other user defined condition.

2) Vacuum Carburization

Variable operating temperature;

Constant flux process design;

Cementite transformation indication;

Cyclic and non-cyclic boost-diffuse process design;

Data export of carbon profile at certain interval and final time;

Effective case depth indication at 0.35 wt.% carbon or other user defined condition.

Gas Carburizing Model

Gas carburizing is a complex phenomenon which involves three distinct stages [3]: 1) carbon transport from the atmosphere to the steel surface, 2) surface reductive chemical reactions, and 3) diffusion of the absorbed carbon atoms towards the bulk of the steel down the chemical potential gradient. Total carbon transfer from the atmosphere to the steel is thus determined by the limiting process, which kinetically becomes the rate controlling stage of carburizing. Figure 1 shows the mechanisms of carbon transfer during carburizing and the primary control parameters: the mass transfer coefficient (β) defining carbon atoms flux (J) from the atmosphere to the steel surface and the coefficient of carbon diffusion in steel (D) at Austenizing temperatures [2].

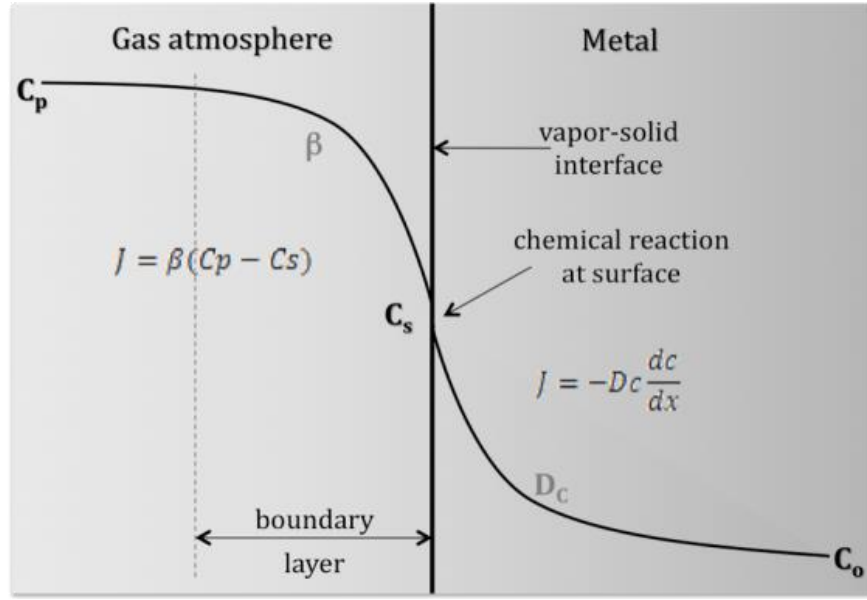


Fig. 1 Schematic of gas carburization process [2].

Mass Transfer Coefficient

A constant value for the mass transfer coefficient is applicable for most cases since once the carbon potential approaches the near-solubility limit in Austenite with carbon content greater than 0.5 wt.%, the value of β becomes consistent with temperature and has little relation with gas compositions [5].

The carbon potential of the carburizing atmosphere is set as the boundary condition to define the physical problem. The mass balance of the steel is

$$\beta(C_p - C_s) = -D_c \frac{dc}{dx} \quad (1)$$

Vacuum Carburization Model

Boundary Conditions

In vacuum carburizing, a small quantity of hydrocarbon gas (i.e. C_2H_2 , C_6H_{12}) is added to a vacuum furnace. The addition creates a very high carbon potential. In fact, in some cases soot may form. Therefore, the mass balance boundary condition is not applicable for this process. However, a constant surface flux can be used. It is assumed that the

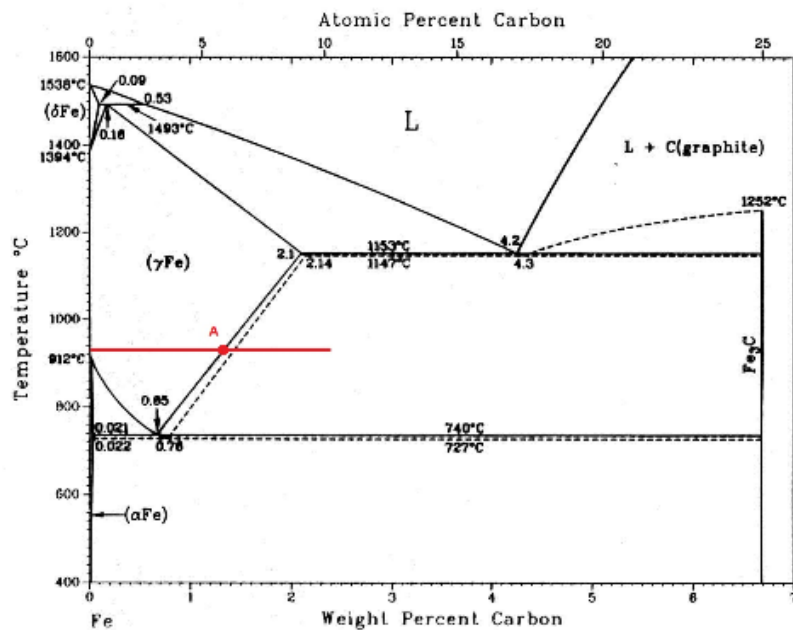
amount of carbon produced by the surface reactions is equal to the mass flow rate for diffusion described by Fick's first law.

$$J|_{x=0} = -D|_{x=0} \cdot \frac{dC}{dx}|_{x=0} \quad (2)$$

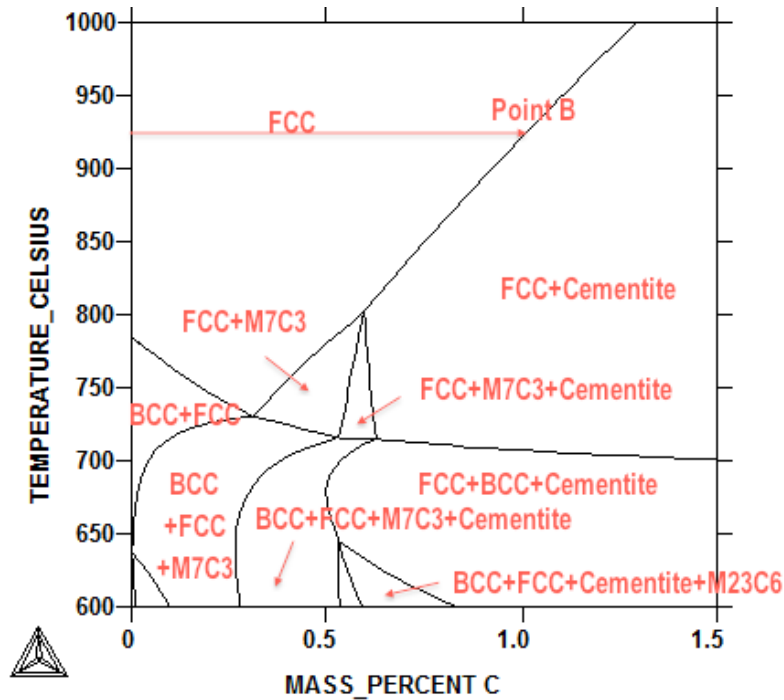
where $x=0$ at the gas-steel surface.

Process Control – Surface Carbon Saturation

During vacuum carburizing, the surface concentration of carbon can exceed the Austenite solubility limit due to the high carbon flux and might form carbides [5,6]. In plain carbon steel, cementite will start forming at 1.3 wt.% carbon (point A) at 925 °C, as shown in Figure 2 (a). In alloy steel, the saturation point is reached at 1.0 wt.% carbon (point B) at the same temperature, as shown in Figure 2 (b).



(a)



(b)

Fig. 2 Fe-Fe₃C phase diagram (a) and 93xx isopleth diagram (b).

Current commercial carburization simulation software does not consider the formation of carbides on the steel surface [8]. When surface carbon concentration of 93xx steel is plotted as a function of time, the surface carbon concentration will increase beyond the solubility limit, as seen in Figure 3. But in reality, the steel will start to form cementite at 1.03 wt.% carbon (as seen in Figure 4). Therefore in simulation it is necessary to consider the maximum solubility of carbon in Austenite, otherwise, the formation of carbides will not be identified. CarbTool© indicates at which carbon concentration cementite will start to form, and shows the cementite volume fraction along with increasing total carbon content. In this case, cementite formation in processes can be controlled.

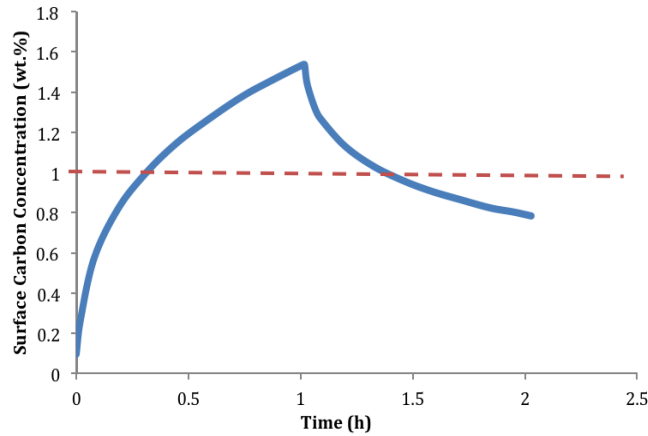


Fig. 3 Output of carbon concentration as the function of time of single boost and diffuse vacuum carburizing

To determine the Austenite maximum carbon solubility, ThermoCalc was utilized to draw the diagram of mole fraction of cementite for alloys. The diagram for 93xx, 86xx, 51xx, 43xx and 10xx was drawn and presented in Figure 4. As seen in Figure 4, the carbon solubility of 93xx is the least, approximately at 1.0 wt. % carbon, while the limits of other alloys are larger.

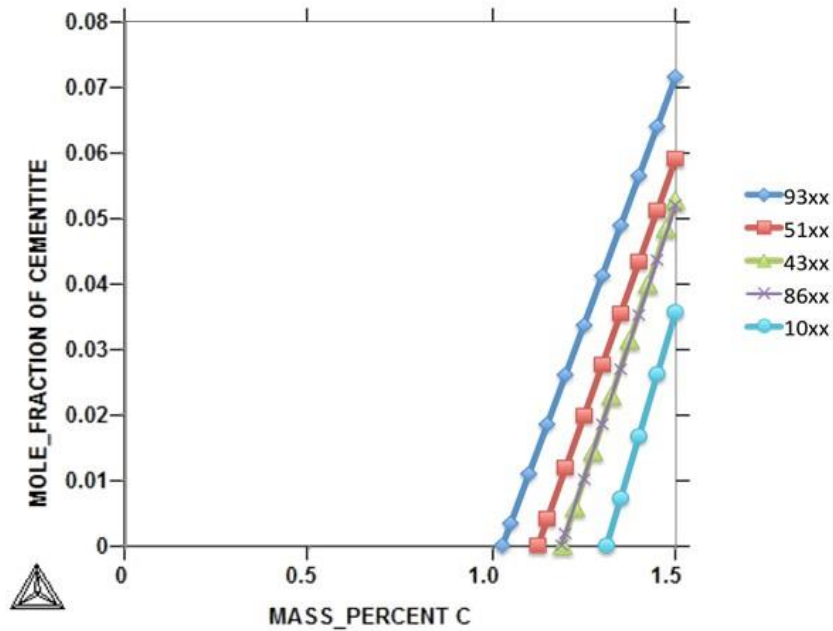


Fig. 4 Mole fraction diagram of AISI 93xx, 86xx, 51xx, 43xx and 10xx.

Case Study

In a current case, identical carbon profiles for a series of steels are required for fatigue testing. These profiles need to be achieved by gas carburizing as well as vacuum carburizing in cyclohexane. The modeling was used to revise the processes to achieve the same surface carbon concentration and effective case depth.

Carburizing Samples

Chemistry

Four materials were chosen, which need to obtain the same carburized properties after both gas and vacuum carburizing. Table 1 is the chemistry (AISI and UNS) of each steel.

Table 1 Chemical Composition (wt %) at room temperature

	C	Cr	Fe	Mn	Mo	Ni	P	S	Si
9310	0.08 – 0.13	1.00 – 1.40	Bal.	0.45 – 0.65	0.08 – 0.15	3.00 – 3.50	0 – 0.025	0 – 0.035	0.15 – 0.30
8620	0.18 – 0.23	0.40 – 0.60	Bal.	0.70 – 0.90	0.15 – 0.25	0.40 – 0.70	0 – 0.035	0 – 0.040	0.15 – 0.30
5120	0.17 – 0.22	0.70 – 0.90	Bal.	0.70 – 0.90	0	0	0 – 0.035	0 – 0.040	0.15 – 0.30
4320H	0.17 – 0.23	0.35 – 0.65	Bal.	0.40 – 0.70	0.20 – 0.30	1.55 – 2.00	0 – 0.035	0 – 0.040	0.15 – 0.30

Carburizing Objective

Case depth: 0.035” (0.9mm) at C=0.35 wt. %.

Surface carbon: 0.80 ± 0.05 for 8620 and 5120, 0.70 ± 0.05 for 4320 and 9310

Geometry

The geometry is shown in Figure 5.

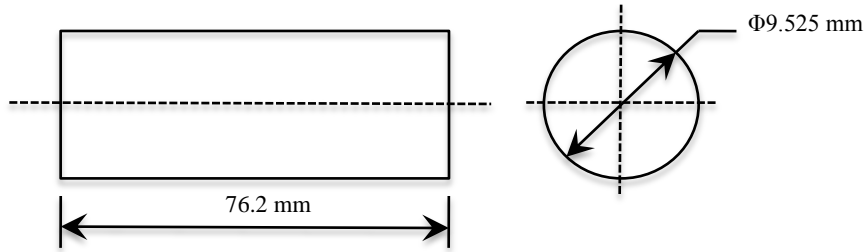


Fig. 5 Geometry of sample

Gas Carburizing Process Development

Test samples were gas carburized in an industrial furnace using a boost and diffuse method. The heat treating process is to heat up to 1700 °F and hold 3.5 hours in endothermic gas at carbon potential of 0.95%, then diffuse at 1550 °F for 1 hour in carbon potential of 0.8%, quench in oil at 140 °F and temper at 350 °F for 2 hours. Figure 6 presents the process schematic.

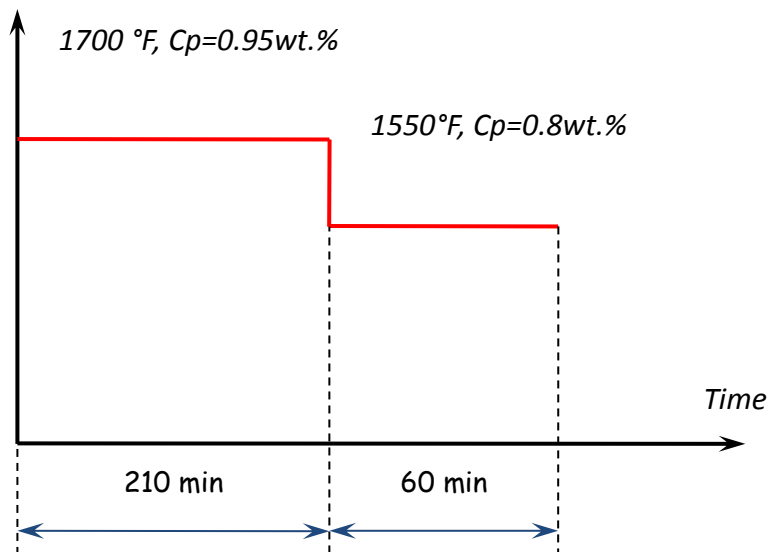
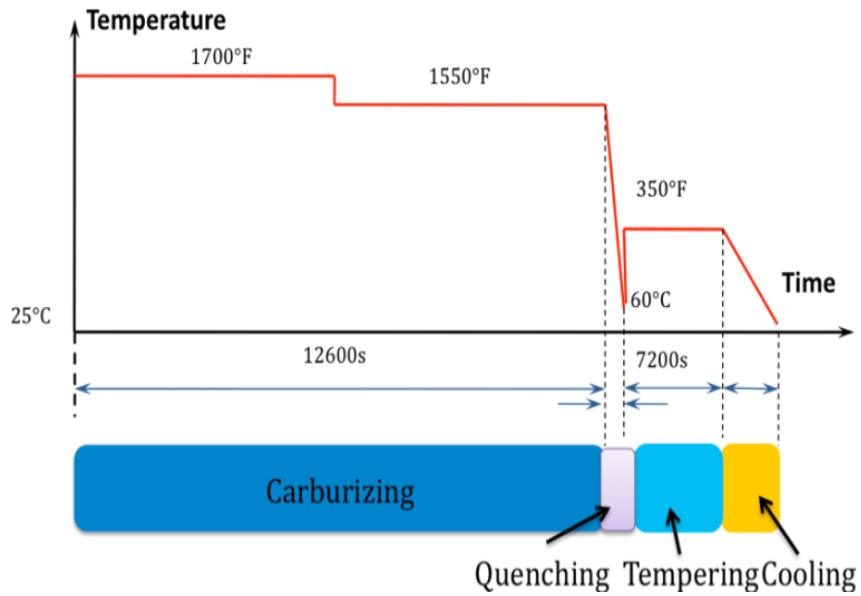


Fig. 6 Process schematic of gas carburizing

The carbon-depth profile measurements of the carburized parts are performed using the Optical Emission Spectrometer (OES). The model was calculated by inputting the parameters of boost and diffuse cycles. Figure 7 presents the measured results and model predictions from CarbTool©. These results agreed very well, which verified the effectiveness of CarbTool© on predicting gas carburizing.

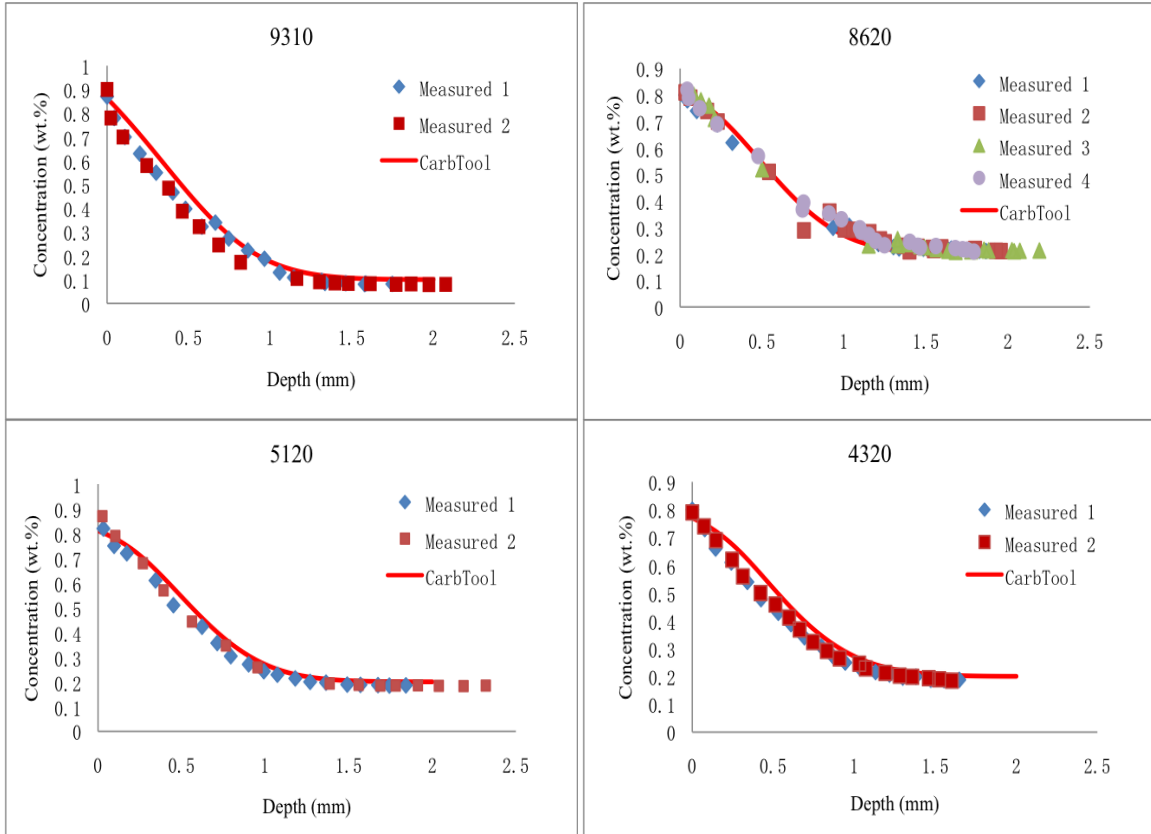


Fig. 7 Comparison between Measured and Predicted Carbon Profile of Four Alloys.

The accuracy of CarbTool© was demonstrated in Table 2; CarbTool©’s calculated surface concentration is compared with the measured result.

Table 2 Comparison of Surface Carbon Concentration between Measured Results and Prediction

	9310	8620	5120	4320
Measured (wt. %)	0.885	0.81	0.85	0.80
CarbTool© (wt. %)	0.86	0.81	0.84	0.77

Table 3 presents a difference between the experiments and specifications. The data shows CarbTool© is able to predict the experimental carbon profile; it was used to revise the industry processes. After changing the inputs in CarbTool©, the corresponding results were obtained in Table 4.

Table 3 Comparison between objective and experimental results

Materials	Surface concentration (wt. %)		Case depth (mm)		Retained Austenite (%)	
	Specification	Experimental	Specification	Experimental	Specification	Experimental
9310	0.70 ±0.05	0.885(higher)	0.889	0.65(shallower)	20% - 30%	33.08
4320		0.8(higher)		0.67(shallower)		37.21
8620	0.80 ±0.05	0.81		0.80(shallower)		19.04
5120		0.85		0.74(shallower)		23.54

Table 4 Gas carburizing predictions from CarbTool©

		9310	4320	8620	5120
Specification	Surface concentration (wt.%)	0.7±0.05		0.8±0.05	
	Depth at 0.35 wt% carbon (mm)	0.889		0.889	
Modeling Results	Surface concentration (wt.%)	0.74	0.74	0.84	0.84
	Depth at 0.35 wt% carbon (mm)	0.888	0.889	0.889	0.889

Process Determination of Vacuum Carburizing in Cyclohexane (C6H6)

9310 and 8620 were used for process development. Processes of the four alloys were set up by industry based on experience and their own databases. In 9310 process, 9310 and 8620 were used. In the other three processes, 8620 coupons with different dimensions were used. Table 5 demonstrates the trial tests.

From Figure 8, the flux of each process was calculated.

Table 5 Tentative test cycles

	Process	Test Material	Diameter (mm)	Calculated flux
Coupon 1	9310	9310	25.4	Flux 1
Coupon 2	9310	8620	12.7	Flux 2

Coupon 3	8620/5120	8620	25.4	Flux 3
Coupon 4	8620/5120	8620	12.7	Flux 4
Coupon 5	4320	8620	25.4	Flux 5

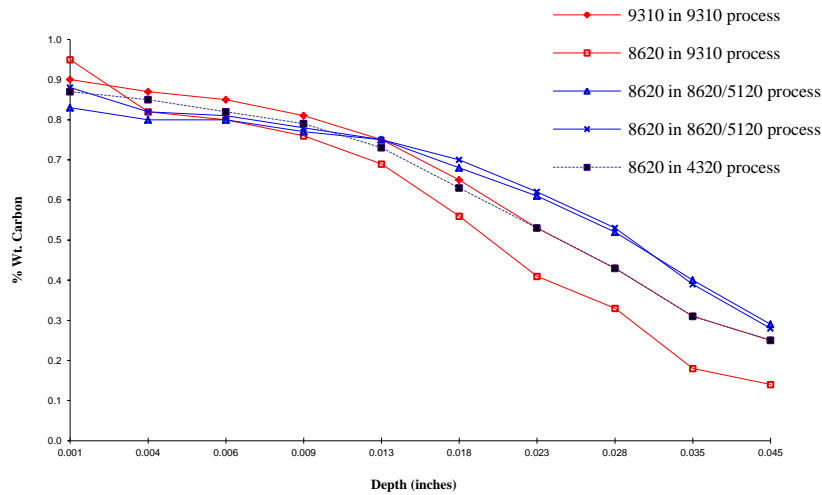


Fig. 8 Carbon profiles of test coupons.

The calculated flux was an input into CarbTool© as a boundary condition; other carburizing parameters (temperature, time and dimension) were kept the same with industry process. The model then predicted carbon profiles of test coupons.

Although we already verified the effectiveness of CarbTool© in gas carburizing, this process has new feature in terms of temperature. Thus, here we verify CarbTool© again. As seen in Figure 9, the modeling results and experimental results agreed with each other very well.

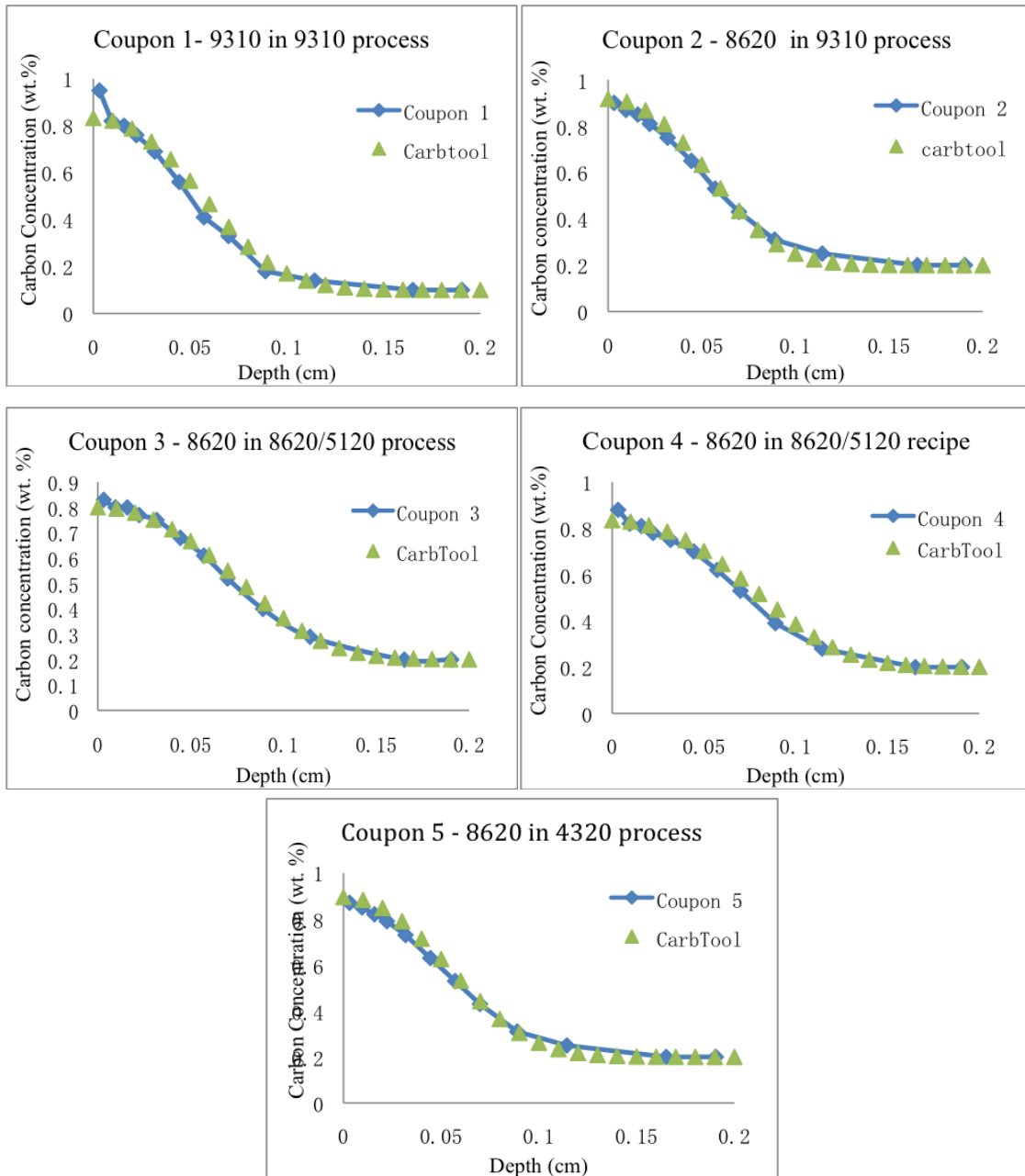


Fig. 9 Carbon profiles of test coupons and their modeling results.

Since the effectiveness of CarbTool© has been proved in this process, the software was utilized to model the fatigue test samples in their corresponding processes. In each process, the calculated flux from the trial test was used as the boundary condition. Meanwhile, diffusivity was changed from the test material (9310 or 8620) to the corresponding material, and the diameter was changed to the correct size (9.525 mm diameter).

At first, the industry processes were conducted, the results were shown in “Modeling 1” column in Table 6. The results do not match specification. Then carburized parameters were tentatively changed in CarbTool©, based on the basic knowledge of diffusion. Once the results (shown in “Modeling 2” column in Table 6) matched the objective, the final processes were obtained.

Table 6 Comparison between objective and different modeling

Process with corresponding material	Flux	Surface concentration (wt. %)			Case depth (mm)		
		Specification	Modeling 1	Modeling 2	Specification	Modeling 1	Modeling 2
9310	Flux 1	0.70 ±0.05	0.82(higher)	0.72	0.889	0.717(shallower)	0.878
	Flux 2		0.84(higher)	0.73		0.727(shallower)	0.891
4320	Flux 5		0.94(higher)	0.69		0.829(shallower)	0.886
8620	Flux 3	0.80 ±0.05	0.83(higher)	0.78		1.063(deeper)	0.883
	Flux 4		0.85	0.8		1.079(deeper)	0.896
5120	Flux 3		0.84	0.8		1.040(deeper)	0.866
	Flux 4		0.86(higher)	0.82	1.057(deeper)	0.878	

Conclusion

The modeling tool, CarbTool©, is effective in predicting the carbon profile for gas carburizing and vacuum carburizing.

Carburization modeling will assist heat treaters to better understand the effects of process parameters on the diffusion process, distribution of carbon concentration, and effective case depth.

Effective modeling will save time and money over a variety of experimental trial.

Finally, the model will give engineers the possibility of optimizing the material, process and design for achieving the optimum performance.

Acknowledgments

The support of the Center for Heat Treating Excellence (CHTE) at Worcester Polytechnic Institute and the member companies is gratefully acknowledged. The author would thank Timken Inc. for providing the raw materials and supporting in this work. The carburization heat treatments were performed at Bodycote Inc. and Surface Combustion Inc. Their support through facilities and experimental work is greatly appreciated.

References

- [1] Sahay, S.S., “Cost Model Based Optimisation of Carburising Operation”, *Surf. Eng.*, 2004, Vol. 20 No. 5, pp. 379.
- [2] Karabelchtchikova, O., “Fundamentals of Mass Transfer in Gas Carburizing”, Ph.D. Dissertation, Worcester Polytechnic Institute, 2007.
- [3] Karabelchtchikova, O., “Carburization Process Modeling and Sensitivity Analysis using Numerical Simulation”, *MS&T '06: Materials Science and Technology 2006 Conference and Exhibition*, 2007.
- [4] Munts, V.A. et al, “Rate of Carburizing of Steel”, *Met. Sci. Heat Treat. (English Translation of Metallovedenie i Termicheskaya Obrabotka Metallov)*, Vol. 22, No. 5-6 (1980), pp. 358-360.
- [5] Baran, Ya. et al, “Gyulihandanov, Vysokotemperaturnaya nitrotsementatsiya spitchenykh staliv vysokoy plotnosti”, *MITOM*, Vol. 9, (1986), pp. 8-10 (in Russian).
- [6] Grafem, W. et al, “Acetylene low-pressure carburizing – a novel and superior carburizing technology”, *Heat Treatment of Metals*, Vol. 4, (1999), pp. 79-85.
- [7] Kula, P. et al, “Vacuum carburizing - process optimization”, *13th International Scientific Conference on Achievement in Mechanical and Materials Engineering*, 2005, Poland.

CHAPTER IV. RESEARCH CONCLUSIONS

This thesis presents results of our works on simulation, development and optimization of thermo-chemical processes, specifically, carburizing and nitriding.

In case hardening processes, there are many process parameters can affect the microstructure and mechanical properties through concentration distribution of interstitial atoms, case depth and hardness.

Regarding to nitriding process, elevated processing temperature within subcritical austenite region replaced the hardened case layers from traditional two layers (compound layer and diffusion zone) to three layers (compound layer, N-austenite layer and diffusion zone if fast cooled). Due to the increased diffusion coefficient at elevated temperature, the nitriding rate was increased leading to more nitrogen flux from atmosphere to metal load and thicker nitride case. The nitrogen flux has been increased to one magnitude larger, while the hardened case was increased from 10 micron to 40 micron.

Liquid nitrogen quenching and soaking utilized on austenitic nitride components increased the hardness of the diffusion zone in the subcritically nitrified steel. Due to the nitrogen stabilized retained austenite, the hardness peak appears at inner part of diffusion zone. The hardness increase is proportional to the soaking time suggesting cryogenic aging and isothermal martensitic transformation as the operating mechanisms. Thus the continuous hardness profile for subcritical temperature austenitic nitriding can be achieved under prolonged soaking in liquid nitrogen.

In nitrogen diluted ammonia atmosphere, the local equilibrium between nitriding medium and metal load surface has not built up yet during the period in this experiment. The intrinsic character of nitrogen diluted ammonia atmosphere makes nitriding potential not sufficiently represents the nitriding capability. Therefore, if quasi-equilibrium (the local equilibrium only at solid interfaces) is assume in the system, the layer growth kinetics can be controlled by the nitrogen flux from the atmosphere into metal surface and the interface migration. Based on parabolic growth of diffusion controlled layers, a

mathematic model has been derived. Once two of three major components, diffusion coefficient, growth rate constant and layer depth, are measured, the other one is accessible from the mathematical calculation. When local equilibrium is reached, the excessive nitrogen atoms constitute the growth of top compound layer, as suggested, boost and diffuse conditions are beneficial to control the thickness of each layer.

In carburizing section, first, the atmosphere effects have been discussed. The carburizing atmosphere is divided into two categories: equilibrium and non-equilibrium. Simulation tool CarbTool© has been built up for these two kinds of atmosphere by Center for Heat Treating Excellence at Worcester Polytechnic Institute, using finite difference method. This work has improved both gas and vacuum models in it using experimental data and thermodynamic predictions. The validation of the models has been implemented by creating recipes in CarbTool© for both industrial atmosphere and low pressure carburizing, as well as comparing the concentration profiles between two processes and between experimental and simulation results. It has been proven that the improved models are capable of creating desired carbon profiles for the carburizing processes in both kinds of atmospheres.

Non-equilibrium atmosphere is used in plasma activated nitrogen-hydrocarbons mixture atmosphere carburizing. The first industrial scale demonstrations confirmed its utility in eliminating intergranular oxides and promoting carburizing process in one atmosphere pressure furnace. In N₂ - 0.4% C₃H₈ - 1% CH₄ atmosphere, sufficient carbon absorption has been achieved with less soot deposition on the metal surface and in the atmosphere.

Secondly, the effect of loading configuration on carburizing uniformity over different locations in the charge and between different sides on the components is investigated with assistance of computational fluid dynamics study. A center channel configuration modification improved the gas stream uniformity, therefore reduced the hardness deviation among stacked trays as well as carburizing unevenness between two sides on the components.

Thirdly, graphite filaments growth on metal surface are investigated, its formation is associated with hydrocarbons type, cementite/carbides formation and surface catalytic

sites. The soot formation mechanism is proposed in three steps: 1) soot particles and PAH formation in atmosphere; 2) pyrolytic soot deposition on metal surface, depending on the gas composition, hydrocarbons and hydrogen concentration ratio; 3) graphite filaments growth, depending on the conditions described above.